Systematics of midrapidity transverse energy distributions in limited apertures from p+Be to Au+Au collisions at relativistic energies

T. Abbott,[4,a] L. Ahle,[12,b] Y. Akiba,[14,7] D. Alburger,[2] D. Beavis,[2] L. Birstein,[2] M. A. Bloomer,[12] P. D. Bond,[2] H. C. Britt,[11] B. Budick,[13] C. Chasman,[2] Z. Chen,[2,c] C. Y. Chi,[5] Y. Y. Chu,[2] V. Cianciolo,[12,d] B. A. Cole,[12,5] J. B. Costales,[12,11,e] H. J. Crawford,[3] J. B. Cumming,[2] R. Debbe,[2] E. Duek,[2,f] J. Engelage,[3] S. Y. Fung,[4] M. Gonin,[2,g] L. Grodzins,[12] S. Gushue,[2] H. Hamagaki,[14] O. Hansen,[2,h] R. S. Hayano,[15] S. Hayashi,[14,2] S. Homma,[14] H. Z. Huang,[12,i] Y. Ikeda,[10,j] I. Juricic,[5,k] H. Kaneko,[9] J. Kang,[4,17] S. Katcoff,[2,l] S. Kaufman,[1] W. L. Kehoe,[12,m] K. Kimura,[10] K. Kitamura,[8,n] K. Kurita,[16,o] R. J. Ledoux,[12,p] M. J. LeVine,[2] Y. Miake,[16] D. P. Morrison,[12,2] R. J. Morse,[12] B. Moskowitz,[2] S. Nagamiya,[5,6] M. N. Namboodiri,[11] T. K. Nayak,[5,q] J. Olness,[2] C. G. Parsons,[12,r] L. P. Remsberg,[2] P. Rothschild,[12] H. Sakurai,[15] T. C. Sangster,[11] M. Sarabura,[12] R. Seto,[4] K. Shigaki,[15,6] A. Shor,[2] R. Soltz,[12,11] P. Stankus,[5,d] S. G. Steadman,[12,s] G. S. F. Stephans,[12] T. Sugitate,[8] T. Sung,[12] M. Tanaka,[2,l] M. J. Tannenbaum,[2] J. Thomas,[11,t] S. Tonse,[11] M. Torikoshi,[14,u] S. Ueno-Hayashi,[16] J. H. van Dijk,[2] F. Videbæk,[2] M. Vient,[4,v] P. Vincent,[2,w] O. Vossnack,[5] E. Vulgaris,[12,x] V. Vutsadakis,[12] F. Q. Wang,[5,t] Y. Wang,[5] W. A. Watson III,[2,y] H. E. Wegner,[2,l] D. S. Woodruff,[12] Y. D. Wu,[5] K. Yagi,[16] X. Yang,[5] D. Zachary,[12] and W. A. Zajc[5]

(E-802 Collaboration)

[1]*Argonne National Laboratory, Argonne, Illinois 60439-4843*
[2]*Brookhaven National Laboratory, Upton, New York 11973*
[3]*University of California, Space Sciences Laboratory, Berkeley, California 94720*
[4]*University of California, Riverside, California 92507*
[5]*Columbia University, New York, New York 10027*
and Nevis Laboratories, Irvington, New York 10533
[6]*High Energy Accelerator Research Organization (KEK), Tsukuba, Ibaraki 305, Japan*
[7]*High Energy Accelerator Research Organization (KEK), Tanashi Branch, (Tanashi) Tokyo 188, Japan*
[8]*Hiroshima University, Hiroshima 730, Japan*
[9]*Kyoto University, Sakyo-Ku, Kyoto 606, Japan*
[10]*Kyushu University, Fukuoka 812, Japan*
[11]*Lawrence Livermore National Laboratory, Livermore, California 94550*
[12]*Massachusetts Institute of Technology, Cambridge, Massachusetts 02139*
[13]*New York University, New York, New York 10003*
[14]*Center for Nuclear Study, School of Science, University of Tokyo, Tanashi, Tokyo 188, Japan*
[15]*Department of Physics, University of Tokyo, Tokyo 113, Japan*
[16]*University of Tsukuba, Tsukuba, Ibaraki 305, Japan*
[17]*Yonsei University, Seoul 120-749, Korea*

(Received 8 September 2000; published 1 May 2001)

Measurements of the A dependence and pseudorapidity interval ($\delta\eta$) dependence of midrapidity E_T distributions in a half-azimuth ($\Delta\phi=\pi$) electromagnetic calorimeter are presented for $p+$Be, $p+$Au, O+Cu, Si+Au, and Au+Au collisions at the BNL-AGS (Alternating-Gradient Synchrotron). The shapes of the upper edges of midrapidity E_T distributions as a function of the pseudorapidity interval $\delta\eta$ in the range 0.3 to 1.3, roughly centered at midrapidity, are observed to vary with $\delta\eta$, like multiplicity—the upper edges of the distributions flatten as $\delta\eta$ is reduced. At the typical fixed upper percentiles of E_T distributions used for *nuclear geometry* characterization by *centrality* definition—7 percentile, 4 percentile, 2 percentile, 1 percentile, 0.5 percentile—the effect of this variation in shape on the measured projectile A_p dependence for ^{16}O, ^{28}Si, ^{197}Au projectiles on an Au target is small for the ranges of $\delta\eta$ and percentile examined. The E_T distributions for $p+$Au and $p+$Be change in shape with $\delta\eta$; but in each $\delta\eta$ interval the shapes of the $p+$Au and $p+$Be distributions remain indentical with each other—a striking confirmation of the absence of multiple-collision effects at midrapidity at AGS energies. The validity of the *nuclear geometry* characterization versus $\delta\eta$ is illustrated by plots of the $E_T(\delta\eta)$ distribution in each $\delta\eta$ interval in units of the measured $\langle E_T(\delta\eta)\rangle_{p+\mathrm{Au}}$ in the same $\delta\eta$ interval for $p+$Au collisions. These plots, in the physically meaningful units of ‘‘number of average $p+$Au collisions,’’ are nearly universal as a function of $\delta\eta$, confirming that the reaction dynamics for E_T production at midrapidity at AGS energies is governed by the number of projectile participants and can be well characterized by measurements in apertures as small as $\Delta\phi=\pi$, $\delta\eta=0.3$.

DOI: 10.1103/PhysRevC.63.064602 PACS number(s): 12.38.Mh, 13.60.Le, 13.85.Hd, 25.75.$-$q

I. INTRODUCTION

A. E_T—from jet probe to global variable

Transverse energy (E_T) measurements using 4π hadron calorimeters in p-p collisions were proposed [1–3] for the purpose of detecting and studying the hard scattering of constituents of the proton (discovered at the CERN ISR via high p_T leading particles [4]) by finding localized cores of energy deposition, ''jets,'' in an unbiased manner. However, the first published measurement [5] of an E_T distribution—where E_T is defined as

$$E_T=\sum_i E_i \sin\theta_i \quad \text{and} \quad dE_T(\eta)/d\eta=\sin\theta(\eta)\, dE(\eta)/d\eta, \tag{1}$$

where $\eta=-\ln\tan\theta/2$ is the pseudorapidity and the sum is taken over all particles emitted on an event[1] into a fixed but large solid angle—utilized a full azimuth hadron calorimeter that covered only the midrapidity region in p-p collisions at c.m. energy $\sqrt{s}=24$ GeV, $-0.88\leqslant\eta\leqslant 0.67$ in the c.m. system. The experimental result was striking—the predominant source of transverse energy turned out to be ''soft'' multiparticle production, not jets.

E_T distributions are composed of a large number of particles with relatively small transverse momenta, the random product of the particle multiplicity and p_T distributions [5]. As the p_T distribution in p-p collisions is largely independent of rapidity and multiplicity [6], the E_T and multiplicity distributions are simply related[2]

$$dE_T/d\eta \sim \langle p_T\rangle \times dn/d\eta, \tag{2}$$

where $\langle p_T\rangle$ is the average transverse momentum per particle.

According to Bjorken [8], dE_T/dy is thought to be related to the comoving energy density in a longitudinal expansion, and proportional to the energy density (ϵ) in space

$$\epsilon_{Bj}=\frac{dE_T}{dy}\,\frac{1}{2\tau_0\pi R^2}, \tag{3}$$

where τ_0, the formation time, is usually taken as 1 (or $\frac{1}{2}$) fm, πR^2 is the effective area of the collision, and dE_T/dy is the co-moving (i.e. transverse) energy density in rapidity. Many authors have suggested that since the transverse energy in both hard [2,9] and softer [10] collisions is created before the hadronization stage, E_T distributions may carry more direct information than may be reflected in multiplicity distributions.

With the advent of the Alternating-Gradient Synchrotron (AGS) and CERN relativistic heavy ion (RHI) programs in the later 1980s, E_T distributions have come to play a leading role as a ''global variable'' to define the overall character or *centrality* of individual RHI interactions: as the impact parameter is reduced from grazing impact, more nucleons participate (there are fewer spectators) so more energy is transferred from the projectile and target rapidity regions to the transverse direction and toward midrapidity. Extensive measurements at the BNL-AGS [11–16] and the CERN SPS

[1]Note that E_T is an ''event-by-event'' variable.

[2]In detail, the relationship is much more complicated [7].

[a]Present address: Reedley College, Reedley, CA 93654.

[b]Present address: Lawrence Livermore National Laboratory, Livermore, CA 94550.

[c]Present address: Renaissance Technologies Corp., East Setauket, NY 11790.

[d]Present address: Oak Ridge National Laboratory, Oak Ridge, TN 37831.

[e]Present address: Radionics Software Applications, Inc., Burlington, MA 01803.

[f]Present address: New Side S.A., Buenos Aires, Argentina.

[g]Present address: LPNHE, Ecole Polytechnique, IN2P3-CNRS, Palaiseau, France.

[h]Present address: Niels Bohr Institute for Astronomy, Physics and Geophysics, DK-1200 Copenhagen Ø, Denmark.

[i]Present address: University of California, Los Angeles, CA 90095.

[j]Present address: Hitachi Limited, Hitachi, Ibaraki 316, Japan.

[k]Present address: Schlumberger Corp., Houston, TX 77210.

[l]Deceased.

[m]Present address: Integral, Inc., Cambridge, MA 02138.

[n]Present address: Nippon Telegraph and Telephone Co., Tsuyama, Okayama 708, Japan.

[o]Present address: The Institute of Physical and Chemical Research (RIKEN), Saitama 351-01, Japan.

[p]Present address: Radionics Software Applications, Inc., Burlington, MA 01803.

[q]Present address: VECC, Calcutta 700064, India.

[r]Present address: NITON, Bedford, MA 01730.

[s]Present address: Office of Science, Department of Energy, Germantown, MD 20874-1290.

[t]Present address: Lawrence Berkeley National Laboratory, Berkeley, CA 94720.

[u]Present address: Mitsubishi Electric Co., Hyogo 652, Japan.

[v]Present address: UC Irvine, Irvine, CA 92717.

[w]Present address: Friedrichstrasse 67, Karlsruhe, Germany.

[x]Present address: Bell Telephone Laboratory, Naperville, IL 60566.

[y]Present address: Thomas Jefferson National Accelerator Facility, Newport News, VA 23606.

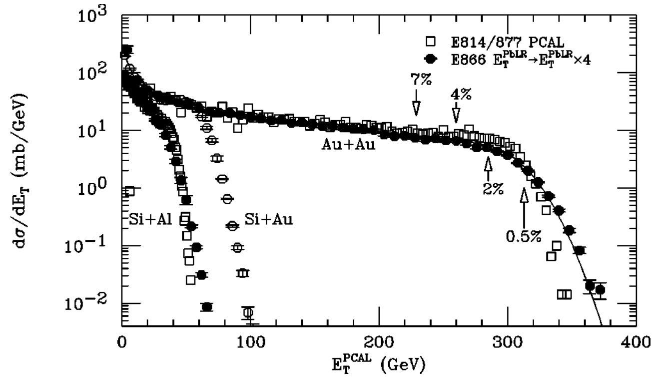

FIG. 1. E814/E877 E_T spectra [31] in a full-azimuth hadron calorimeter covering $0.83 \leqslant \eta \leqslant 4.7$, denoted E_T^{PCAL}, compared to E802/E866 E_T spectra [15] in a full-azimuth mid-rapidity EM calorimeter covering $1.3 \leqslant \eta \leqslant 2.4$, denoted E_T^{PbLR}. The E866 E_T spectra are scaled by an empirical factor of 4 in E_T^{PbLR} to match the E_T^{PCAL} spectra. Some upper percentiles of the E802/E866 Au+Au spectrum are indicated by arrows. The solid line on the E802/E866 Au+Au data is a WPNM calculation to be discussed later.

[17–22] have shown that E_T distributions in $A+A$ collisions are largely dominated by the *nuclear geometry* of the reaction, at the present level of sensitivity, so that ''a very modest quality E_T measurement over a limited region of phase space will provide sufficiently accurate information for impact parameter tagging [23].'' At the 160–200 A GeV/c incident beam momentum at CERN ($\sqrt{s_{NN}} \sim 19$ GeV), midrapidity E_T for $A+A$ collisions [24] is largely proportional to the total number of participants (wounded nucleons) as it was for $p+A$ and light-ion collisions in this energy range [25,26]. The situation at AGS energies of 11.6–14.6A GeV/c ($\sqrt{s_{NN}} \sim 5$ GeV) is quite different—midrapidity E_T distributions in $A+A$ collisions are generally described by a superposition of $p+A$ collisions [11–15,27]. The E_T measurements provided the first indication of significant projectile stopping at AGS energies, subsequently confirmed by direct measurements of the nucleon rapidity distributions [28–30].

B. Centrality definition via E_T—midrapidity versus 4π

At the AGS, where midrapidity is $y_{\mathrm{c.m.}}^{NN} \simeq 1.6-1.7$, both E802/E866 [14] and E814/E877 [31] use E_T distributions to define *centrality*, typically by a certain upper percentile of the distribution: Ref. [14] measures E_T in a midrapidity electromagnetic calorimeter that is sensitive predominantly to produced particles [14,15] while [31] employs a nearly 4π hadronic calorimeter (see Fig. 1). The upper tails of the less-constrained distributions measured by [14] in the smaller aperture, midrapidity, electromagnetic calorimeter (scaled by a factor of 4 in E_T for visual effect) fluctuate more (i.e., have a less steep upper edge) than the more constrained distributions measured by [31] in the nearly 4π hadron calorimeter; but for the most part the distributions are very similar in shape, and therefore in centrality definition.

The utility of *hermetic* 4π detectors to search for *missing energy* in nucleon-nucleon collisions is beyond debate [32,33]. However, when nuclei are involved, the situation is considerably more complicated. The physics may be different for outgoing nucleons, which are overwhelmingly fragments from the original projectile and target, and for produced particles, which are typically mesons (mainly pions). This leads to a philosophical issue: one may use the overall 4π multiplicity or E_T to try to learn the physics from a measurement, or one may distinguish among the target fragmentation, midrapidity, and projectile-fragmentation rapidity regions where, furthermore, the systematics may be quite different for the different particle types. As the projectile dependence of a reaction is emphasized by measurements in the projectile-fragmentation region [25,18,34], while the target dependence is emphasized by measurements in the target-fragmentation region [17,35,7], midrapidity measurements might represent a reasonable global average for centrality definition or studies of reaction dynamics.

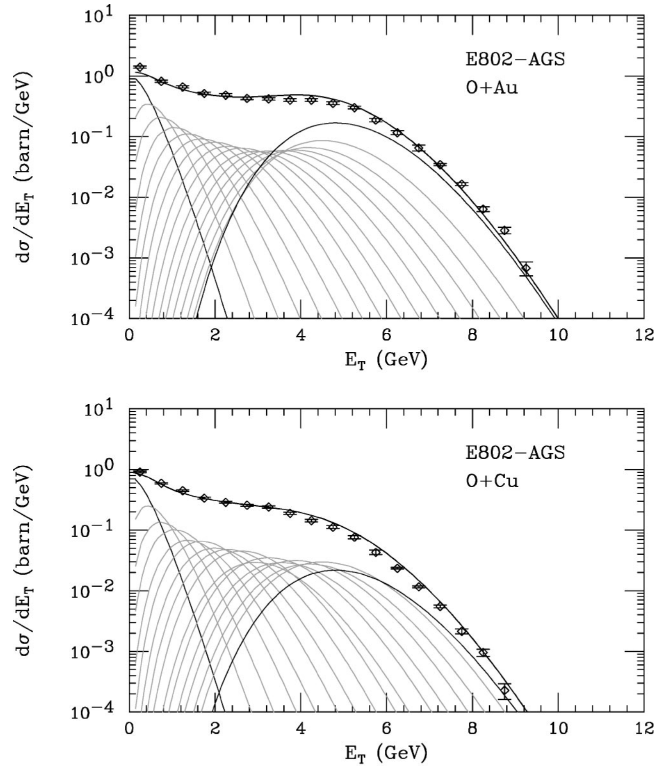

FIG. 2. Previously published [14] measured energy emission in the E802 electromagnetic calorimeter ($\Delta\phi=\pi$, $1.22 \leqslant \eta \leqslant 2.50$) for ^{16}O+Au and ^{16}O+Cu interactions at 14.6A GeV/c. The solid curve through the data is the sum of the 1-fold to 16-fold convolution of the measured $p+$Au spectrum weighted according to the probability for 1, 2, . . . ,16 of the projectile nucleons to interact in the target (wounded projected nucleon model). The individual components of the sum are shown, with the 1-fold and 16-fold $p+$Au convolutions emphasized.

C. Previous measurements and open issues

Previous measurements [11–15] of midrapidity E_T distributions have demonstrated that beyond simple issues of nuclear geometry, dynamics plays a significant role. Once the maximum number of participants is reached in central collisions, the geometrical effect is exhausted leaving the detailed shape of the sharp drop-off of the upper edge of the spectrum to reveal possible underlying dynamics. Two early measurements illustrate this effect. The first midrapidity E_T spectra ($1.22 \leqslant \eta \leqslant 2.50$) measured at the AGS with a ^{16}O beam [11–13] showed saturation in targets of Cu or heavier (see Fig. 2). The maximum transverse energy is roughly the same in ^{16}O+Cu and ^{16}O+Au reactions, even though the maximum thickness of a Cu nucleus is only ~2/3 that of Au. Also, the shapes of the upper edges of both spectra are identical, with a constant ratio $(d\sigma/dE_T)_{\mathrm{O+Au}}/(d\sigma/dE_T)_{\mathrm{O+Cu}} \sim 6$, which is close to the ratio of the areas (~5) for the ^{16}O projectile to fit within the Au or Cu target nucleus [11,12]. The same trend was observed in the $p+A$ E_T spectra, which have the same shape and $\langle E_T \rangle$ for p+Be, p+Al, p+Cu and p+Au reactions—a striking absence of the successive collision effect seen at higher energies [21].

These two observations, together with the success in reconstructing the measured O+A [36], Si+A ($B+A$) midrapidity E_T spectra as the sum of the 1 to B-fold convolutions of the measured p+Au spectrum, weighted according to the *geometric* probability for 1, 2, ..., B of the projectile nucleons to interact in the target (wounded projectile nucleon model, or WPNM, see curves on Fig. 2), could be explained if the projectiles were presumed to exhaust their ability to produce pions after only a few nucleon-nucleon collisions [11–14,27]. It is also conceivable [19,37] that the saturation of the upper edges of the E802 midrapidity E_T spectra at AGS energies could be an artifact of the limited angular (η) acceptance.

The pseudorapidity acceptance is an issue because nonquantum mechanical models, based on solid-body kinematics [38], which work well at nonrelativistic energies [39–41], predict that the rapidity of the c.m. system will shift such that the maximum in dn/dy (and presumably $dE_T/d\eta$) moves towards the rapidity of the larger nucleus in an asymmetric $B+A$ reaction. Similar but quantitatively different shifts are also predicted in relativistic successive collision models [42] since the excitation of a nucleon by a collision causes its rapidity to decrease. These effects are observed in [29,43]. Therefore, an important issue to address is whether the pseudorapidity acceptance of the midrapidity E_T distributions affects the interpretation of the measurements—i.e., are the saturation observation, the stopping inference, and the WPNM calculations something fundamental, or are they just an artifact of a particular $\delta\eta$ acceptance? An additional issue is whether the shapes of E_T distributions change with the $\delta\eta$ interval, like multiplicity, and if so, how this affects the event characterization and *centrality* definition.

II. NEW MEASUREMENTS OF MIDRAPIDITY E_T DISTRIBUTIONS VERSUS $\delta\eta$

A. Overview

Systematic measurements of midrapidity E_T distributions are presented as a function of $\delta\eta$ using the E802 lead glass (PbGl) EM calorimeter (see Fig. 3) that covered half the azimuth ($\Delta\phi=\pi$), with a total pseudorapidity acceptance of $1.22 \leqslant \eta \leqslant 2.50$ (where midrapidity for these energies is $y^{NN}_{\mathrm{c.m.}} \simeq 1.6$–1.7 depending on the species). It is important to note that the PbGl EM calorimeter accurately measures electromagnetic energy deposited by photons (typically produced by $\pi^0 \to \gamma\gamma$ and $\eta \to$ neutral decays), but also responds to the Čerenkov radiation from relativistic charged hadrons [14,15]. The overall response of the detector may be simply represented as

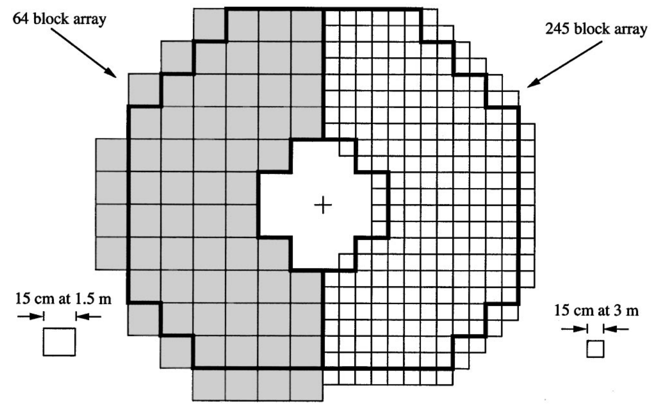

FIG. 3. E802/E859/E866 lead glass electromagnetic calorimeter. The $\delta\eta$ dependence reported here is made using the more highly segmented right half of the calorimeter that covers $\Delta\phi=\pi$, $1.22 \leqslant \eta \leqslant 2.50$. The heavy lines define the fiducial volume for a previous measurement [15] (Fig. 1) and are not relevant for the present data.

$$E_T \equiv \sum_{\text{photons}} E_\gamma \sin\theta + \sum_{\text{charged, } \beta \geqslant 0.8} (0.45\,\text{GeV}) \times \sin\theta. \quad (4)$$

No correction is made for the average charged hadron signal since an unknown model-dependent systematic error would accrue. Thus, E_T is a composite but precisely measured quantity that has linear response for multiple collisions.[3] Details on the linearity, response, and calibration of the detectors may be found elsewhere [14,35,44]. For the present purposes, it is important to note that at least 85% of the measured E_T in the PbGl is due to produced particles (i.e., not nucleons).

The pseudorapidity distributions, $dE_T/d\eta$ for fixed E_T, have already been published [14,15]. In the present study, the full η acceptance of the half-azimuth calorimeter, $1.22 \leqslant \eta \leqslant 2.50$, is subdivided into eight nominally equal bins of 0.16 in pseudorapidity, i.e., $1.22 \leqslant \eta \leqslant 1.38$, $1.38 \leqslant \eta \leqslant 1.54, \ldots, 2.34 \leqslant \eta \leqslant 2.50$. The acceptance ($\Delta\eta \times \Delta\phi$) of each bin varies compared to the ideal $0.16 \times \pi$, and is corrected by quoting an effective $\delta\eta$ rather than simply the difference of the boundaries of the interval. The E_T distributions (in $\Delta\phi=\pi$) are then measured for $\delta\eta$ intervals composed of groups of 1,2,4,6,8 bins centered (except for the smallest) on $\eta=1.86$: $\delta\eta=1.30$, the full η acceptance of the calorimeter (actually $1.22 \leqslant \eta \leqslant 2.50$); $\delta\eta=0.966$ ($1.38 \leqslant \eta \leqslant 2.34$); $\delta\eta=0.624$ ($1.54 \leqslant \eta \leqslant 2.18$); $\delta\eta=0.378$

[3] In previous publications [13,14], this same quantity was denoted E_T^{PbGl}.

TABLE I. Beams and targets used in the reported data.

Beam(s)	Target	Thickness (mg/cm^2)	Percent of interaction length
p	Be	1480	2
Si	Al	817	3 (Si)
O	Cu	1440	3 (Si)
p, O	Au	2939	3 (Si)
Si	Au	1846	2 (Si)
Au	Au	944	1 (Si)

$(1.70 \leqslant \eta \leqslant 2.02)$; $\delta\eta = 0.170$ $(1.70 \leqslant \eta \leqslant 1.86)$. The data and method of analysis are the same as reported in Refs. [14,15] where full details are given. A brief description follows.

All the data presented here come from the right half azimuth of the calorimeter (Fig. 3). Data from previous publications [12–14] use the same setup. (Different setups were used for Fig. 1 [15] and Ref. [11].) The data were taken over the period 1987–1992 with beams of p, ^{16}O, ^{28}Si, and ^{197}Au on various targets (see Table I). Several triggers were used to acquire the data: the minimum bias interaction trigger ''INT'' and hardware high-E_T trigger, ''PB2,'' described in Ref. [14]; and an alternative minimum-bias trigger ''EMIN'' defined by any hit on the PbGl ($E_T \sim 15-75$ MeV, depending on the species) in coincidence with a good beam count, described in Ref. [15]. Pile-up was eliminated by vetoing events with more than one beam particle within a ± 500-ns window. Target-out contributions were measured and subtracted for all beam-target-trigger combinations. The stability of the E_T calibration over the five year period, checked by remeasurement of the $\delta\eta = 1.30$ Si+Al and Si+Au E_T spectra [13], was within $\pm 3\%$ (see Fig. 4).

B. Proton-nucleus spectra

The original Abbott *et al.* measurements [12,14] in the full η acceptance of the half-azimuth calorimeter showed that the midrapidity E_T spectra of $p+$Au, $p+$Cu, $p+$Al, and $p+$Be all exhibit the same shape over roughly five decades of cross section—no obvious multiple-collisions effects were evident at midrapidity for $p+A$ collisions at AGS energies. In the present measurement, the E_T distributions of $p+$Au and $p+$Be at 14.6 GeV/c (see Fig. 5 and Tables II and III) are obtained as a function of the smaller $\delta\eta$ intervals listed in Sec. II A. It is evident in Fig. 5 that as the $\delta\eta$ interval is reduced, the shapes of the E_T spectra clearly change with $\delta\eta$ for both $p+$Au and $p+$Be; but in each $\delta\eta$ interval, the shapes of the $p+$Au and $p+$Be distributions remain essentially *identical* to each other. This striking effect is exhibited quantitatively by fits of each spectrum to a single-Gamma distribution [45] that result in the equality of the $p+$Au and $p+$Be fit parameters, b and p, in each $\delta\eta$ interval as indicated on Fig. 5 (see also Table IV). The near indistinguishability of the $p+$Au and $p+$Be E_T distributions for the smaller $\delta\eta$ intervals is striking confirmation of the previous explanation of the same effect in the full η acceptance [14] by a class of events where the pion distribution exhibits a large backward shift in rapidity, $\gtrsim 0.8$ units

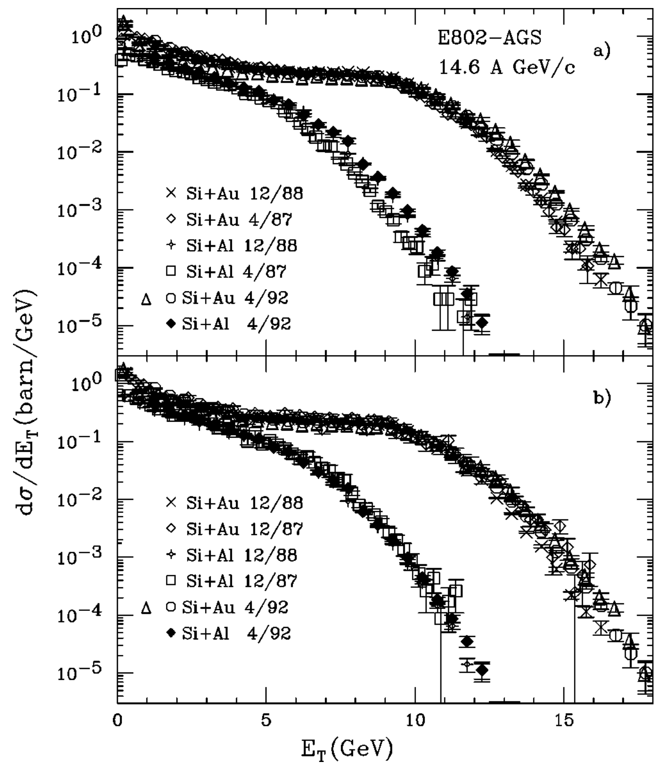

FIG. 4. E_T distributions ($\Delta\phi = \pi$, $1.22 \leqslant \delta\eta \leqslant 2.50$) at 14.6$A$ GeV/c for Si+Al (filled diamonds) and Si+Au (open triangles, open circles) from the April 1992 run, which includes the Au+Au measurement, compared to measurements in previous runs [14]. Note that the filled diamonds and open circles represent an analysis done just after the data were taken in April 1992, while the present analysis of the Si+Au data is shown as the open triangles.

[46,47], leaving little energy in the midrapidity acceptance of the calorimeter. This is further evidence that the large stopping observed in nucleus-nucleus collisions at AGS energies is also manifest in $p+A$ collisions [12,14,27].

C. Nucleus-nucleus spectra

Measurements of the E_T distributions for $p+$Au (Sec. II B), ^{16}O+Cu, ^{16}O+Cu(central), ^{28}Si+Au at 14.6A GeV/c and ^{197}Au+Au, ^{197}Au+Au(central) at 11.6A GeV/c as a function of $\delta\eta$ are shown in Fig. 6. The plots are strikingly similar in all $\delta\eta$ intervals, but there is a clear flattening of the upper edges of the distributions with decreasing $\delta\eta$. The centrality is defined by a zero degree calorimeter [13,48], which, for O+Cu [49], required a forward-going kinetic energy of less than that of a single projectile spectator (13.6 GeV), indicating that all 16 projectile nucleons had interacted, and, for Au+Au [48], selected the most central 8.4 percentile of the projectile spectator distribution corresponding to collisions with less than 40 projectile spectators (out of 197), with a mean value of $\langle N_{pp} \rangle = 197 - 20 = 177$ projectile participants. The data are tabulated in Tables V–IX. See Refs. [13,48,49] for further details pertaining to the zero degree calorimeter.

The flattening of the upper edges of the distributions and the broadening of the central collision spectra with decreas-

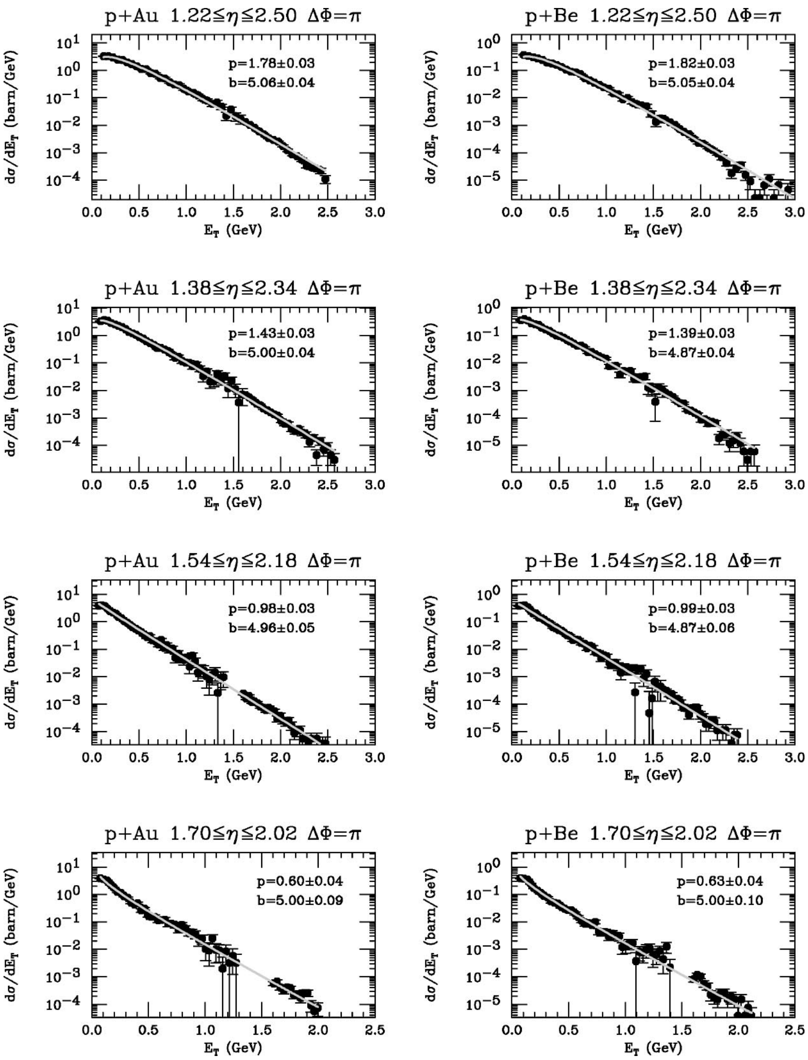

FIG. 5. E_T distributions for $p+\mathrm{Au}$ (left) and $p+\mathrm{Be}$ (right) at 14.6 GeV/c as a function of decreasing $\delta\eta$ from top to bottom. Adjacent $p+\mathrm{Au}$ and $p+\mathrm{Be}$ plots have the same $\delta\eta$. The gaps in the spectra for smaller $\delta\eta$ intervals are due to the fact that the high-E_T trigger was operative on the full η acceptance, thus not fully efficient in the smaller intervals, requiring inefficient points to be deleted. As described in the text, minimum-bias triggers are used to obtain the lower E_T segments of the spectra. The solid lines on the figure are Gamma distribution fits with parameters indicated.

ing $\delta\eta$, evident in Fig. 6, is emphasized by plotting the central collision spectrum in each $\delta\eta$ interval scaled by its mean (see Fig. 7). Since measurements of the shapes of multiplicity distributions for central $^{16}\mathrm{O}+\mathrm{Cu}$ collisions [49] have been made with exactly the same data sets used in the present E_T analysis, they are shown as a reminder on Fig. 8. Evidently, the shapes of the upper edges of E_T distributions change with $\delta\eta$, like multiplicity.

III. FITS

In the mid 1980s, the close connection between E_T and multiplicity distributions in p-p collisions was reinforced by the fact that both could be described by relatively simple and closely related functions, the negative binomial distribution (NBD) for multiplicity [50] and the Gamma distribution for E_T [51–54]. In fact, Gamma distributions were found to provide excellent representations of midrapidity E_T distributions for ten decades in cross section for both p-p and α-α collisions [53].

A. Gamma and negative binomial distributions

The Gamma distribution represents the probability density for a continuous variable x, and has two parameters b and p:

$$f(x)=\frac{b}{\Gamma(p)}(bx)^{p-1}e^{-bx}, \tag{5}$$

where

$$p>0, \quad b>0, \quad 0\leqslant x\leqslant\infty,$$

$\Gamma(p)$ is the Gamma function, which equals $(p-1)!$ if p is an integer, and $f(x)$ is normalized. The first few moments of the distribution are

$$\mu\equiv\langle x\rangle=\frac{p}{b}, \quad \sigma=\frac{\sqrt{p}}{b}, \quad \frac{\sigma^2}{\mu^2}=\frac{1}{p}. \tag{6}$$

The negative binomial distribution of an integer m is defined as

$$P(m)=\frac{(m+k-1)!}{m!(k-1)!}\frac{\left(\frac{\mu}{k}\right)^m}{\left(1+\frac{\mu}{k}\right)^{m+k}}, \tag{7}$$

where $P(m)$ is normalized for $0\leqslant m\leqslant\infty$, $\mu\equiv\langle m\rangle$, and some higher moments are

TABLE II. $d\sigma/dE_T$ (b/GeV) versus E_T (GeV) for $p+\mathrm{Be}$ at 14.6A GeV/c for four $\delta\eta$ intervals. Errors quoted are statistical only; systematic errors are estimated to be less than $\pm3\%$ on the E_T scale.

$p+\mathrm{Be}$							
E_T	$\delta\eta$=1.30	E_T	$\delta\eta$=0.966	E_T	$\delta\eta$=0.624	E_T	$\delta\eta$=0.378
0.125	$3.66\times10^{-1}\pm1.09\times10^{-2}$	0.094	$3.63\times10^{-1}\pm1.24\times10^{-2}$	0.075	$3.82\times10^{-1}\pm1.41\times10^{-2}$	0.075	$3.88\times10^{-1}\pm1.42\times10^{-2}$
0.175	$3.32\times10^{-1}\pm1.03\times10^{-2}$	0.131	$3.93\times10^{-1}\pm1.29\times10^{-2}$	0.105	$3.91\times10^{-1}\pm1.43\times10^{-2}$	0.105	$3.72\times10^{-1}\pm1.39\times10^{-2}$
0.225	$3.02\times10^{-1}\pm9.83\times10^{-3}$	0.169	$3.51\times10^{-1}\pm1.22\times10^{-2}$	0.135	$3.98\times10^{-1}\pm1.44\times10^{-2}$	0.135	$3.51\times10^{-1}\pm1.34\times10^{-2}$
0.275	$2.69\times10^{-1}\pm9.21\times10^{-3}$	0.206	$2.79\times10^{-1}\pm1.09\times10^{-2}$	0.165	$3.45\times10^{-1}\pm1.33\times10^{-2}$	0.165	$2.45\times10^{-1}\pm1.13\times10^{-2}$
0.325	$2.37\times10^{-1}\pm8.62\times10^{-3}$	0.244	$2.62\times10^{-1}\pm1.05\times10^{-2}$	0.195	$2.62\times10^{-1}\pm1.16\times10^{-2}$	0.195	$1.69\times10^{-1}\pm9.31\times10^{-3}$
0.375	$1.89\times10^{-1}\pm7.72\times10^{-3}$	0.281	$2.47\times10^{-1}\pm1.00\times10^{-2}$	0.225	$1.98\times10^{-1}\pm1.02\times10^{-2}$	0.225	$1.37\times10^{-1}\pm8.36\times10^{-3}$
0.425	$1.81\times10^{-1}\pm7.44\times10^{-3}$	0.319	$1.90\times10^{-1}\pm8.87\times10^{-3}$	0.255	$1.99\times10^{-1}\pm1.01\times10^{-2}$	0.255	$1.14\times10^{-1}\pm7.53\times10^{-3}$
0.475	$1.56\times10^{-1}\pm6.91\times10^{-3}$	0.356	$1.66\times10^{-1}\pm8.25\times10^{-3}$	0.285	$1.40\times10^{-1}\pm8.56\times10^{-3}$	0.285	$8.78\times10^{-2}\pm6.76\times10^{-3}$
0.525	$1.33\times10^{-1}\pm6.45\times10^{-3}$	0.394	$1.51\times10^{-1}\pm7.86\times10^{-3}$	0.315	$1.36\times10^{-1}\pm8.31\times10^{-3}$	0.315	$7.71\times10^{-2}\pm6.21\times10^{-3}$
0.575	$1.06\times10^{-1}\pm5.69\times10^{-3}$	0.431	$1.21\times10^{-1}\pm7.06\times10^{-3}$	0.345	$1.17\times10^{-1}\pm7.77\times10^{-3}$	0.345	$5.47\times10^{-2}\pm5.41\times10^{-3}$
0.625	$8.92\times10^{-2}\pm5.19\times10^{-3}$	0.469	$1.03\times10^{-1}\pm6.54\times10^{-3}$	0.375	$9.85\times10^{-2}\pm7.06\times10^{-3}$	0.375	$4.99\times10^{-2}\pm5.10\times10^{-3}$
0.675	$8.63\times10^{-2}\pm5.11\times10^{-3}$	0.506	$9.57\times10^{-2}\pm6.24\times10^{-3}$	0.405	$8.66\times10^{-2}\pm6.64\times10^{-3}$	0.405	$4.59\times10^{-2}\pm4.72\times10^{-3}$
0.725	$7.36\times10^{-2}\pm4.67\times10^{-3}$	0.544	$8.67\times10^{-2}\pm5.89\times10^{-3}$	0.435	$6.23\times10^{-2}\pm5.77\times10^{-3}$	0.435	$3.59\times10^{-2}\pm4.26\times10^{-3}$
0.775	$5.14\times10^{-2}\pm2.80\times10^{-3}$	0.581	$7.02\times10^{-2}\pm5.33\times10^{-3}$	0.465	$6.35\times10^{-2}\pm5.61\times10^{-3}$	0.465	$3.00\times10^{-2}\pm3.87\times10^{-3}$
0.825	$4.30\times10^{-2}\pm2.57\times10^{-3}$	0.619	$5.98\times10^{-2}\pm4.90\times10^{-3}$	0.495	$4.96\times10^{-2}\pm5.08\times10^{-3}$	0.495	$2.65\times10^{-2}\pm3.61\times10^{-3}$
0.875	$3.55\times10^{-2}\pm2.36\times10^{-3}$	0.656	$4.99\times10^{-2}\pm3.18\times10^{-3}$	0.525	$4.84\times10^{-2}\pm3.50\times10^{-3}$	0.525	$2.64\times10^{-2}\pm2.57\times10^{-3}$
0.925	$2.99\times10^{-2}\pm2.12\times10^{-3}$	0.694	$4.17\times10^{-2}\pm2.93\times10^{-3}$	0.555	$3.94\times10^{-2}\pm3.18\times10^{-3}$	0.555	$2.05\times10^{-2}\pm2.29\times10^{-3}$
0.975	$2.40\times10^{-2}\pm1.92\times10^{-3}$	0.731	$4.34\times10^{-2}\pm2.94\times10^{-3}$	0.585	$3.23\times10^{-2}\pm2.86\times10^{-3}$	0.585	$1.50\times10^{-2}\pm1.98\times10^{-3}$
1.025	$2.18\times10^{-2}\pm1.82\times10^{-3}$	0.769	$3.62\times10^{-2}\pm2.71\times10^{-3}$	0.615	$3.04\times10^{-2}\pm2.77\times10^{-3}$	0.615	$1.10\times10^{-2}\pm1.72\times10^{-3}$
1.075	$1.46\times10^{-2}\pm1.48\times10^{-3}$	0.806	$2.45\times10^{-2}\pm2.28\times10^{-3}$	0.645	$2.16\times10^{-2}\pm2.37\times10^{-3}$	0.645	$8.50\times10^{-3}\pm1.48\times10^{-3}$
1.125	$1.37\times10^{-2}\pm1.44\times10^{-3}$	0.844	$2.49\times10^{-2}\pm2.26\times10^{-3}$	0.675	$2.26\times10^{-2}\pm2.39\times10^{-3}$	0.675	$9.09\times10^{-3}\pm1.54\times10^{-3}$
1.175	$8.79\times10^{-3}\pm1.16\times10^{-3}$	0.881	$2.08\times10^{-2}\pm2.05\times10^{-3}$	0.705	$2.21\times10^{-2}\pm2.36\times10^{-3}$	0.705	$7.79\times10^{-3}\pm1.41\times10^{-3}$
1.225	$1.00\times10^{-2}\pm1.22\times10^{-3}$	0.919	$1.80\times10^{-2}\pm1.91\times10^{-3}$	0.735	$1.67\times10^{-2}\pm2.06\times10^{-3}$	0.735	$9.99\times10^{-3}\pm1.55\times10^{-3}$
1.275	$6.99\times10^{-3}\pm1.04\times10^{-3}$	0.956	$1.60\times10^{-2}\pm1.77\times10^{-3}$	0.765	$1.61\times10^{-2}\pm2.03\times10^{-3}$	0.765	$4.57\times10^{-3}\pm1.09\times10^{-3}$
1.325	$5.79\times10^{-3}\pm9.32\times10^{-4}$	0.994	$1.46\times10^{-2}\pm1.72\times10^{-3}$	0.795	$1.08\times10^{-2}\pm1.72\times10^{-3}$	0.795	$4.03\times10^{-3}\pm1.02\times10^{-3}$
1.375	$5.33\times10^{-3}\pm8.93\times10^{-4}$	1.031	$7.61\times10^{-3}\pm1.29\times10^{-3}$	0.825	$1.39\times10^{-2}\pm1.84\times10^{-3}$	0.825	$4.31\times10^{-3}\pm1.01\times10^{-3}$
1.425	$4.98\times10^{-3}\pm8.50\times10^{-4}$	1.069	$7.79\times10^{-3}\pm1.27\times10^{-3}$	0.855	$1.18\times10^{-2}\pm1.72\times10^{-3}$	0.855	$2.99\times10^{-3}\pm8.93\times10^{-4}$
1.475	$2.62\times10^{-3}\pm6.24\times10^{-4}$	1.106	$7.85\times10^{-3}\pm1.26\times10^{-3}$	0.885	$7.79\times10^{-3}\pm1.41\times10^{-3}$	0.885	$3.82\times10^{-3}\pm9.65\times10^{-4}$
1.525	$1.37\times10^{-3}\pm4.86\times10^{-4}$	1.144	$3.78\times10^{-3}\pm9.13\times10^{-4}$	0.915	$7.37\times10^{-3}\pm1.33\times10^{-3}$	0.915	$3.22\times10^{-3}\pm8.85\times10^{-4}$
1.575	$1.77\times10^{-3}\pm5.16\times10^{-4}$	1.181	$5.19\times10^{-3}\pm1.02\times10^{-3}$	0.945	$4.76\times10^{-3}\pm1.19\times10^{-3}$	0.945	$2.93\times10^{-3}\pm8.95\times10^{-4}$
1.625	$1.58\times10^{-3}\pm5.95\times10^{-5}$	1.219	$4.97\times10^{-3}\pm1.01\times10^{-3}$	0.975	$6.10\times10^{-3}\pm1.24\times10^{-3}$	0.975	$1.20\times10^{-3}\pm5.43\times10^{-4}$
1.675	$1.30\times10^{-3}\pm5.40\times10^{-5}$	1.256	$5.10\times10^{-3}\pm1.02\times10^{-3}$	1.005	$5.39\times10^{-3}\pm1.18\times10^{-3}$	1.005	$1.30\times10^{-3}\pm5.91\times10^{-4}$
1.725	$1.05\times10^{-3}\pm4.86\times10^{-5}$	1.294	$2.79\times10^{-3}\pm7.55\times10^{-4}$	1.035	$3.14\times10^{-3}\pm9.54\times10^{-4}$	1.035	$1.63\times10^{-3}\pm6.72\times10^{-4}$
1.775	$7.45\times10^{-4}\pm4.09\times10^{-5}$	1.331	$2.70\times10^{-3}\pm7.57\times10^{-4}$	1.065	$2.78\times10^{-3}\pm8.30\times10^{-4}$	1.065	$1.70\times10^{-3}\pm6.22\times10^{-4}$
1.825	$5.67\times10^{-4}\pm3.57\times10^{-5}$	1.369	$3.15\times10^{-3}\pm7.69\times10^{-4}$	1.095	$3.21\times10^{-3}\pm9.19\times10^{-4}$	1.095	$3.71\times10^{-4}\pm4.00\times10^{-4}$
1.875	$4.77\times10^{-4}\pm3.28\times10^{-5}$	1.406	$3.28\times10^{-3}\pm7.90\times10^{-4}$	1.125	$2.46\times10^{-3}\pm7.65\times10^{-4}$	1.125	$8.19\times10^{-4}\pm4.42\times10^{-4}$
1.925	$3.31\times10^{-4}\pm2.73\times10^{-5}$	1.444	$1.26\times10^{-3}\pm5.39\times10^{-4}$	1.155	$1.41\times10^{-3}\pm6.35\times10^{-4}$	1.155	$7.62\times10^{-4}\pm4.45\times10^{-4}$
1.975	$2.32\times10^{-4}\pm2.28\times10^{-5}$	1.481	$1.13\times10^{-3}\pm5.08\times10^{-4}$	1.185	$2.18\times10^{-3}\pm7.35\times10^{-4}$	1.185	$9.81\times10^{-4}\pm4.96\times10^{-4}$
2.025	$2.14\times10^{-4}\pm2.19\times10^{-5}$	1.519	$3.89\times10^{-4}\pm3.14\times10^{-4}$	1.215	$1.96\times10^{-3}\pm7.02\times10^{-4}$	1.215	$1.10\times10^{-3}\pm4.90\times10^{-4}$
2.075	$1.60\times10^{-4}\pm1.90\times10^{-5}$	1.556	$1.26\times10^{-3}\pm5.02\times10^{-4}$	1.245	$1.80\times10^{-3}\pm6.65\times10^{-4}$	1.245	$6.00\times10^{-4}\pm3.84\times10^{-4}$
2.125	$1.26\times10^{-4}\pm1.68\times10^{-5}$	1.594	$1.01\times10^{-3}\pm4.32\times10^{-4}$	1.275	$2.08\times10^{-3}\pm6.97\times10^{-4}$	1.275	$6.57\times10^{-4}\pm3.79\times10^{-4}$
2.175	$9.68\times10^{-5}\pm1.48\times10^{-5}$	1.631	$7.98\times10^{-4}\pm4.89\times10^{-5}$	1.305	$2.67\times10^{-4}\pm3.25\times10^{-4}$	1.305	$8.76\times10^{-4}\pm4.38\times10^{-4}$
2.225	$6.75\times10^{-5}\pm1.23\times10^{-5}$	1.669	$6.84\times10^{-4}\pm4.53\times10^{-5}$	1.335	$1.91\times10^{-3}\pm6.60\times10^{-4}$	1.335	$4.38\times10^{-4}\pm3.10\times10^{-4}$
2.275	$4.28\times10^{-5}\pm9.81\times10^{-6}$	1.706	$5.82\times10^{-4}\pm4.18\times10^{-5}$	1.365	$1.91\times10^{-3}\pm6.60\times10^{-4}$	1.365	$1.26\times10^{-3}\pm5.40\times10^{-4}$
2.325	$1.80\times10^{-5}\pm6.36\times10^{-6}$	1.744	$4.20\times10^{-4}\pm3.55\times10^{-5}$	1.395	$8.76\times10^{-4}\pm4.38\times10^{-4}$	1.395	$2.19\times10^{-4}\pm2.19\times10^{-4}$
2.375	$2.70\times10^{-5}\pm7.79\times10^{-6}$	1.781	$3.48\times10^{-4}\pm3.23\times10^{-5}$	1.425	$1.26\times10^{-3}\pm5.40\times10^{-4}$	1.605	$8.25\times10^{-5}\pm1.76\times10^{-5}$
2.425	$3.60\times10^{-5}\pm9.00\times10^{-6}$	1.819	$3.42\times10^{-4}\pm3.20\times10^{-5}$	1.455	$4.76\times10^{-5}\pm2.40\times10^{-4}$	1.635	$1.16\times10^{-4}\pm2.09\times10^{-5}$
2.475	$1.58\times10^{-5}\pm5.95\times10^{-6}$	1.856	$1.98\times10^{-4}\pm2.44\times10^{-5}$	1.485	$1.62\times10^{-4}\pm2.26\times10^{-4}$	1.665	$1.05\times10^{-4}\pm1.98\times10^{-5}$
2.525	$9.00\times10^{-6}\pm4.50\times10^{-6}$	1.894	$1.86\times10^{-4}\pm2.36\times10^{-5}$	1.515	$6.57\times10^{-4}\pm3.79\times10^{-4}$	1.695	$5.63\times10^{-5}\pm1.45\times10^{-5}$

TABLE II. (*Continued*).

			$p+\mathrm{Be}$				
E_T	$\delta\eta=1.30$	E_T	$\delta\eta=0.966$	E_T	$\delta\eta=0.624$	E_T	$\delta\eta=0.378$
2.575	$2.25\times10^{-6}\pm2.25\times10^{-6}$	1.931	$1.59\times10^{-4}\pm2.18\times10^{-5}$	1.545	$4.38\times10^{-4}\pm3.10\times10^{-4}$	1.725	$4.50\times10^{-5}\pm1.30\times10^{-5}$
2.625	$2.25\times10^{-6}\pm2.25\times10^{-6}$	1.969	$1.35\times10^{-4}\pm2.01\times10^{-5}$	1.575	$4.38\times10^{-4}\pm3.10\times10^{-4}$	1.755	$2.25\times10^{-5}\pm9.19\times10^{-6}$
2.675	$6.75\times10^{-6}\pm3.90\times10^{-6}$	2.006	$8.70\times10^{-5}\pm1.62\times10^{-5}$	1.605	$3.45\times10^{-4}\pm3.60\times10^{-5}$	1.785	$1.88\times10^{-5}\pm8.39\times10^{-6}$
2.725	$1.13\times10^{-5}\pm5.03\times10^{-6}$	2.044	$9.00\times10^{-5}\pm1.64\times10^{-5}$	1.635	$3.15\times10^{-4}\pm3.44\times10^{-5}$	1.815	$1.50\times10^{-5}\pm7.50\times10^{-6}$
2.775	$2.25\times10^{-6}\pm2.25\times10^{-6}$	2.081	$6.30\times10^{-5}\pm1.37\times10^{-5}$	1.665	$2.14\times10^{-4}\pm2.83\times10^{-5}$	1.845	$2.63\times10^{-5}\pm9.92\times10^{-6}$
2.825	$6.75\times10^{-6}\pm3.90\times10^{-6}$	2.119	$7.20\times10^{-5}\pm1.47\times10^{-5}$	1.695	$2.36\times10^{-4}\pm2.98\times10^{-5}$	1.875	$2.63\times10^{-5}\pm9.92\times10^{-6}$
2.925	$4.50\times10^{-6}\pm3.18\times10^{-6}$	2.156	$6.60\times10^{-5}\pm1.41\times10^{-5}$	1.725	$1.31\times10^{-4}\pm2.22\times10^{-5}$	1.905	$1.50\times10^{-5}\pm7.50\times10^{-6}$
		2.194	$1.80\times10^{-5}\pm7.35\times10^{-6}$	1.755	$1.58\times10^{-4}\pm2.43\times10^{-5}$	1.935	$1.88\times10^{-5}\pm8.39\times10^{-6}$
		2.231	$2.40\times10^{-5}\pm8.49\times10^{-6}$	1.785	$1.20\times10^{-4}\pm2.12\times10^{-5}$	1.965	$1.50\times10^{-5}\pm7.50\times10^{-6}$
		2.269	$2.70\times10^{-5}\pm9.00\times10^{-6}$	1.815	$7.88\times10^{-5}\pm1.72\times10^{-5}$	1.995	$3.75\times10^{-6}\pm3.75\times10^{-6}$
		2.306	$1.20\times10^{-5}\pm6.00\times10^{-6}$	1.845	$7.13\times10^{-5}\pm1.63\times10^{-5}$	2.025	$1.50\times10^{-5}\pm7.50\times10^{-6}$
		2.344	$1.50\times10^{-5}\pm6.71\times10^{-6}$	1.875	$4.13\times10^{-5}\pm1.24\times10^{-5}$	2.055	$3.75\times10^{-6}\pm3.75\times10^{-6}$
		2.381	$2.10\times10^{-5}\pm7.94\times10^{-6}$	1.905	$7.13\times10^{-5}\pm1.63\times10^{-5}$	2.085	$7.50\times10^{-6}\pm5.30\times10^{-6}$
		2.419	$1.20\times10^{-5}\pm6.00\times10^{-6}$	1.935	$7.50\times10^{-5}\pm1.68\times10^{-5}$	2.115	$3.75\times10^{-6}\pm3.75\times10^{-6}$
		2.456	$6.00\times10^{-6}\pm4.24\times10^{-6}$	1.965	$7.50\times10^{-5}\pm1.68\times10^{-5}$		
		2.494	$3.00\times10^{-6}\pm3.00\times10^{-6}$	1.995	$4.13\times10^{-5}\pm1.24\times10^{-5}$		
		2.531	$6.00\times10^{-6}\pm4.24\times10^{-6}$	2.025	$3.38\times10^{-5}\pm1.13\times10^{-5}$		
		2.569	$6.00\times10^{-6}\pm4.24\times10^{-6}$	2.055	$1.88\times10^{-5}\pm8.39\times10^{-6}$		
				2.085	$1.88\times10^{-5}\pm8.39\times10^{-6}$		
				2.115	$2.63\times10^{-5}\pm9.92\times10^{-6}$		
				2.145	$2.25\times10^{-5}\pm9.19\times10^{-6}$		
				2.175	$1.13\times10^{-5}\pm6.50\times10^{-6}$		
				2.235	$1.13\times10^{-5}\pm6.50\times10^{-6}$		
				2.265	$1.13\times10^{-5}\pm6.50\times10^{-6}$		
				2.325	$3.75\times10^{-6}\pm3.75\times10^{-6}$		
				2.355	$7.50\times10^{-6}\pm5.30\times10^{-6}$		
				2.385	$7.50\times10^{-6}\pm5.30\times10^{-6}$		

$$\sigma=\sqrt{\mu\left(1+\frac{\mu}{k}\right)},\quad \frac{\sigma^2}{\mu^2}=\frac{1}{\mu}+\frac{1}{k}. \tag{8}$$

The NBD, with an additional parameter k compared to a Poisson distribution, becomes Poisson in the limit $k\to\infty$ and binomial for k equal to a negative integer (hence the name). The negative binomial distribution bears a strong relationship to the Gamma distribution, and becomes a Gamma distribution in the limit $\mu\gg k>1$. In fact, many times, Gamma distributions are substituted for NBD to prove various theorems [55]. One important difference between between NBD and Gamma distributions is in the limit m or $x\to 0$: for $p>1$ the limit is always zero for a Gamma distribution, whereas for the NBD it is always finite.

The Gamma distribution has an important property under convolution. Define the n-fold convolution of a distribution with itself as

$$f_n(x)=\int_0^x dy\, f(y)\, f_{n-1}(x-y); \tag{9}$$

then for a Gamma distribution [Eq. (5)], the n-fold convolution is simply given by the function

$$f_n(x)=\frac{b}{\Gamma(np)}(bx)^{np-1}e^{-bx}, \tag{10}$$

i.e., $p\to np$ and b remains unchanged. Notice that the mean μ_n and standard deviation σ_n of the n-fold convolution obey the familiar rule

$$\mu_n=n\mu,\quad \sigma_n=\sigma\sqrt{n}. \tag{11}$$

The convolution property of the Gamma distribution also holds for the NBD, with $\mu\to n\mu$, $k\to nk$, so that μ/k remains constant [49].

B. Gamma distribution fits

Again referring to Figs. 7 and 8, the solid lines in Fig. 7 are fits of the E_T distributions to a single Gamma distribution [see Table X for the fitted parameters to Eq. (5)] and the solid lines in Fig. 8 are NBD fits to the multiplicity distributions. The NBD provides excellent fits to the O+Cu central multiplicity distributions [49], while the Gamma distribution provides a reasonable ($\chi^2\sim 1.5$/dof) fit to the O+Cu central E_T distributions and a fair fit ($\chi^2\sim 3-6$/dof) to the Au+Au central E_T distributions. Since the centrality trigger for the Au+Au data is relatively weak [48], corresponding to

TABLE III. $d\sigma/dE_T$ (b/GeV) versus E_T (GeV) for $p+\mathrm{Au}$ at 14.6A GeV/c for four $\delta\eta$ intervals. Errors quoted are statistical only; systematic errors are estimated to be less than $\pm3\%$ on the E_T scale.

$p+\mathrm{Au}$							
E_T	$\delta\eta=1.30$	E_T	$\delta\eta=0.966$	E_T	$\delta\eta=0.624$	E_T	$\delta\eta=0.378$
0.125	$3.28\times10^{0}\pm9.97\times10^{-2}$	0.094	$3.32\times10^{0}\pm1.13\times10^{-1}$	0.075	$3.87\times10^{0}\pm1.35\times10^{-1}$	0.075	$3.83\times10^{0}\pm1.34\times10^{-1}$
0.175	$3.29\times10^{0}\pm9.73\times10^{-2}$	0.131	$3.71\times10^{0}\pm1.20\times10^{-1}$	0.105	$4.04\times10^{0}\pm1.38\times10^{-1}$	0.105	$3.56\times10^{0}\pm1.30\times10^{-1}$
0.225	$2.95\times10^{0}\pm9.25\times10^{-2}$	0.169	$3.46\times10^{0}\pm1.15\times10^{-1}$	0.135	$3.77\times10^{0}\pm1.34\times10^{-1}$	0.135	$3.18\times10^{0}\pm1.21\times10^{-1}$
0.275	$2.45\times10^{0}\pm8.42\times10^{-2}$	0.206	$2.84\times10^{0}\pm1.05\times10^{-1}$	0.165	$3.05\times10^{0}\pm1.20\times10^{-1}$	0.165	$2.30\times10^{0}\pm1.04\times10^{-1}$
0.325	$2.37\times10^{0}\pm8.17\times10^{-2}$	0.244	$2.57\times10^{0}\pm9.86\times10^{-2}$	0.195	$2.43\times10^{0}\pm1.07\times10^{-1}$	0.195	$1.76\times10^{0}\pm8.94\times10^{-2}$
0.375	$1.96\times10^{0}\pm7.42\times10^{-2}$	0.281	$2.24\times10^{0}\pm9.09\times10^{-2}$	0.225	$2.15\times10^{0}\pm1.00\times10^{-1}$	0.225	$1.26\times10^{0}\pm7.63\times10^{-2}$
0.425	$1.68\times10^{0}\pm6.83\times10^{-2}$	0.319	$2.04\times10^{0}\pm8.65\times10^{-2}$	0.255	$1.96\times10^{0}\pm9.46\times10^{-2}$	0.255	$1.13\times10^{0}\pm7.10\times10^{-2}$
0.475	$1.43\times10^{0}\pm6.31\times10^{-2}$	0.356	$1.74\times10^{0}\pm7.96\times10^{-2}$	0.285	$1.48\times10^{0}\pm8.30\times10^{-2}$	0.285	$8.58\times10^{-1}\pm6.35\times10^{-2}$
0.525	$1.13\times10^{0}\pm5.72\times10^{-2}$	0.394	$1.34\times10^{0}\pm7.10\times10^{-2}$	0.315	$1.33\times10^{0}\pm7.80\times10^{-2}$	0.315	$7.56\times10^{-1}\pm5.82\times10^{-2}$
0.575	$1.11\times10^{0}\pm5.49\times10^{-2}$	0.431	$1.21\times10^{0}\pm6.69\times10^{-2}$	0.345	$1.06\times10^{0}\pm7.09\times10^{-2}$	0.345	$5.05\times10^{-1}\pm4.99\times10^{-2}$
0.625	$7.94\times10^{-1}\pm4.67\times10^{-2}$	0.469	$1.05\times10^{0}\pm6.26\times10^{-2}$	0.375	$9.20\times10^{-1}\pm6.49\times10^{-2}$	0.375	$4.34\times10^{-1}\pm4.57\times10^{-2}$
0.675	$7.48\times10^{-1}\pm4.55\times10^{-2}$	0.506	$8.80\times10^{-1}\pm5.71\times10^{-2}$	0.405	$7.69\times10^{-1}\pm5.98\times10^{-2}$	0.405	$4.71\times10^{-1}\pm4.50\times10^{-2}$
0.725	$5.36\times10^{-1}\pm3.87\times10^{-2}$	0.544	$7.68\times10^{-1}\pm5.29\times10^{-2}$	0.435	$6.22\times10^{-1}\pm5.47\times10^{-2}$	0.435	$2.62\times10^{-1}\pm3.55\times10^{-2}$
0.775	$5.04\times10^{-1}\pm3.71\times10^{-2}$	0.581	$6.21\times10^{-1}\pm4.79\times10^{-2}$	0.465	$5.58\times10^{-1}\pm5.02\times10^{-2}$	0.465	$3.04\times10^{-1}\pm3.68\times10^{-2}$
0.825	$3.71\times10^{-1}\pm3.22\times10^{-2}$	0.619	$5.30\times10^{-1}\pm4.41\times10^{-2}$	0.495	$4.85\times10^{-1}\pm4.77\times10^{-2}$	0.495	$1.76\times10^{-1}\pm2.87\times10^{-2}$
0.875	$3.08\times10^{-1}\pm2.91\times10^{-2}$	0.656	$4.63\times10^{-1}\pm4.15\times10^{-2}$	0.525	$4.18\times10^{-1}\pm4.37\times10^{-2}$	0.525	$1.51\times10^{-1}\pm2.68\times10^{-2}$
0.925	$2.91\times10^{-1}\pm2.81\times10^{-2}$	0.694	$3.49\times10^{-1}\pm3.65\times10^{-2}$	0.555	$3.44\times10^{-1}\pm3.92\times10^{-2}$	0.555	$1.52\times10^{-1}\pm2.60\times10^{-2}$
0.975	$2.15\times10^{-1}\pm2.44\times10^{-2}$	0.731	$3.51\times10^{-1}\pm3.56\times10^{-2}$	0.585	$2.78\times10^{-1}\pm3.63\times10^{-2}$	0.585	$1.16\times10^{-1}\pm2.30\times10^{-2}$
1.025	$1.71\times10^{-1}\pm2.00\times10^{-2}$	0.769	$3.12\times10^{-1}\pm3.34\times10^{-2}$	0.615	$2.94\times10^{-1}\pm3.76\times10^{-2}$	0.615	$1.17\times10^{-1}\pm2.30\times10^{-2}$
1.075	$1.54\times10^{-1}\pm1.85\times10^{-2}$	0.806	$2.77\times10^{-1}\pm3.13\times10^{-2}$	0.645	$2.06\times10^{-1}\pm3.06\times10^{-2}$	0.645	$1.21\times10^{-1}\pm2.33\times10^{-2}$
1.125	$1.23\times10^{-1}\pm1.68\times10^{-2}$	0.844	$2.17\times10^{-1}\pm2.82\times10^{-2}$	0.675	$1.99\times10^{-1}\pm3.02\times10^{-2}$	0.675	$8.63\times10^{-2}\pm1.93\times10^{-2}$
1.175	$9.33\times10^{-2}\pm1.45\times10^{-2}$	0.881	$1.54\times10^{-1}\pm2.40\times10^{-2}$	0.705	$1.48\times10^{-1}\pm2.54\times10^{-2}$	0.705	$8.63\times10^{-2}\pm1.93\times10^{-2}$
1.225	$7.78\times10^{-2}\pm1.33\times10^{-2}$	0.919	$1.70\times10^{-1}\pm2.52\times10^{-2}$	0.735	$2.18\times10^{-1}\pm3.03\times10^{-2}$	0.735	$7.79\times10^{-2}\pm1.74\times10^{-2}$
1.275	$6.03\times10^{-2}\pm1.20\times10^{-2}$	0.956	$1.19\times10^{-1}\pm2.12\times10^{-2}$	0.765	$1.13\times10^{-1}\pm2.36\times10^{-2}$	0.765	$5.38\times10^{-2}\pm1.42\times10^{-2}$
1.325	$6.84\times10^{-2}\pm1.22\times10^{-2}$	0.994	$1.05\times10^{-1}\pm1.94\times10^{-2}$	0.795	$1.42\times10^{-1}\pm2.47\times10^{-2}$	0.795	$7.77\times10^{-2}\pm1.66\times10^{-2}$
1.375	$4.78\times10^{-2}\pm1.04\times10^{-2}$	1.031	$1.02\times10^{-1}\pm1.95\times10^{-2}$	0.825	$9.55\times10^{-2}\pm2.20\times10^{-2}$	0.825	$5.82\times10^{-2}\pm1.41\times10^{-2}$
1.425	$2.26\times10^{-2}\pm7.37\times10^{-3}$	1.069	$7.64\times10^{-2}\pm1.76\times10^{-2}$	0.855	$1.06\times10^{-1}\pm2.16\times10^{-2}$	0.855	$4.28\times10^{-2}\pm1.26\times10^{-2}$
1.475	$3.77\times10^{-2}\pm8.94\times10^{-3}$	1.106	$8.89\times10^{-2}\pm1.75\times10^{-2}$	0.885	$4.96\times10^{-2}\pm1.70\times10^{-2}$	0.885	$4.14\times10^{-2}\pm1.22\times10^{-2}$
1.525	$2.14\times10^{-2}\pm7.09\times10^{-3}$	1.144	$6.33\times10^{-2}\pm1.53\times10^{-2}$	0.915	$6.94\times10^{-2}\pm1.79\times10^{-2}$	0.915	$3.56\times10^{-2}\pm1.13\times10^{-2}$
1.575	$1.71\times10^{-2}\pm6.20\times10^{-3}$	1.181	$3.36\times10^{-2}\pm1.29\times10^{-2}$	0.945	$4.97\times10^{-2}\pm1.44\times10^{-2}$	0.945	$2.28\times10^{-2}\pm9.89\times10^{-3}$
1.625	$1.34\times10^{-2}\pm3.86\times10^{-4}$	1.219	$4.98\times10^{-2}\pm1.23\times10^{-2}$	0.975	$4.12\times10^{-2}\pm1.49\times10^{-2}$	0.975	$2.46\times10^{-2}\pm9.18\times10^{-3}$
1.675	$1.04\times10^{-2}\pm3.39\times10^{-4}$	1.256	$2.09\times10^{-2}\pm8.79\times10^{-3}$	1.005	$4.99\times10^{-2}\pm1.39\times10^{-2}$	1.005	$1.04\times10^{-2}\pm6.58\times10^{-3}$
1.725	$8.11\times10^{-3}\pm3.00\times10^{-4}$	1.294	$2.18\times10^{-2}\pm8.29\times10^{-3}$	1.035	$2.35\times10^{-2}\pm1.05\times10^{-2}$	1.035	$9.14\times10^{-3}\pm6.64\times10^{-3}$
1.775	$5.99\times10^{-3}\pm2.58\times10^{-4}$	1.331	$4.15\times10^{-2}\pm1.11\times10^{-2}$	1.065	$5.82\times10^{-2}\pm1.41\times10^{-2}$	1.065	$2.52\times10^{-2}\pm9.15\times10^{-3}$
1.825	$4.64\times10^{-3}\pm2.27\times10^{-4}$	1.369	$2.38\times10^{-2}\pm8.23\times10^{-3}$	1.095	$3.63\times10^{-2}\pm1.18\times10^{-2}$	1.095	$9.77\times10^{-3}\pm6.61\times10^{-3}$
1.875	$3.43\times10^{-3}\pm1.95\times10^{-4}$	1.406	$3.37\times10^{-2}\pm9.73\times10^{-3}$	1.125	$1.43\times10^{-2}\pm7.30\times10^{-3}$	1.125	$9.06\times10^{-3}\pm5.63\times10^{-3}$
1.925	$2.96\times10^{-3}\pm1.81\times10^{-4}$	1.444	$1.20\times10^{-2}\pm6.47\times10^{-3}$	1.155	$1.88\times10^{-2}\pm8.68\times10^{-3}$	1.155	$1.97\times10^{-3}\pm3.35\times10^{-3}$
1.975	$2.53\times10^{-3}\pm1.67\times10^{-4}$	1.481	$2.28\times10^{-2}\pm8.26\times10^{-3}$	1.185	$1.69\times10^{-2}\pm8.01\times10^{-3}$	1.185	$8.43\times10^{-3}\pm5.66\times10^{-3}$
2.025	$1.75\times10^{-3}\pm1.39\times10^{-4}$	1.519	$1.14\times10^{-2}\pm5.84\times10^{-3}$	1.215	$1.04\times10^{-2}\pm6.58\times10^{-3}$	1.215	$3.23\times10^{-3}\pm3.23\times10^{-3}$
2.075	$1.22\times10^{-3}\pm1.16\times10^{-4}$	1.556	$3.66\times10^{-3}\pm3.75\times10^{-3}$	1.245	$7.80\times10^{-3}\pm5.70\times10^{-3}$	1.245	$5.83\times10^{-3}\pm4.61\times10^{-3}$
2.125	$8.65\times10^{-4}\pm9.80\times10^{-5}$	1.594	$7.25\times10^{-3}\pm4.50\times10^{-3}$	1.275	$1.17\times10^{-2}\pm6.52\times10^{-3}$	1.275	$3.23\times10^{-3}\pm3.23\times10^{-3}$
2.175	$7.43\times10^{-4}\pm9.08\times10^{-5}$	1.631	$6.77\times10^{-3}\pm3.17\times10^{-4}$	1.305	$1.43\times10^{-2}\pm7.30\times10^{-3}$	1.605	$5.73\times10^{-4}\pm1.03\times10^{-4}$
2.225	$5.55\times10^{-4}\pm7.84\times10^{-5}$	1.669	$5.49\times10^{-3}\pm2.85\times10^{-4}$	1.335	$2.60\times10^{-3}\pm3.29\times10^{-3}$	1.635	$6.66\times10^{-4}\pm1.11\times10^{-4}$
2.275	$3.44\times10^{-4}\pm6.18\times10^{-5}$	1.706	$4.47\times10^{-3}\pm2.57\times10^{-4}$	1.365	$9.06\times10^{-3}\pm5.63\times10^{-3}$	1.665	$4.07\times10^{-4}\pm8.67\times10^{-5}$
2.325	$3.00\times10^{-4}\pm5.76\times10^{-5}$	1.744	$3.37\times10^{-3}\pm2.23\times10^{-4}$	1.395	$9.69\times10^{-3}\pm5.59\times10^{-3}$	1.695	$3.14\times10^{-4}\pm7.62\times10^{-5}$
2.375	$2.66\times10^{-4}\pm5.43\times10^{-5}$	1.781	$3.02\times10^{-3}\pm2.11\times10^{-4}$	1.605	$2.42\times10^{-3}\pm2.12\times10^{-4}$	1.725	$4.25\times10^{-4}\pm8.87\times10^{-5}$
2.425	$2.22\times10^{-4}\pm4.96\times10^{-5}$	1.819	$2.20\times10^{-3}\pm1.81\times10^{-4}$	1.635	$1.61\times10^{-3}\pm1.72\times10^{-4}$	1.755	$3.70\times10^{-4}\pm8.27\times10^{-5}$
2.475	$1.11\times10^{-4}\pm3.51\times10^{-5}$	1.856	$1.94\times10^{-3}\pm1.69\times10^{-4}$	1.665	$1.98\times10^{-3}\pm1.91\times10^{-4}$	1.785	$2.22\times10^{-4}\pm6.40\times10^{-5}$

TABLE III. (*Continued*).

			$p+\mathrm{Au}$				
E_T	$\delta\eta=1.30$	E_T	$\delta\eta=0.966$	E_T	$\delta\eta=0.624$	E_T	$\delta\eta=0.378$
		1.894	$1.60\times10^{-3}\pm1.54\times10^{-4}$	1.695	$1.20\times10^{-3}\pm1.49\times10^{-4}$	1.815	$2.40\times10^{-4}\pm6.67\times10^{-5}$
		1.931	$1.38\times10^{-3}\pm1.43\times10^{-4}$	1.725	$1.24\times10^{-3}\pm1.51\times10^{-4}$	1.845	$1.66\times10^{-4}\pm5.55\times10^{-5}$
		1.969	$1.21\times10^{-3}\pm1.34\times10^{-4}$	1.755	$1.09\times10^{-3}\pm1.42\times10^{-4}$	1.875	$2.59\times10^{-4}\pm6.92\times10^{-5}$
		2.006	$7.84\times10^{-4}\pm1.08\times10^{-4}$	1.785	$8.32\times10^{-4}\pm1.24\times10^{-4}$	1.905	$2.59\times10^{-4}\pm6.92\times10^{-5}$
		2.044	$6.06\times10^{-4}\pm9.47\times10^{-5}$	1.815	$7.40\times10^{-4}\pm1.17\times10^{-4}$	1.935	$9.24\times10^{-5}\pm4.13\times10^{-5}$
		2.081	$6.21\times10^{-4}\pm9.59\times10^{-5}$	1.845	$6.10\times10^{-4}\pm1.06\times10^{-4}$	1.965	$5.55\times10^{-5}\pm3.20\times10^{-5}$
		2.119	$3.99\times10^{-4}\pm7.69\times10^{-5}$	1.875	$7.40\times10^{-4}\pm1.17\times10^{-4}$	1.995	$7.40\times10^{-5}\pm3.70\times10^{-5}$
		2.156	$3.25\times10^{-4}\pm6.94\times10^{-5}$	1.905	$6.10\times10^{-4}\pm1.06\times10^{-4}$		
		2.194	$3.99\times10^{-4}\pm7.69\times10^{-5}$	1.935	$5.55\times10^{-4}\pm1.01\times10^{-4}$		
		2.231	$2.96\times10^{-4}\pm6.61\times10^{-5}$	1.965	$2.96\times10^{-4}\pm7.40\times10^{-5}$		
		2.269	$2.51\times10^{-4}\pm6.10\times10^{-5}$	1.995	$3.88\times10^{-4}\pm8.47\times10^{-5}$		
		2.306	$1.33\times10^{-4}\pm4.44\times10^{-5}$	2.025	$2.59\times10^{-4}\pm6.92\times10^{-5}$		
		2.344	$1.92\times10^{-4}\pm5.33\times10^{-5}$	2.055	$2.22\times10^{-4}\pm6.40\times10^{-5}$		
		2.381	$4.44\times10^{-5}\pm2.56\times10^{-5}$	2.085	$2.59\times10^{-4}\pm6.92\times10^{-5}$		
		2.419	$1.48\times10^{-4}\pm4.68\times10^{-5}$	2.115	$1.66\times10^{-4}\pm5.55\times10^{-5}$		
		2.456	$7.40\times10^{-5}\pm3.31\times10^{-5}$	2.145	$9.24\times10^{-5}\pm4.13\times10^{-5}$		
		2.494	$8.87\times10^{-5}\pm3.62\times10^{-5}$	2.175	$1.11\times10^{-4}\pm4.53\times10^{-5}$		
		2.531	$4.44\times10^{-5}\pm2.56\times10^{-5}$	2.205	$1.11\times10^{-4}\pm4.53\times10^{-5}$		
		2.569	$2.96\times10^{-5}\pm2.09\times10^{-5}$	2.235	$5.55\times10^{-5}\pm3.20\times10^{-5}$		
				2.265	$5.55\times10^{-5}\pm3.20\times10^{-5}$		
				2.295	$3.70\times10^{-5}\pm2.61\times10^{-5}$		
				2.325	$5.55\times10^{-5}\pm3.20\times10^{-5}$		
				2.385	$5.55\times10^{-5}\pm3.20\times10^{-5}$		
				2.445	$3.70\times10^{-5}\pm2.61\times10^{-5}$		
				2.475	$3.70\times10^{-5}\pm2.61\times10^{-5}$		

a range of from 0 to 40 projectile spectators, it is perhaps not surprising that the lower edges of the data do not follow a simple Gamma distribution, thus causing the relatively poor quality of the fits.

The $p(\delta\eta)$ parameters from the fits to the $p+\mathrm{Au}$ (Fig. 5), O+Cu central and Au+Au central E_T distributions (Fig. 7) are shown as filled circles on Fig. 9 and vary systematically with $\delta\eta$, similarly to the $k(\delta\eta)$ from multiplicity distributions [49]. However, in contrast to the situation for multiplicity distributions, where the shape as characterized by the NBD parameter $k(\delta\eta)$ can be related to the two-particle short-range correlation length [56–58], there is at present no

TABLE IV. Parameters from Gamma distribution fits to $p+\mathrm{Au}$ and $p+\mathrm{Be}$ data. Errors quoted are statistical only. The fit parameters are σ, p, and b. The $\langle E_T\rangle = p/b$ on each interval is computed from the fitted parameters of the distribution. The probability p_0 for a $p+\mathrm{Au}$ ($p+$ Be) reaction to produce zero signal on the interval $\delta\eta$ is computed by taking $1-p_0$ as the ratio of σ, the observed cross section on the interval, to the inelastic $p+\mathrm{Au}$ ($p+\mathrm{Be}$) cross section of 1.662 (0.176) barn from the nuclear geometry calculation [14,64].

		Gamma fit parameters			
$\delta\eta$	σ (b)	$\langle E_T\rangle$ (GeV)	p	b (GeV^{-1})	1-p_0
		$p+\mathrm{Au}$			
1.30	1.52 ± 0.02	0.353 ± 0.007	1.78 ± 0.03	5.06 ± 0.04	0.917 ± 0.011
0.966	1.40 ± 0.02	0.286 ± 0.006	1.43 ± 0.03	5.00 ± 0.04	0.844 ± 0.011
0.624	1.29 ± 0.02	0.197 ± 0.006	0.98 ± 0.03	4.96 ± 0.05	0.774 ± 0.014
0.378	1.29 ± 0.06	0.119 ± 0.007	0.60 ± 0.04	5.00 ± 0.09	0.774 ± 0.034
		$p+\mathrm{Be}$			
1.30	0.161 ± 0.002	0.360 ± 0.006	1.82 ± 0.03	5.05 ± 0.04	0.915 ± 0.011
0.966	0.147 ± 0.002	0.286 ± 0.006	1.39 ± 0.03	4.87 ± 0.04	0.838 ± 0.011
0.624	0.131 ± 0.002	0.204 ± 0.006	0.99 ± 0.03	4.87 ± 0.06	0.742 ± 0.013
0.378	0.130 ± 0.006	0.125 ± 0.008	0.63 ± 0.04	5.00 ± 0.10	0.739 ± 0.032

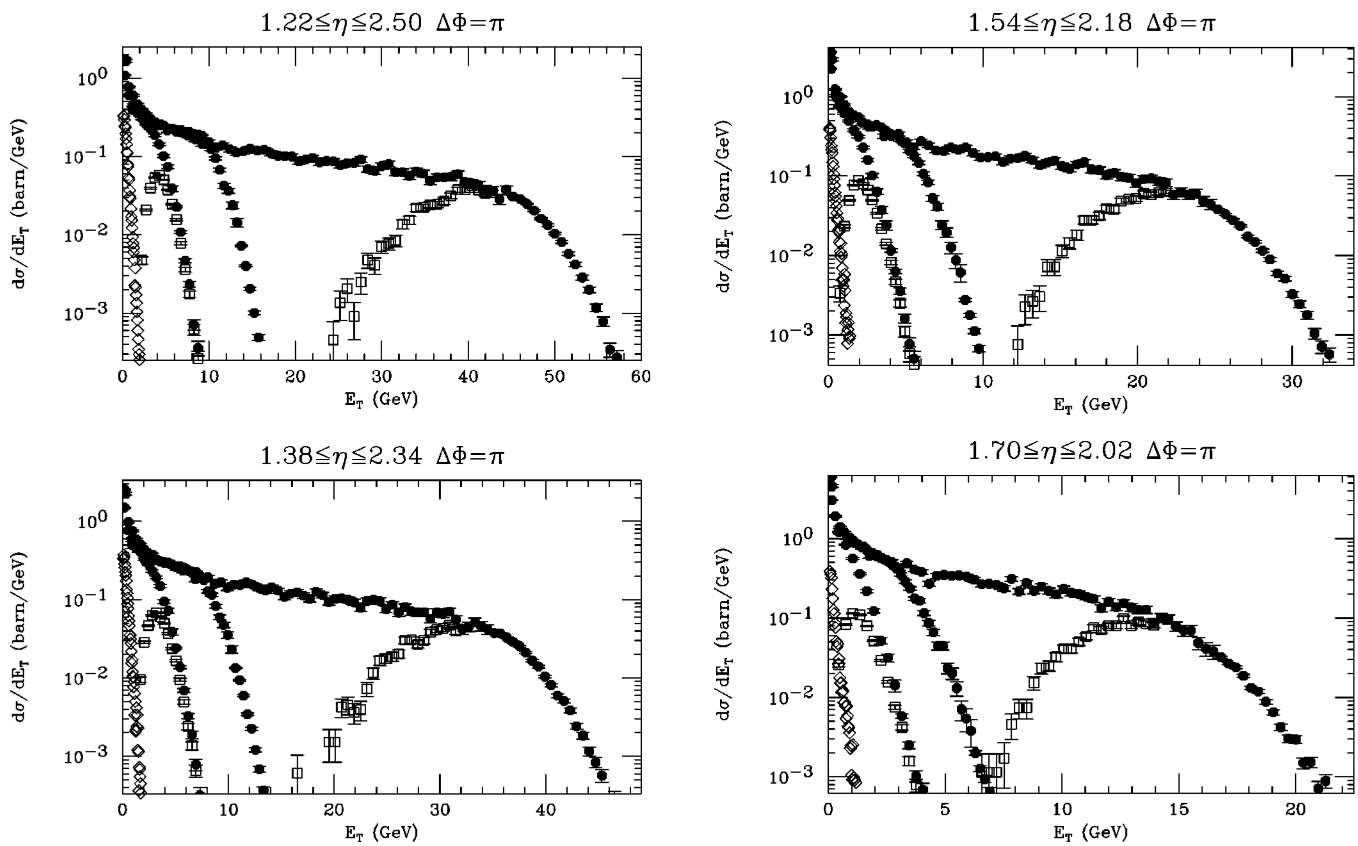

FIG. 6. E_T ($\Delta\phi=\pi$) distributions for the four $\delta\eta$ intervals indicated for $p+$Au (open diamonds) and (filled points) for the reactions (in order of increasing maximum E_T) O+Cu, Si+Au at 14.6A GeV/c and Au+Au, at 11.6A GeV/c. The open squares on the O+Cu and Au+Au distributions represent the centrally triggered O+Cu (ZCAL) and Au+Au (ZCAL) data. The $p+$Au cross section is multiplied by 0.10 for clarity of presentation. The plotting ranges in E_T for each $\delta\eta$ interval are chosen by eye so that the Au+Au distribution is near full scale on all plots.

theoretical framework to relate the systematic variation in the Gamma-distribution parameter $p(\delta\eta)$ to other physical quantities. On the other hand, Gamma distribution fits to the ^{16}O+Cu multiplicity distributions [49] (open diamonds on Fig. 9) give $p(\delta\eta)$ in excellent agreement with the E_T results.

C. Is E_T or multiplicity primary?

An interesting issue is whether E_T production is primary, followed by fragmentation to particles, or whether E_T is composed of the random product of the particle multiplicity and p_T distributions [59–61]. If E_T production were the result of the creation of particles according to the semi-inclusive multiplicity distribution followed by the random assignment of transverse momentum to each particle according to the single-particle semi-inclusive p_T distribution [59–61], the process would be described by the equation

$$\frac{d\sigma}{dE_T}=\sigma\sum_{n=1}^{n_{\max}} f_{\mathrm{NBD}}(n,1/k,\mu)\, f_{\Gamma}(E_T,np,b), \tag{12}$$

where the multiplicity distribution for O+Cu central collisions is represented by a NBD [49], $f_{\mathrm{NBD}}(n,1/k,\mu)$, the E_T distribution for n particles is represented by the Gamma distribution, $f_{\Gamma}(E_T,np,b)$, where p and b are the parameters of the E_T distribution for a single particle [48]; and it is assumed that the E_T spectra for individual particles are independent of each other and independent of the multiplicity n so that the E_T spectrum for n particles is the nth convolution of the spectrum for a single particle [Eq. (10)]. Satisfactory convergence of fits to Eq. (12) could not be obtained, so the NBD was restricted to be Poisson, by fixing $1/k=0$, which led to convergence. These fits are shown as dots on Fig. 7. A simpler fit based on Eq. (2) was also tried that assumed a simple proportionality between E_T and n, so that the number of particles n for a given E_T was taken as $n=E_T/\langle p_T\rangle$ (nearest integer) and fit to a NBD

$$\frac{d\sigma}{dE_T}=\sigma\, f_{\mathrm{NBD}}(E_T/\langle p_T\rangle,1/k,\mu). \tag{13}$$

These fits are shown as dashed lines on Fig. 7. Neither of the more complicated forms fit the central collision data as well as a single-Gamma distribution. The tendency is for the NBD based fits to be lower than the single-Gamma distribution fits at the higher values of E_T and higher than the

TABLE V. $d\sigma/dE_T$ (b/GeV) versus E_T (GeV) for O+Cu at 14.6A GeV/c for four $\delta\eta$ intervals. Errors quoted are statistical only; systematic errors are estimated to be less than ±3% on the E_T scale.

O+Cu							
E_T	$\delta\eta$=1.30	E_T	$\delta\eta$=0.966	E_T	$\delta\eta$=0.624	E_T	$\delta\eta$=0.378
0.25	$1.08\times10^{0}\pm2.04\times10^{-2}$	0.19	$1.49\times10^{0}\pm2.76\times10^{-2}$	0.15	$2.23\times10^{0}\pm3.70\times10^{-2}$	0.15	$3.05\times10^{0}\pm4.21\times10^{-2}$
0.75	$6.06\times10^{-1}\pm1.36\times10^{-2}$	0.56	$7.67\times10^{-1}\pm1.77\times10^{-2}$	0.45	$1.03\times10^{0}\pm2.25\times10^{-2}$	0.45	$1.22\times10^{0}\pm2.38\times10^{-2}$
1.25	$4.59\times10^{-1}\pm1.15\times10^{-2}$	0.94	$6.02\times10^{-1}\pm1.52\times10^{-2}$	0.75	$7.53\times10^{-1}\pm1.87\times10^{-2}$	0.75	$8.31\times10^{-1}\pm1.91\times10^{-2}$
1.75	$3.58\times10^{-1}\pm9.97\times10^{-3}$	1.31	$4.55\times10^{-1}\pm1.30\times10^{-2}$	1.05	$6.17\times10^{-1}\pm1.67\times10^{-2}$	1.05	$5.60\times10^{-1}\pm1.55\times10^{-2}$
2.25	$3.05\times10^{-1}\pm9.03\times10^{-3}$	1.69	$4.11\times10^{-1}\pm1.21\times10^{-2}$	1.35	$4.95\times10^{-1}\pm1.47\times10^{-2}$	1.35	$3.59\times10^{-1}\pm1.23\times10^{-2}$
2.75	$2.58\times10^{-1}\pm8.11\times10^{-3}$	2.06	$3.28\times10^{-1}\pm1.07\times10^{-2}$	1.65	$3.81\times10^{-1}\pm1.28\times10^{-2}$	1.65	$2.17\times10^{-1}\pm9.52\times10^{-3}$
3.25	$2.27\times10^{-1}\pm7.55\times10^{-3}$	2.44	$2.87\times10^{-1}\pm9.81\times10^{-3}$	1.95	$3.14\times10^{-1}\pm1.15\times10^{-2}$	1.95	$1.23\times10^{-1}\pm7.09\times10^{-3}$
3.75	$1.87\times10^{-1}\pm6.82\times10^{-3}$	2.81	$2.31\times10^{-1}\pm8.78\times10^{-3}$	2.25	$2.29\times10^{-1}\pm9.69\times10^{-3}$	2.25	$5.17\times10^{-2}\pm4.63\times10^{-3}$
4.25	$1.43\times10^{-1}\pm5.92\times10^{-3}$	3.19	$1.94\times10^{-1}\pm8.01\times10^{-3}$	2.55	$1.60\times10^{-1}\pm8.10\times10^{-3}$	2.55	$3.14\times10^{-2}\pm3.63\times10^{-3}$
4.75	$1.02\times10^{-1}\pm5.00\times10^{-3}$	3.56	$1.49\times10^{-1}\pm6.98\times10^{-3}$	2.85	$1.01\times10^{-1}\pm6.49\times10^{-3}$	2.85	$1.41\times10^{-2}\pm2.39\times10^{-3}$
5.25	$7.37\times10^{-2}\pm4.23\times10^{-3}$	3.94	$9.48\times10^{-2}\pm5.58\times10^{-3}$	3.15	$6.38\times10^{-2}\pm5.09\times10^{-3}$	3.15	$5.81\times10^{-3}\pm3.96\times10^{-4}$
5.75	$3.89\times10^{-2}\pm3.06\times10^{-3}$	4.31	$7.23\times10^{-2}\pm4.82\times10^{-3}$	3.45	$3.75\times10^{-2}\pm3.91\times10^{-3}$	3.45	$2.51\times10^{-3}\pm2.59\times10^{-4}$
6.25	$2.27\times10^{-2}\pm6.03\times10^{-4}$	4.69	$3.87\times10^{-2}\pm3.54\times10^{-3}$	3.75	$2.41\times10^{-2}\pm3.11\times10^{-3}$	3.75	$1.03\times10^{-3}\pm1.69\times10^{-4}$
6.75	$1.08\times10^{-2}\pm4.16\times10^{-4}$	5.06	$2.41\times10^{-2}\pm7.19\times10^{-4}$	4.05	$1.16\times10^{-2}\pm5.56\times10^{-4}$	4.05	$6.89\times10^{-4}\pm1.35\times10^{-4}$
7.25	$4.69\times10^{-3}\pm2.74\times10^{-4}$	5.44	$1.38\times10^{-2}\pm5.42\times10^{-4}$	4.35	$6.30\times10^{-3}\pm4.10\times10^{-4}$	4.35	$2.39\times10^{-4}\pm7.95\times10^{-5}$
7.75	$2.35\times10^{-3}\pm1.94\times10^{-4}$	5.81	$6.92\times10^{-3}\pm3.84\times10^{-4}$	4.65	$3.57\times10^{-3}\pm3.10\times10^{-4}$	4.65	$2.65\times10^{-5}\pm2.65\times10^{-5}$
8.25	$7.16\times10^{-4}\pm1.07\times10^{-4}$	6.19	$3.26\times10^{-3}\pm2.63\times10^{-4}$	4.95	$1.62\times10^{-3}\pm2.07\times10^{-4}$	4.95	$2.65\times10^{-5}\pm2.65\times10^{-5}$
8.75	$3.59\times10^{-4}\pm7.66\times10^{-5}$	6.56	$1.88\times10^{-3}\pm2.00\times10^{-4}$	5.25	$7.69\times10^{-4}\pm1.43\times10^{-4}$	5.25	$2.65\times10^{-5}\pm2.65\times10^{-5}$
9.25	$6.36\times10^{-5}\pm3.18\times10^{-5}$	6.94	$7.85\times10^{-4}\pm1.29\times10^{-4}$	5.55	$5.04\times10^{-4}\pm1.16\times10^{-4}$		
9.75	$3.18\times10^{-5}\pm2.25\times10^{-5}$	7.31	$3.18\times10^{-4}\pm8.21\times10^{-5}$	5.85	$6.81\times10^{-5}\pm4.73\times10^{-5}$		
10.25	$1.59\times10^{-5}\pm1.59\times10^{-5}$	7.69	$9.69\times10^{-5}\pm4.83\times10^{-5}$	6.15	$9.46\times10^{-5}\pm5.42\times10^{-5}$		
		8.06	$4.24\times10^{-5}\pm3.00\times10^{-5}$	6.45	$2.65\times10^{-5}\pm2.65\times10^{-5}$		

TABLE VI. $d\sigma/dE_T$ (b/GeV) versus E_T (GeV) for O+Cu (ZCAL) at 14.6A GeV/c for four $\delta\eta$ intervals. Errors quoted are statistical only; systematic errors are estimated to be less than ±3% on the E_T scale.

O+Cu (ZCAL)							
E_T	$\delta\eta$=1.30	E_T	$\delta\eta$=0.966	E_T	$\delta\eta$=0.624	E_T	$\delta\eta$=0.378
2.25	$4.72\times10^{-3}\pm5.22\times10^{-4}$	1.69	$9.52\times10^{-3}\pm7.18\times10^{-4}$	0.75	$3.37\times10^{-3}\pm7.72\times10^{-4}$	0.45	$2.55\times10^{-2}\pm1.21\times10^{-3}$
2.75	$2.07\times10^{-2}\pm7.02\times10^{-4}$	2.06	$2.86\times10^{-2}\pm9.38\times10^{-4}$	1.05	$2.33\times10^{-2}\pm1.06\times10^{-3}$	0.75	$8.26\times10^{-2}\pm1.69\times10^{-3}$
3.25	$3.94\times10^{-2}\pm8.68\times10^{-4}$	2.44	$4.67\times10^{-2}\pm1.09\times10^{-3}$	1.35	$4.90\times10^{-2}\pm1.33\times10^{-3}$	1.05	$1.14\times10^{-1}\pm1.86\times10^{-3}$
3.75	$5.38\times10^{-2}\pm9.66\times10^{-4}$	2.81	$6.31\times10^{-2}\pm1.22\times10^{-3}$	1.65	$7.69\times10^{-2}\pm1.54\times10^{-3}$	1.35	$1.09\times10^{-1}\pm1.77\times10^{-3}$
4.25	$5.76\times10^{-2}\pm9.82\times10^{-4}$	3.19	$6.80\times10^{-2}\pm1.24\times10^{-3}$	1.95	$8.74\times10^{-2}\pm1.59\times10^{-3}$	1.65	$7.89\times10^{-2}\pm1.49\times10^{-3}$
4.75	$5.04\times10^{-2}\pm9.09\times10^{-4}$	3.56	$6.03\times10^{-2}\pm1.16\times10^{-3}$	2.25	$8.02\times10^{-2}\pm1.50\times10^{-3}$	1.95	$5.17\times10^{-2}\pm1.20\times10^{-3}$
5.25	$3.75\times10^{-2}\pm7.79\times10^{-4}$	3.94	$4.97\times10^{-2}\pm1.04\times10^{-3}$	2.55	$6.72\times10^{-2}\pm1.37\times10^{-3}$	2.25	$2.92\times10^{-2}\pm8.97\times10^{-4}$
5.75	$2.47\times10^{-2}\pm6.31\times10^{-4}$	4.31	$3.70\times10^{-2}\pm8.95\times10^{-4}$	2.85	$4.98\times10^{-2}\pm1.17\times10^{-3}$	2.55	$1.57\times10^{-2}\pm6.58\times10^{-4}$
6.25	$1.56\times10^{-2}\pm5.02\times10^{-4}$	4.69	$2.36\times10^{-2}\pm7.15\times10^{-4}$	3.15	$3.40\times10^{-2}\pm9.65\times10^{-4}$	2.85	$7.55\times10^{-3}\pm4.55\times10^{-4}$
6.75	$7.77\times10^{-3}\pm3.52\times10^{-4}$	5.06	$1.66\times10^{-2}\pm5.98\times10^{-4}$	3.45	$2.17\times10^{-2}\pm7.67\times10^{-4}$	3.15	$4.20\times10^{-3}\pm3.39\times10^{-4}$
7.25	$3.59\times10^{-3}\pm2.40\times10^{-4}$	5.44	$9.48\times10^{-3}\pm4.50\times10^{-4}$	3.75	$1.41\times10^{-2}\pm6.16\times10^{-4}$	3.45	$1.58\times10^{-3}\pm2.06\times10^{-4}$
7.75	$1.75\times10^{-3}\pm1.68\times10^{-4}$	5.81	$4.94\times10^{-3}\pm3.25\times10^{-4}$	4.05	$8.19\times10^{-3}\pm4.68\times10^{-4}$	3.75	$7.88\times10^{-4}\pm1.49\times10^{-4}$
8.25	$6.20\times10^{-4}\pm9.93\times10^{-5}$	6.19	$2.41\times10^{-3}\pm2.27\times10^{-4}$	4.35	$4.68\times10^{-3}\pm3.54\times10^{-4}$	4.05	$4.77\times10^{-4}\pm1.12\times10^{-4}$
8.75	$2.64\times10^{-4}\pm6.59\times10^{-5}$	6.56	$1.37\times10^{-3}\pm1.71\times10^{-4}$	4.65	$2.51\times10^{-3}\pm2.60\times10^{-4}$	4.35	$2.12\times10^{-4}\pm7.50\times10^{-5}$
9.25	$4.77\times10^{-5}\pm2.75\times10^{-5}$	6.94	$6.57\times10^{-4}\pm1.18\times10^{-4}$	4.95	$1.11\times10^{-3}\pm1.72\times10^{-4}$	4.65	$3.33\times10^{-8}\pm2.33\times10^{-5}$
9.75	$3.18\times10^{-5}\pm2.25\times10^{-5}$	7.31	$1.91\times10^{-4}\pm6.36\times10^{-5}$	5.25	$5.83\times10^{-4}\pm1.24\times10^{-4}$	4.95	$2.65\times10^{-5}\pm2.65\times10^{-5}$
10.25	$1.59\times10^{-5}\pm1.59\times10^{-5}$	7.69	$9.69\times10^{-5}\pm4.83\times10^{-5}$	5.55	$4.24\times10^{-4}\pm1.06\times10^{-4}$		
		8.06	$2.12\times10^{-5}\pm2.12\times10^{-5}$	5.85	$4.16\times10^{-5}\pm3.92\times10^{-5}$		
				6.15	$6.81\times10^{-5}\pm4.73\times10^{-5}$		
				6.45	$2.65\times10^{-5}\pm2.65\times10^{-5}$		

TABLE VII. $d\sigma/dE_T$ (b/GeV) versus E_T (GeV) for Si+Au at 14.6A GeV/c for four $\delta\eta$ intervals. Errors quoted are statistical only; systematic errors are estimated to be less than $\pm$3% on the E_T scale.

			Si+Au				
E_T	$\delta\eta$=1.30	E_T	$\delta\eta$=0.966	E_T	$\delta\eta$=0.624	E_T	$\delta\eta$=0.378
0.25	$1.78\times10^{0}\pm4.2310\times^{-2}$	0.19	$2.54\times10^{0}\pm5.72\times10^{-2}$	0.15	$3.63\times10^{0}\pm7.33\times10^{-2}$	0.10	$5.91\times10^{0}\pm1.12\times10^{-1}$
0.75	$7.71\times10^{-1}\pm1.76\times10^{-2}$	0.56	$9.81\times10^{-1}\pm2.26\times10^{-2}$	0.45	$1.24\times10^{0}\pm2.86\times10^{-2}$	0.30	$1.90\times10^{0}\pm4.28\times10^{-2}$
1.25	$6.03\times10^{-1}\pm1.49\times10^{-2}$	0.94	$7.55\times10^{-1}\pm1.92\times10^{-2}$	0.75	$9.95\times10^{-1}\pm2.45\times10^{-2}$	0.50	$1.39\times10^{0}\pm3.58\times10^{-2}$
1.75	$4.61\times10^{-1}\pm1.27\times10^{-2}$	1.31	$5.88\times10^{-1}\pm1.70\times10^{-2}$	1.05	$7.90\times10^{-1}\pm2.15\times10^{-2}$	0.70	$1.20\times10^{0}\pm3.18\times10^{-2}$
2.25	$3.93\times10^{-1}\pm1.19\times10^{-2}$	1.69	$5.05\times10^{-1}\pm1.54\times10^{-2}$	1.35	$6.42\times10^{-1}\pm1.90\times10^{-2}$	0.90	$1.04\times10^{0}\pm2.84\times10^{-2}$
2.75	$3.46\times10^{-1}\pm1.07\times10^{-2}$	2.06	$4.37\times10^{-1}\pm1.40\times10^{-2}$	1.65	$5.84\times10^{-1}\pm1.72\times10^{-2}$	1.10	$9.16\times10^{-1}\pm2.59\times10^{-2}$
3.25	$3.03\times10^{-1}\pm9.67\times10^{-3}$	2.44	$3.93\times10^{-1}\pm1.28\times10^{-2}$	1.95	$5.52\times10^{-1}\pm1.58\times10^{-2}$	1.30	$8.42\times10^{-1}\pm2.36\times10^{-2}$
3.75	$2.74\times10^{-1}\pm9.03\times10^{-3}$	2.81	$3.78\times10^{-1}\pm1.19\times10^{-2}$	2.25	$4.77\times10^{-1}\pm1.45\times10^{-2}$	1.50	$7.98\times10^{-1}\pm2.21\times10^{-2}$
4.25	$2.50\times10^{-1}\pm8.24\times10^{-3}$	3.19	$3.20\times10^{-1}\pm1.09\times10^{-2}$	2.55	$4.49\times10^{-1}\pm1.36\times10^{-2}$	1.70	$6.98\times10^{-1}\pm2.08\times10^{-2}$
4.75	$2.49\times10^{-1}\pm7.93\times10^{-3}$	3.56	$3.09\times10^{-1}\pm1.02\times10^{-2}$	2.85	$4.22\times10^{-1}\pm1.30\times10^{-2}$	1.90	$6.59\times10^{-1}\pm1.97\times10^{-2}$
5.25	$2.27\times10^{-1}\pm7.35\times10^{-3}$	3.94	$2.96\times10^{-1}\pm9.76\times10^{-3}$	3.15	$4.29\times10^{-1}\pm1.27\times10^{-2}$	2.10	$6.22\times10^{-1}\pm1.91\times10^{-2}$
5.75	$2.25\times10^{-1}\pm7.11\times10^{-3}$	4.31	$2.98\times10^{-1}\pm9.59\times10^{-3}$	3.45	$4.11\times10^{-1}\pm1.24\times10^{-2}$	2.30	$5.68\times10^{-1}\pm1.79\times10^{-2}$
6.25	$2.06\times10^{-1}\pm6.81\times10^{-3}$	4.69	$2.80\times10^{-1}\pm9.15\times10^{-3}$	3.75	$3.71\times10^{-1}\pm1.17\times10^{-2}$	2.50	$5.37\times10^{-1}\pm1.72\times10^{-2}$
6.75	$2.19\times10^{-1}\pm6.94\times10^{-3}$	5.06	$2.59\times10^{-1}\pm8.79\times10^{-3}$	4.05	$3.32\times10^{-1}\pm1.10\times10^{-2}$	2.70	$4.79\times10^{-1}\pm1.62\times10^{-2}$
7.25	$2.07\times10^{-1}\pm6.71\times10^{-3}$	5.44	$2.68\times10^{-1}\pm8.88\times10^{-3}$	4.35	$3.28\times10^{-1}\pm1.09\times10^{-2}$	2.90	$4.28\times10^{-1}\pm1.53\times10^{-2}$
7.75	$2.05\times10^{-1}\pm6.67\times10^{-3}$	5.81	$2.58\times10^{-1}\pm8.68\times10^{-3}$	4.65	$2.86\times10^{-1}\pm1.02\times10^{-2}$	3.10	$3.53\times10^{-1}\pm1.39\times10^{-2}$
8.25	$1.94\times10^{-1}\pm6.50\times10^{-3}$	6.19	$2.38\times10^{-1}\pm8.30\times10^{-3}$	4.95	$2.57\times10^{-1}\pm9.64\times10^{-3}$	3.30	$2.87\times10^{-1}\pm1.25\times10^{-2}$
8.75	$1.93\times10^{-1}\pm6.48\times10^{-3}$	6.56	$2.29\times10^{-1}\pm8.14\times10^{-3}$	5.25	$2.07\times10^{-1}\pm8.66\times10^{-3}$	3.50	$2.36\times10^{-1}\pm1.13\times10^{-2}$
9.25	$1.81\times10^{-1}\pm6.28\times10^{-3}$	6.94	$2.25\times10^{-1}\pm8.07\times10^{-3}$	5.55	$1.79\times10^{-1}\pm8.05\times10^{-3}$	3.70	$1.75\times10^{-1}\pm9.75\times10^{-3}$
9.75	$1.48\times10^{-1}\pm5.68\times10^{-3}$	7.31	$2.01\times10^{-1}\pm7.64\times10^{-3}$	5.85	$1.47\times10^{-1}\pm7.30\times10^{-3}$	3.90	$1.65\times10^{-1}\pm9.50\times10^{-3}$
10.25	$1.24\times10^{-1}\pm5.19\times10^{-3}$	7.69	$1.77\times10^{-1}\pm7.17\times10^{-3}$	6.15	$1.07\times10^{-1}\pm6.21\times10^{-3}$	4.10	$1.15\times10^{-1}\pm7.90\times10^{-3}$
10.75	$9.47\times10^{-2}\pm4.53\times10^{-3}$	8.06	$1.28\times10^{-1}\pm6.08\times10^{-3}$	6.45	$8.39\times10^{-2}\pm5.51\times10^{-3}$	4.30	$8.63\times10^{-2}\pm6.84\times10^{-3}$
11.25	$6.75\times10^{-2}\pm3.83\times10^{-3}$	8.44	$1.15\times10^{-1}\pm5.77\times10^{-3}$	6.75	$5.25\times10^{-2}\pm4.36\times10^{-3}$	4.50	$6.62\times10^{-2}\pm5.99\times10^{-3}$
11.75	$4.23\times10^{-2}\pm3.03\times10^{-3}$	8.81	$8.25\times10^{-2}\pm4.89\times10^{-3}$	7.05	$4.12\times10^{-2}\pm3.86\times10^{-3}$	4.70	$4.45\times10^{-2}\pm4.98\times10^{-3}$
12.25	$3.65\times10^{-2}\pm2.81\times10^{-3}$	9.19	$5.96\times10^{-2}\pm4.15\times10^{-3}$	7.35	$2.42\times10^{-2}\pm2.96\times10^{-3}$	4.90	$4.45\times10^{-2}\pm4.91\times10^{-3}$
12.75	$2.39\times10^{-2}\pm2.28\times10^{-3}$	9.56	$4.75\times10^{-2}\pm3.71\times10^{-3}$	7.65	$1.95\times10^{-2}\pm2.66\times10^{-3}$	5.10	$2.33\times10^{-2}\pm3.56\times10^{-3}$
13.25	$1.43\times10^{-2}\pm1.76\times10^{-3}$	9.94	$3.53\times10^{-2}\pm3.20\times10^{-3}$	7.95	$1.27\times10^{-2}\pm2.14\times10^{-3}$	5.30	$2.01\times10^{-2}\pm3.30\times10^{-3}$
13.75	$7.29\times10^{-3}\pm1.57\times10^{-4}$	10.31	$2.32\times10^{-2}\pm2.59\times10^{-3}$	8.25	$8.68\times10^{-3}\pm1.77\times10^{-3}$	5.50	$1.30\times10^{-2}\pm2.66\times10^{-3}$
14.25	$4.01\times10^{-3}\pm1.17\times10^{-4}$	10.69	$1.34\times10^{-2}\pm2.46\times10^{-4}$	8.55	$6.15\times10^{-3}\pm1.49\times10^{-3}$	5.70	$7.06\times10^{-3}\pm1.96\times10^{-3}$
14.75	$2.05\times10^{-3}\pm8.33\times10^{-5}$	11.06	$9.31\times10^{-3}\pm2.05\times10^{-4}$	8.85	$2.75\times10^{-3}\pm1.25\times10^{-4}$	5.90	$5.43\times10^{-3}\pm1.72\times10^{-3}$
15.25	$1.01\times10^{-3}\pm5.84\times10^{-5}$	11.44	$5.96\times10^{-3}\pm1.64\times10^{-4}$	9.15	$1.78\times10^{-3}\pm1.00\times10^{-4}$	6.10	$3.80\times10^{-3}\pm1.44\times10^{-3}$
15.75	$4.88\times10^{-4}\pm4.06\times10^{-5}$	11.81	$3.44\times10^{-3}\pm1.25\times10^{-4}$	9.45	$1.12\times10^{-3}\pm7.94\times10^{-5}$	6.30	$2.00\times10^{-3}\pm1.30\times10^{-4}$
16.25	$2.13\times10^{-4}\pm2.69\times10^{-5}$	12.19	$2.25\times10^{-3}\pm1.01\times10^{-4}$	9.75	$6.72\times10^{-4}\pm6.16\times10^{-5}$	6.50	$1.27\times10^{-3}\pm1.04\times10^{-4}$
16.75	$1.35\times10^{-4}\pm2.14\times10^{-5}$	12.56	$1.21\times10^{-3}\pm7.38\times10^{-5}$	10.05	$3.39\times10^{-4}\pm4.37\times10^{-5}$	6.70	$9.40\times10^{-4}\pm8.92\times10^{-5}$
17.25	$3.73\times10^{-5}\pm1.12\times10^{-5}$	12.94	$6.86\times10^{-4}\pm5.57\times10^{-5}$	10.35	$2.37\times10^{-4}\pm3.66\times10^{-5}$	6.90	$6.52\times10^{-4}\pm7.43\times10^{-5}$
17.75	$1.02\times10^{-5}\pm5.87\times10^{-6}$	13.31	$3.66\times10^{-4}\pm4.06\times10^{-5}$	10.65	$1.07\times10^{-4}\pm2.46\times10^{-5}$	7.10	$3.81\times10^{-4}\pm5.68\times10^{-5}$
18.25	$1.02\times10^{-5}\pm5.87\times10^{-6}$	13.69	$2.30\times10^{-4}\pm3.22\times10^{-5}$	10.95	$3.39\times10^{-5}\pm1.38\times10^{-5}$	7.30	$2.79\times10^{-4}\pm4.86\times10^{-5}$
18.75	$1.35\times10^{-5}\pm6.77\times10^{-6}$	14.06	$1.17\times10^{-4}\pm2.30\times10^{-5}$	11.25	$2.82\times10^{-5}\pm1.26\times10^{-5}$	7.50	$1.27\times10^{-4}\pm3.28\times10^{-5}$
19.25	$6.77\times10^{-6}\pm4.79\times10^{-6}$	14.44	$5.42\times10^{-5}\pm1.56\times10^{-5}$	11.55	$3.39\times10^{-5}\pm1.38\times10^{-5}$	7.70	$1.35\times10^{-4}\pm3.39\times10^{-5}$
		14.81	$3.16\times10^{-5}\pm1.19\times10^{-5}$	11.85	$5.64\times10^{-6}\pm5.64\times10^{-6}$	7.90	$6.77\times10^{-5}\pm2.39\times10^{-5}$
		15.19	$1.81\times10^{-5}\pm9.03\times10^{-6}$	12.15	$1.13\times10^{-5}\pm7.98\times10^{-6}$	8.10	$8.47\times10^{-6}\pm8.47\times10^{-6}$
						8.30	$1.69\times10^{-5}\pm1.20\times10^{-5}$
						8.50	$1.69\times10^{-5}\pm1.20\times10^{-5}$
						8.70	$8.47\times10^{-6}\pm8.47\times10^{-6}$
						8.90	$8.47\times10^{-6}\pm8.47\times10^{-6}$
						9.10	$1.69\times10^{-5}\pm1.20\times10^{-5}$
						9.30	$8.47\times10^{-6}\pm8.47\times10^{-6}$

TABLE VIII. $d\sigma/dE_T$ (b/GeV) versus E_T (GeV) for Au+Au at 11.6A GeV/c for four $\delta\eta$ intervals. Errors quoted are statistical only; systematic errors are estimated to be less than $\pm3\%$ on the E_T scale.

			Au+Au				
E_T	$\delta\eta$=1.30	E_T	$\delta\eta$=0.966	E_T	$\delta\eta$=0.624	E_T	$\delta\eta$=0.378
0.40	$1.65\times10^{0}\pm7.37\times10^{-2}$	0.30	$2.26\times10^{0}\pm9.90\times10^{-2}$	0.24	$2.94\times10^{0}\pm1.29\times10^{-1}$	0.16	$4.59\times10^{0}\pm1.97\times10^{-1}$
1.20	$3.91\times10^{-1}\pm4.04\times10^{-2}$	0.90	$5.00\times10^{-1}\pm5.26\times10^{-2}$	0.72	$8.07\times10^{-1}\pm6.37\times10^{-2}$	0.48	$1.23\times10^{0}\pm9.27\times10^{-2}$
2.00	$3.59\times10^{-1}\pm2.72\times10^{-2}$	1.50	$4.39\times10^{-1}\pm3.66\times10^{-2}$	1.20	$6.02\times10^{-1}\pm4.48\times10^{-2}$	0.80	$1.04\times10^{0}\pm6.77\times10^{-2}$
2.80	$2.84\times10^{-1}\pm2.22\times10^{-2}$	2.10	$3.92\times10^{-1}\pm2.96\times10^{-2}$	1.68	$5.79\times10^{-1}\pm3.75\times10^{-2}$	1.12	$8.84\times10^{-1}\pm5.45\times10^{-2}$
3.60	$2.69\times10^{-1}\pm1.96\times10^{-2}$	2.70	$3.63\times10^{-1}\pm2.58\times10^{-2}$	2.16	$4.72\times10^{-1}\pm3.11\times10^{-2}$	1.44	$7.75\times10^{-1}\pm4.69\times10^{-2}$
4.40	$2.57\times10^{-1}\pm1.69\times10^{-2}$	3.30	$3.23\times10^{-1}\pm2.27\times10^{-2}$	2.64	$4.18\times10^{-1}\pm2.75\times10^{-2}$	1.76	$6.06\times10^{-1}\pm4.10\times10^{-2}$
5.20	$2.17\times10^{-1}\pm1.54\times10^{-2}$	3.90	$3.04\times10^{-1}\pm2.04\times10^{-2}$	3.12	$4.37\times10^{-1}\pm2.55\times10^{-2}$	2.08	$5.96\times10^{-1}\pm3.61\times10^{-2}$
6.00	$2.21\times10^{-1}\pm1.44\times10^{-2}$	4.50	$2.85\times10^{-1}\pm1.88\times10^{-2}$	3.60	$3.18\times10^{-1}\pm2.20\times10^{-2}$	2.40	$5.42\times10^{-1}\pm3.37\times10^{-2}$
6.80	$2.00\times10^{-1}\pm1.35\times10^{-2}$	5.10	$2.55\times10^{-1}\pm1.75\times10^{-2}$	4.08	$3.19\times10^{-1}\pm2.09\times10^{-2}$	2.72	$5.07\times10^{-1}\pm3.16\times10^{-2}$
7.60	$1.83\times10^{-1}\pm1.20\times10^{-2}$	5.70	$2.33\times10^{-1}\pm1.60\times10^{-2}$	4.56	$3.39\times10^{-1}\pm2.09\times10^{-2}$	3.04	$4.24\times10^{-1}\pm2.85\times10^{-2}$
8.40	$1.67\times10^{-1}\pm1.17\times10^{-2}$	6.30	$2.29\times10^{-1}\pm1.58\times10^{-2}$	5.04	$2.68\times10^{-1}\pm1.85\times10^{-2}$	3.36	$4.86\times10^{-1}\pm2.92\times10^{-2}$
9.20	$1.46\times10^{-1}\pm1.08\times10^{-2}$	6.90	$1.83\times10^{-1}\pm1.43\times10^{-2}$	5.52	$2.32\times10^{-1}\pm1.67\times10^{-2}$	3.68	$4.06\times10^{-1}\pm2.65\times10^{-2}$
10.00	$1.53\times10^{-1}\pm1.03\times10^{-2}$	7.50	$1.91\times10^{-1}\pm1.36\times10^{-2}$	6.00	$2.75\times10^{-1}\pm1.74\times10^{-2}$	4.00	$3.79\times10^{-1}\pm2.52\times10^{-2}$
10.80	$1.29\times10^{-1}\pm9.64\times10^{-3}$	8.10	$1.93\times10^{-1}\pm1.32\times10^{-2}$	6.48	$2.44\times10^{-1}\pm1.62\times10^{-2}$	4.32	$2.70\times10^{-1}\pm2.14\times10^{-2}$
11.60	$1.40\times10^{-1}\pm9.84\times10^{-3}$	8.70	$1.59\times10^{-1}\pm1.24\times10^{-2}$	6.96	$2.10\times10^{-1}\pm1.48\times10^{-2}$	4.64	$3.38\times10^{-1}\pm2.31\times10^{-2}$
12.40	$1.24\times10^{-1}\pm8.86\times10^{-3}$	9.30	$1.67\times10^{-1}\pm1.21\times10^{-2}$	7.44	$2.06\times10^{-1}\pm1.48\times10^{-2}$	4.96	$3.49\times10^{-1}\pm2.35\times10^{-2}$
13.20	$1.12\times10^{-1}\pm8.46\times10^{-3}$	9.90	$1.42\times10^{-1}\pm1.11\times10^{-2}$	7.92	$2.30\times10^{-1}\pm1.57\times10^{-2}$	5.28	$3.38\times10^{-1}\pm2.26\times10^{-2}$
14.00	$1.17\times10^{-1}\pm8.55\times10^{-3}$	10.50	$1.55\times10^{-1}\pm1.12\times10^{-2}$	8.40	$2.14\times10^{-1}\pm1.48\times10^{-2}$	5.60	$3.41\times10^{-1}\pm2.30\times10^{-2}$
14.80	$1.26\times10^{-1}\pm8.88\times10^{-3}$	11.10	$1.53\times10^{-1}\pm1.14\times10^{-2}$	8.88	$2.30\times10^{-1}\pm1.53\times10^{-2}$	5.92	$3.31\times10^{-1}\pm2.24\times10^{-2}$
15.60	$1.19\times10^{-1}\pm8.61\times10^{-3}$	11.70	$1.67\times10^{-1}\pm1.17\times10^{-2}$	9.36	$1.95\times10^{-1}\pm1.40\times10^{-2}$	6.24	$3.04\times10^{-1}\pm2.15\times10^{-2}$
16.40	$1.21\times10^{-1}\pm8.61\times10^{-3}$	12.30	$1.55\times10^{-1}\pm1.13\times10^{-2}$	9.84	$1.72\times10^{-1}\pm1.32\times10^{-2}$	6.56	$2.66\times10^{-1}\pm2.00\times10^{-2}$
17.20	$1.10\times10^{-1}\pm8.20\times10^{-3}$	12.90	$1.42\times10^{-1}\pm1.07\times10^{-2}$	10.32	$1.73\times10^{-1}\pm1.33\times10^{-2}$	6.88	$2.69\times10^{-1}\pm2.03\times10^{-2}$
18.00	$1.02\times10^{-1}\pm7.90\times10^{-3}$	13.50	$1.31\times10^{-1}\pm1.04\times10^{-2}$	10.80	$1.77\times10^{-1}\pm1.34\times10^{-2}$	7.20	$2.60\times10^{-1}\pm1.98\times10^{-2}$
18.80	$1.02\times10^{-1}\pm7.83\times10^{-3}$	14.10	$1.43\times10^{-1}\pm1.08\times10^{-2}$	11.28	$1.51\times10^{-1}\pm1.23\times10^{-2}$	7.52	$2.37\times10^{-1}\pm1.89\times10^{-2}$
19.60	$1.00\times10^{-1}\pm7.83\times10^{-3}$	14.70	$1.31\times10^{-1}\pm1.03\times10^{-2}$	11.76	$1.66\times10^{-1}\pm1.30\times10^{-2}$	7.84	$3.11\times10^{-1}\pm2.17\times10^{-2}$
20.40	$8.64\times10^{-2}\pm7.23\times10^{-3}$	15.30	$1.09\times10^{-1}\pm9.43\times10^{-3}$	12.24	$1.68\times10^{-1}\pm1.30\times10^{-2}$	8.16	$2.16\times10^{-1}\pm1.81\times10^{-2}$
21.20	$9.19\times10^{-2}\pm7.50\times10^{-3}$	15.90	$1.19\times10^{-1}\pm9.80\times10^{-3}$	12.72	$1.79\times10^{-1}\pm1.35\times10^{-2}$	8.48	$2.75\times10^{-1}\pm2.05\times10^{-2}$
22.00	$9.61\times10^{-2}\pm7.67\times10^{-3}$	16.50	$1.24\times10^{-1}\pm1.01\times10^{-2}$	13.20	$1.60\times10^{-1}\pm1.27\times10^{-2}$	8.80	$2.21\times10^{-1}\pm1.83\times10^{-2}$
22.80	$8.40\times10^{-2}\pm7.13\times10^{-3}$	17.10	$1.13\times10^{-1}\pm9.53\times10^{-3}$	13.68	$1.38\times10^{-1}\pm1.18\times10^{-2}$	9.12	$2.49\times10^{-1}\pm1.94\times10^{-2}$
23.60	$8.76\times10^{-2}\pm7.33\times10^{-3}$	17.70	$1.02\times10^{-1}\pm9.15\times10^{-3}$	14.16	$1.48\times10^{-1}\pm1.22\times10^{-2}$	9.44	$2.19\times10^{-1}\pm1.83\times10^{-2}$
24.40	$8.64\times10^{-2}\pm7.23\times10^{-3}$	18.30	$1.27\times10^{-1}\pm1.01\times10^{-2}$	14.64	$1.56\times10^{-1}\pm1.25\times10^{-2}$	9.76	$1.96\times10^{-1}\pm1.72\times10^{-2}$
25.20	$7.80\times10^{-2}\pm6.86\times10^{-3}$	18.90	$1.14\times10^{-1}\pm9.60\times10^{-3}$	15.12	$1.33\times10^{-1}\pm1.16\times10^{-2}$	10.08	$2.33\times10^{-1}\pm1.87\times10^{-2}$
26.00	$8.22\times10^{-2}\pm7.05\times10^{-3}$	19.50	$9.35\times10^{-2}\pm8.68\times10^{-3}$	15.60	$1.24\times10^{-1}\pm1.12\times10^{-2}$	10.40	$2.07\times10^{-1}\pm1.78\times10^{-2}$
26.80	$8.28\times10^{-2}\pm7.07\times10^{-3}$	20.10	$1.02\times10^{-1}\pm9.08\times10^{-3}$	16.08	$1.41\times10^{-1}\pm1.19\times10^{-2}$	10.72	$1.99\times10^{-1}\pm1.74\times10^{-2}$
27.60	$9.13\times10^{-2}\pm7.43\times10^{-3}$	20.70	$1.05\times10^{-1}\pm9.19\times10^{-3}$	16.56	$1.50\times10^{-1}\pm1.23\times10^{-2}$	11.04	$1.84\times10^{-1}\pm1.67\times10^{-2}$
28.40	$6.95\times10^{-2}\pm6.48\times10^{-3}$	21.30	$9.99\times10^{-2}\pm8.97\times10^{-3}$	17.04	$1.21\times10^{-1}\pm1.10\times10^{-2}$	11.36	$1.74\times10^{-1}\pm1.62\times10^{-2}$
29.20	$6.53\times10^{-2}\pm6.28\times10^{-3}$	21.90	$9.27\times10^{-2}\pm8.64\times10^{-3}$	17.52	$1.19\times10^{-1}\pm1.10\times10^{-2}$	11.68	$1.33\times10^{-1}\pm1.42\times10^{-2}$
30.00	$7.55\times10^{-2}\pm6.76\times10^{-3}$	22.50	$7.90\times10^{-2}\pm7.98\times10^{-3}$	18.00	$1.03\times10^{-1}\pm1.02\times10^{-2}$	12.00	$1.60\times10^{-1}\pm1.56\times10^{-2}$
30.80	$8.04\times10^{-2}\pm6.97\times10^{-3}$	23.10	$9.59\times10^{-2}\pm8.79\times10^{-3}$	18.48	$1.10\times10^{-1}\pm1.05\times10^{-2}$	12.32	$1.37\times10^{-1}\pm1.44\times10^{-2}$
31.60	$6.28\times10^{-2}\pm6.22\times10^{-3}$	23.70	$9.99\times10^{-2}\pm8.97\times10^{-3}$	18.96	$9.77\times10^{-2}\pm9.92\times10^{-3}$	12.64	$1.53\times10^{-1}\pm1.52\times10^{-2}$
32.40	$6.29\times10^{-2}\pm6.16\times10^{-3}$	24.30	$9.59\times10^{-2}\pm8.79\times10^{-3}$	19.44	$9.47\times10^{-2}\pm9.77\times10^{-3}$	12.96	$1.36\times10^{-1}\pm1.43\times10^{-2}$
33.20	$5.68\times10^{-2}\pm5.86\times10^{-3}$	24.90	$7.57\times10^{-2}\pm7.81\times10^{-3}$	19.92	$8.16\times10^{-2}\pm9.07\times10^{-3}$	13.28	$1.27\times10^{-1}\pm1.38\times10^{-2}$
34.00	$6.47\times10^{-2}\pm6.25\times10^{-3}$	25.50	$8.62\times10^{-2}\pm8.34\times10^{-3}$	20.40	$9.17\times10^{-2}\pm9.61\times10^{-3}$	13.60	$1.27\times10^{-1}\pm1.38\times10^{-2}$
34.80	$6.04\times10^{-2}\pm6.04\times10^{-3}$	26.10	$6.85\times10^{-2}\pm7.43\times10^{-3}$	20.88	$9.37\times10^{-2}\pm9.71\times10^{-3}$	13.92	$8.76\times10^{-2}\pm1.15\times10^{-2}$
35.60	$4.90\times10^{-2}\pm5.44\times10^{-3}$	26.70	$7.98\times10^{-2}\pm8.10\times10^{-3}$	21.36	$8.56\times10^{-2}\pm9.29\times10^{-3}$	14.24	$1.01\times10^{-1}\pm1.24\times10^{-2}$
36.40	$5.44\times10^{-2}\pm5.73\times10^{-3}$	27.30	$7.09\times10^{-2}\pm7.56\times10^{-3}$	21.84	$8.26\times10^{-2}\pm9.12\times10^{-3}$	14.56	$9.67\times10^{-2}\pm1.21\times10^{-2}$
37.20	$5.44\times10^{-2}\pm5.73\times10^{-3}$	27.90	$6.93\times10^{-2}\pm7.47\times10^{-3}$	22.32	$5.84\times10^{-2}\pm7.67\times10^{-3}$	14.88	$7.86\times10^{-2}\pm1.09\times10^{-2}$
38.00	$5.50\times10^{-2}\pm5.77\times10^{-3}$	28.50	$6.93\times10^{-2}\pm7.47\times10^{-3}$	22.80	$6.35\times10^{-2}\pm7.99\times10^{-3}$	15.20	$6.95\times10^{-2}\pm1.02\times10^{-2}$
38.80	$5.92\times10^{-2}\pm5.98\times10^{-3}$	29.10	$5.72\times10^{-2}\pm6.79\times10^{-3}$	23.28	$5.84\times10^{-2}\pm7.67\times10^{-3}$	15.52	$6.95\times10^{-2}\pm1.02\times10^{-2}$
39.60	$4.77\times10^{-2}\pm5.37\times10^{-3}$	29.70	$6.85\times10^{-2}\pm7.43\times10^{-3}$	23.76	$6.04\times10^{-2}\pm7.80\times10^{-3}$	15.84	$4.83\times10^{-2}\pm8.55\times10^{-3}$
40.40	$4.59\times10^{-2}\pm5.27\times10^{-3}$	30.30	$6.61\times10^{-2}\pm7.30\times10^{-3}$	24.24	$4.83\times10^{-2}\pm6.98\times10^{-3}$	16.16	$4.08\times10^{-2}\pm7.85\times10^{-3}$

TABLE VIII. (*Continued*).

Au+Au							
E_T	$\delta\eta$=1.30	E_T	$\delta\eta$=0.966	E_T	$\delta\eta$=0.624	E_T	$\delta\eta$=0.378
41.20	$4.29\times10^{-2}\pm5.09\times10^{-3}$	30.90	$7.01\times10^{-2}\pm7.52\times10^{-3}$	24.72	$4.43\times10^{-2}\pm6.68\times10^{-3}$	16.48	$3.78\times10^{-2}\pm7.55\times10^{-3}$
42.00	$3.81\times10^{-2}\pm4.80\times10^{-3}$	31.50	$5.56\times10^{-2}\pm6.69\times10^{-3}$	25.20	$3.81\times10^{-2}\pm9.51\times10^{-4}$	16.80	$3.20\times10^{-2}\pm1.07\times10^{-3}$
42.80	$3.63\times10^{-2}\pm4.68\times10^{-3}$	32.10	$4.19\times10^{-2}\pm5.81\times10^{-3}$	25.68	$3.31\times10^{-2}\pm8.86\times10^{-4}$	17.12	$2.67\times10^{-2}\pm9.75\times10^{-4}$
43.60	$2.84\times10^{-2}\pm4.14\times10^{-3}$	32.70	$4.51\times10^{-2}\pm6.03\times10^{-3}$	26.16	$2.80\times10^{-2}\pm8.14\times10^{-4}$	17.44	$2.39\times10^{-2}\pm9.23\times10^{-4}$
44.40	$3.75\times10^{-2}\pm4.76\times10^{-3}$	33.30	$5.16\times10^{-2}\pm6.45\times10^{-3}$	26.64	$2.36\times10^{-2}\pm7.48\times10^{-4}$	17.76	$1.87\times10^{-2}\pm8.15\times10^{-4}$
45.20	$3.07\times10^{-2}\pm6.61\times10^{-4}$	33.90	$4.59\times10^{-2}\pm6.08\times10^{-3}$	27.12	$1.74\times10^{-2}\pm6.42\times10^{-4}$	18.08	$1.32\times10^{-2}\pm6.85\times10^{-4}$
46.00	$2.85\times10^{-2}\pm6.37\times10^{-4}$	34.50	$4.19\times10^{-2}\pm5.81\times10^{-3}$	27.60	$1.49\times10^{-2}\pm5.94\times10^{-4}$	18.40	$1.18\times10^{-2}\pm6.49\times10^{-4}$
46.80	$2.49\times10^{-2}\pm5.95\times10^{-4}$	35.10	$3.75\times10^{-2}\pm8.43\times10^{-4}$	28.08	$1.15\times10^{-2}\pm5.23\times10^{-4}$	18.72	$8.79\times10^{-3}\pm5.59\times10^{-4}$
47.60	$2.04\times10^{-2}\pm5.39\times10^{-4}$	35.70	$3.70\times10^{-2}\pm8.38\times10^{-4}$	28.56	$8.92\times10^{-3}\pm4.60\times10^{-4}$	19.04	$6.51\times10^{-3}\pm4.81\times10^{-4}$
48.40	$1.61\times10^{-2}\pm4.78\times10^{-4}$	36.30	$3.28\times10^{-2}\pm7.89\times10^{-4}$	29.04	$5.98\times10^{-3}\pm3.76\times10^{-4}$	19.36	$4.23\times10^{-3}\pm3.88\times10^{-4}$
49.20	$1.33\times10^{-2}\pm4.35\times10^{-4}$	36.90	$2.88\times10^{-2}\pm7.39\times10^{-4}$	29.52	$5.12\times10^{-3}\pm3.49\times10^{-4}$	19.68	$3.02\times10^{-3}\pm3.28\times10^{-4}$
50.00	$1.03\times10^{-2}\pm3.84\times10^{-4}$	37.50	$2.56\times10^{-2}\pm6.97\times10^{-4}$	30.00	$3.25\times10^{-3}\pm2.78\times10^{-4}$	20.00	$2.95\times10^{-3}\pm3.24\times10^{-4}$
50.80	$8.10\times10^{-3}\pm3.39\times10^{-4}$	38.10	$2.11\times10^{-2}\pm6.32\times10^{-4}$	30.48	$2.44\times10^{-3}\pm2.41\times10^{-4}$	20.32	$1.49\times10^{-3}\pm2.31\times10^{-4}$
51.60	$5.73\times10^{-3}\pm2.86\times10^{-4}$	38.70	$1.67\times10^{-2}\pm5.62\times10^{-4}$	30.96	$1.78\times10^{-3}\pm2.05\times10^{-4}$	20.64	$1.53\times10^{-3}\pm2.33\times10^{-4}$
52.40	$4.18\times10^{-3}\pm2.44\times10^{-4}$	39.30	$1.40\times10^{-2}\pm5.15\times10^{-4}$	31.44	$1.04\times10^{-3}\pm1.57\times10^{-4}$	20.96	$7.12\times10^{-4}\pm1.59\times10^{-4}$
53.20	$2.85\times10^{-3}\pm2.01\times10^{-4}$	39.90	$1.04\times10^{-2}\pm4.45\times10^{-4}$	31.92	$7.12\times10^{-4}\pm1.30\times10^{-4}$	21.28	$8.89\times10^{-4}\pm1.78\times10^{-4}$
54.00	$1.99\times10^{-3}\pm1.68\times10^{-4}$	40.50	$8.12\times10^{-3}\pm3.93\times10^{-4}$	32.40	$5.69\times10^{-4}\pm1.16\times10^{-4}$	21.60	$3.91\times10^{-4}\pm1.18\times10^{-4}$
54.80	$1.17\times10^{-3}\pm1.29\times10^{-4}$	41.10	$5.94\times10^{-3}\pm3.36\times10^{-4}$	32.88	$2.61\times10^{-4}\pm7.87\times10^{-5}$	21.92	$2.13\times10^{-4}\pm8.71\times10^{-5}$
55.60	$7.83\times10^{-4}\pm1.06\times10^{-4}$	41.70	$5.10\times10^{-3}\pm3.11\times10^{-4}$	33.36	$1.19\times10^{-4}\pm5.30\times10^{-5}$	22.24	$1.07\times10^{-4}\pm6.16\times10^{-5}$
56.40	$3.42\times10^{-4}\pm6.97\times10^{-5}$	42.30	$3.85\times10^{-3}\pm2.70\times10^{-4}$	33.84	$7.12\times10^{-5}\pm4.11\times10^{-5}$	22.56	$1.78\times10^{-4}\pm7.95\times10^{-5}$
57.20	$2.70\times10^{-4}\pm6.20\times10^{-5}$	42.90	$2.43\times10^{-3}\pm2.15\times10^{-4}$	34.32	$7.12\times10^{-5}\pm4.11\times10^{-5}$	22.88	$1.42\times10^{-4}\pm7.12\times10^{-5}$
58.00	$8.54\times10^{-5}\pm3.49\times10^{-5}$	43.50	$1.84\times10^{-3}\pm1.87\times10^{-4}$	34.80	$4.74\times10^{-5}\pm3.35\times10^{-5}$	23.20	$3.56\times10^{-5}\pm3.56\times10^{-5}$
58.80	$8.54\times10^{-5}\pm3.49\times10^{-5}$	44.10	$1.16\times10^{-3}\pm1.48\times10^{-4}$			23.52	$3.56\times10^{-5}\pm3.56\times10^{-5}$
59.60	$1.42\times10^{-5}\pm1.42\times10^{-5}$	44.70	$8.35\times10^{-4}\pm1.26\times10^{-4}$			23.84	$3.56\times10^{-5}\pm3.56\times10^{-5}$

Gamma fits at the lower values of E_T. Surprisingly, the more complicated fit [Eq. (12)] with more parameters fits the data much worse than the simpler form [Eq. (13)] that again fits the data much more poorly than a single-Gamma distribution. If multiplicity were the primary quantity, leading to an E_T distribution of the form of Eqs. (12) and (13), one would expect these equations to fit the measurements better than the single-Gamma distribution. It is tempting to speculate on the implications of these results for the detailed relationship between E_T and multiplicity distributions and the effect of hadronization; however, the present experiment has significant instrumental effects in both the E_T and multiplicity measurements so that a more controlled experiment to better examine these issues certainly seems desirable.

IV. WOUNDED PROJECTED NUCLEON MODEL

A. Method and results

A simple and elegant method for separating instrumental effects from nuclear geometrical and possible dynamical effects is to use extreme-independent-collision models such as the wounded nucleon model (WNM) [26,62,63] or the wounded projectile nucleon model (WPNM) [36,27,11,12] to relate measurements of different nuclei in the same detector. In these models, the nuclear geometry is represented as the relative probability per interaction for a given number of total participants (WNM) or projectile participants (WPNM) integrated over the impact parameter of the $p+A$ or $B+A$ reaction.[4] Typically, Woods-Saxon densities are used for both the projectile and target nuclei, and a nucleon-nucleon inelastic cross section of 30 mb is taken, corresponding to a nucleon-nucleon mean free path of $\sim$2.2 fm at nuclear density [36,11,12]. Once the nuclear geometry is specified in this manner, experimental measurements can be used to derive the distribution (in the actual detector) of E_T or multiplicity (or other additive quantity) for the elementary collision process, i.e., a wounded nucleon or a wounded projectile nucleon, which is then used as the basis of the analysis of a nuclear scattering as the result of multiple independent elementary collision processes. The key experimental issue then becomes the linearity of the detector response to multiple collisions (better than 1% in the present case), instead of detailed instrumental corrections to obtain, e.g., the ''true E_T'' impinging on the detector from the measured E_T and response function [Eq. (4)].

The WPNM calculation for a $B+A$ reaction is given by the sum

$$\left(\frac{d\sigma}{dE_T}\right)_{\mathrm{WPNM}} = \sigma \sum_{n=1}^{B} w_n P_n(E_T), \tag{14}$$

where σ is the measured $B+A$ cross section in the interval

[4]It can also be done as a function of impact parameter.

TABLE IX. $d\sigma/dE_T$ (b/GeV) versus E_T (GeV) for Au+Au (ZCAL) at 11.6A GeV/c for four $\delta\eta$ intervals. Errors quoted are statistical only; systematic errors are estimated to be less than $\pm3\%$ on the E_T scale.

Au+Au (ZCAL)							
E_T	$\delta\eta$=1.30	E_T	$\delta\eta$=0.966	E_T	$\delta\eta$=0.624	E_T	$\delta\eta$=0.378
24.40	$4.55\times10^{-4}\pm3.22\times10^{-4}$	16.50	$6.07\times10^{-4}\pm4.29\times10^{-4}$	11.28	$3.79\times10^{-4}\pm3.79\times10^{-4}$	5.92	$5.69\times10^{-4}\pm5.69\times10^{-4}$
25.20	$1.37\times10^{-3}\pm5.57\times10^{-4}$	17.10	$3.03\times10^{-4}\pm3.03\times10^{-4}$	11.76	$3.79\times10^{-4}\pm3.79\times10^{-4}$	6.24	$5.69\times10^{-4}\pm5.69\times10^{-4}$
26.00	$2.05\times10^{-3}\pm6.83\times10^{-4}$	17.70	$3.03\times10^{-4}\pm3.03\times10^{-4}$	12.24	$7.59\times10^{-4}\pm5.36\times10^{-4}$	6.56	$1.14\times10^{-3}\pm8.05\times10^{-4}$
26.80	$9.10\times10^{-4}\pm4.55\times10^{-4}$	18.30	$3.03\times10^{-4}\pm3.03\times10^{-4}$	12.72	$2.28\times10^{-3}\pm9.29\times10^{-4}$	6.88	$1.14\times10^{-3}\pm8.05\times10^{-4}$
27.60	$2.50\times10^{-3}\pm7.55\times10^{-4}$	18.90	$3.03\times10^{-4}\pm3.03\times10^{-4}$	13.20	$2.65\times10^{-3}\pm1.00\times10^{-3}$	7.20	$1.14\times10^{-3}\pm8.05\times10^{-4}$
28.40	$4.78\times10^{-3}\pm1.04\times10^{-3}$	19.50	$1.52\times10^{-3}\pm6.79\times10^{-4}$	13.68	$3.03\times10^{-3}\pm1.07\times10^{-3}$	7.52	$1.71\times10^{-3}\pm9.85\times10^{-4}$
29.20	$4.10\times10^{-3}\pm9.66\times10^{-4}$	20.10	$1.52\times10^{-3}\pm6.79\times10^{-4}$	14.16	$7.21\times10^{-3}\pm1.65\times10^{-3}$	7.84	$4.55\times10^{-3}\pm1.61\times10^{-3}$
30.00	$7.05\times10^{-3}\pm1.27\times10^{-3}$	20.70	$4.25\times10^{-3}\pm1.14\times10^{-3}$	14.64	$7.21\times10^{-3}\pm1.65\times10^{-3}$	8.16	$7.40\times10^{-3}\pm2.05\times10^{-3}$
30.80	$7.74\times10^{-3}\pm1.33\times10^{-3}$	21.30	$4.55\times10^{-3}\pm1.18\times10^{-3}$	15.12	$1.14\times10^{-2}\pm2.08\times10^{-3}$	8.48	$7.40\times10^{-3}\pm2.05\times10^{-3}$
31.60	$8.42\times10^{-3}\pm1.38\times10^{-3}$	21.90	$3.64\times10^{-3}\pm1.05\times10^{-3}$	15.60	$1.44\times10^{-2}\pm2.34\times10^{-3}$	8.80	$1.54\times10^{-2}\pm2.96\times10^{-3}$
32.40	$1.37\times10^{-2}\pm1.76\times10^{-3}$	22.50	$3.94\times10^{-3}\pm1.09\times10^{-3}$	16.08	$1.82\times10^{-2}\pm2.63\times10^{-3}$	9.12	$2.33\times10^{-2}\pm3.64\times10^{-3}$
33.20	$1.55\times10^{-2}\pm1.88\times10^{-3}$	23.10	$7.28\times10^{-3}\pm1.49\times10^{-3}$	16.56	$2.81\times10^{-2}\pm3.26\times10^{-3}$	9.44	$2.50\times10^{-2}\pm3.77\times10^{-3}$
34.00	$2.21\times10^{-2}\pm2.24\times10^{-3}$	23.70	$1.15\times10^{-2}\pm1.87\times10^{-3}$	17.04	$2.81\times10^{-2}\pm3.26\times10^{-3}$	9.76	$3.24\times10^{-2}\pm4.30\times10^{-3}$
34.80	$2.23\times10^{-2}\pm2.25\times10^{-3}$	24.30	$1.67\times10^{-2}\pm2.25\times10^{-3}$	17.52	$3.19\times10^{-2}\pm3.48\times10^{-3}$	10.08	$4.10\times10^{-2}\pm4.83\times10^{-3}$
35.60	$2.44\times10^{-2}\pm2.35\times10^{-3}$	24.90	$1.79\times10^{-2}\pm2.33\times10^{-3}$	18.00	$3.91\times10^{-2}\pm3.85\times10^{-3}$	10.40	$4.10\times10^{-2}\pm4.83\times10^{-3}$
36.40	$2.46\times10^{-2}\pm2.37\times10^{-3}$	25.50	$1.88\times10^{-2}\pm2.39\times10^{-3}$	18.48	$3.83\times10^{-2}\pm3.81\times10^{-3}$	10.72	$5.01\times10^{-2}\pm5.34\times10^{-3}$
37.20	$2.69\times10^{-2}\pm2.47\times10^{-3}$	26.10	$2.03\times10^{-2}\pm2.48\times10^{-3}$	18.96	$4.86\times10^{-2}\pm4.29\times10^{-3}$	11.04	$5.86\times10^{-2}\pm5.77\times10^{-3}$
38.00	$3.14\times10^{-2}\pm2.67\times10^{-3}$	26.70	$3.03\times10^{-2}\pm3.03\times10^{-3}$	19.44	$5.16\times10^{-2}\pm4.42\times10^{-3}$	11.36	$7.57\times10^{-2}\pm6.56\times10^{-3}$
38.80	$3.78\times10^{-2}\pm2.93\times10^{-3}$	27.30	$3.06\times10^{-2}\pm3.05\times10^{-3}$	19.92	$5.23\times10^{-2}\pm4.46\times10^{-3}$	11.68	$7.11\times10^{-2}\pm6.36\times10^{-3}$
39.60	$3.78\times10^{-2}\pm2.93\times10^{-3}$	27.90	$2.70\times10^{-2}\pm2.86\times10^{-3}$	20.40	$6.03\times10^{-2}\pm4.78\times10^{-3}$	12.00	$7.97\times10^{-2}\pm6.73\times10^{-3}$
40.40	$4.21\times10^{-2}\pm3.10\times10^{-3}$	28.50	$3.00\times10^{-2}\pm3.02\times10^{-3}$	20.88	$5.84\times10^{-2}\pm4.71\times10^{-3}$	12.32	$7.97\times10^{-2}\pm6.73\times10^{-3}$
41.20	$3.76\times10^{-2}\pm2.92\times10^{-3}$	29.10	$3.85\times10^{-2}\pm3.42\times10^{-3}$	21.36	$6.22\times10^{-2}\pm4.86\times10^{-3}$	12.64	$9.79\times10^{-2}\pm7.46\times10^{-3}$
42.00	$3.37\times10^{-2}\pm2.77\times10^{-3}$	29.70	$4.16\times10^{-2}\pm3.55\times10^{-3}$	21.84	$6.49\times10^{-2}\pm4.96\times10^{-3}$	12.96	$7.97\times10^{-2}\pm6.73\times10^{-3}$
42.80	$3.44\times10^{-2}\pm2.80\times10^{-3}$	30.30	$4.31\times10^{-2}\pm3.62\times10^{-3}$	22.32	$6.45\times10^{-2}\pm4.95\times10^{-3}$	13.28	$8.88\times10^{-2}\pm7.11\times10^{-3}$
43.60	$3.46\times10^{-2}\pm2.81\times10^{-3}$	30.90	$4.76\times10^{-2}\pm3.80\times10^{-3}$	22.80	$6.11\times10^{-2}\pm4.81\times10^{-3}$	13.60	$8.48\times10^{-2}\pm6.95\times10^{-3}$
44.40	$3.37\times10^{-2}\pm2.77\times10^{-3}$	31.50	$3.97\times10^{-2}\pm3.47\times10^{-3}$	23.28	$4.86\times10^{-2}\pm4.29\times10^{-3}$	13.92	$8.08\times10^{-2}\pm6.78\times10^{-3}$
45.20	$3.07\times10^{-2}\pm2.64\times10^{-3}$	32.10	$4.98\times10^{-2}\pm3.89\times10^{-3}$	23.76	$4.67\times10^{-2}\pm4.21\times10^{-3}$	14.24	$7.51\times10^{-2}\pm6.54\times10^{-3}$
46.00	$2.32\times10^{-2}\pm2.30\times10^{-3}$	32.70	$4.98\times10^{-2}\pm3.89\times10^{-3}$	24.24	$4.13\times10^{-2}\pm3.96\times10^{-3}$	14.56	$8.59\times10^{-2}\pm6.99\times10^{-3}$
46.80	$2.25\times10^{-2}\pm2.26\times10^{-3}$	33.30	$4.34\times10^{-2}\pm3.63\times10^{-3}$	24.72	$4.51\times10^{-2}\pm4.14\times10^{-3}$	14.88	$7.62\times10^{-2}\pm6.59\times10^{-3}$
47.60	$1.82\times10^{-2}\pm2.04\times10^{-3}$	33.90	$3.94\times10^{-2}\pm3.46\times10^{-3}$	25.20	$3.53\times10^{-2}\pm3.66\times10^{-3}$	15.20	$5.75\times10^{-2}\pm5.72\times10^{-3}$
48.40	$1.80\times10^{-2}\pm2.02\times10^{-3}$	34.50	$4.25\times10^{-2}\pm3.59\times10^{-3}$	25.68	$3.15\times10^{-2}\pm3.46\times10^{-3}$	15.52	$6.14\times10^{-2}\pm5.91\times10^{-3}$
49.20	$1.59\times10^{-2}\pm1.90\times10^{-3}$	35.10	$3.00\times10^{-2}\pm3.02\times10^{-3}$	26.16	$2.58\times10^{-2}\pm3.13\times10^{-3}$	15.84	$5.46\times10^{-2}\pm5.57\times10^{-3}$
50.00	$1.05\times10^{-2}\pm1.54\times10^{-3}$	35.70	$3.22\times10^{-2}\pm3.12\times10^{-3}$	26.64	$2.73\times10^{-2}\pm3.22\times10^{-3}$	16.16	$3.47\times10^{-2}\pm4.44\times10^{-3}$
50.80	$9.56\times10^{-3}\pm1.47\times10^{-3}$	36.30	$2.76\times10^{-2}\pm2.89\times10^{-3}$	27.12	$1.33\times10^{-2}\pm2.24\times10^{-3}$	16.48	$3.64\times10^{-2}\pm4.55\times10^{-3}$
51.60	$8.19\times10^{-3}\pm1.37\times10^{-3}$	36.90	$2.88\times10^{-2}\pm2.96\times10^{-3}$	27.60	$1.59\times10^{-2}\pm2.46\times10^{-3}$	16.80	$2.90\times10^{-2}\pm4.06\times10^{-3}$
52.40	$5.69\times10^{-3}\pm1.14\times10^{-3}$	37.50	$2.09\times10^{-2}\pm2.52\times10^{-3}$	28.08	$1.48\times10^{-2}\pm2.37\times10^{-3}$	17.12	$3.30\times10^{-2}\pm4.33\times10^{-3}$
53.20	$2.50\times10^{-3}\pm7.55\times10^{-4}$	38.10	$1.97\times10^{-2}\pm2.45\times10^{-3}$	28.56	$1.02\times10^{-2}\pm1.97\times10^{-3}$	17.44	$2.45\times10^{-2}\pm3.73\times10^{-3}$
54.00	$1.14\times10^{-3}\pm5.09\times10^{-4}$	38.70	$1.97\times10^{-2}\pm2.45\times10^{-3}$	29.04	$7.21\times10^{-3}\pm1.65\times10^{-3}$	17.76	$2.16\times10^{-2}\pm3.51\times10^{-3}$
54.80	$9.10\times10^{-4}\pm4.55\times10^{-4}$	39.30	$1.43\times10^{-2}\pm2.08\times10^{-3}$	29.52	$5.31\times10^{-3}\pm1.42\times10^{-3}$	18.08	$1.14\times10^{-2}\pm2.54\times10^{-3}$
55.60	$1.14\times10^{-3}\pm5.09\times10^{-4}$	39.90	$1.40\times10^{-2}\pm2.06\times10^{-3}$	30.00	$3.79\times10^{-3}\pm1.20\times10^{-3}$	18.40	$1.71\times10^{-2}\pm3.12\times10^{-3}$
56.40	$9.10\times10^{-4}\pm4.55\times10^{-4}$	40.50	$1.03\times10^{-2}\pm1.77\times10^{-3}$	30.48	$2.28\times10^{-3}\pm9.29\times10^{-4}$	18.72	$1.19\times10^{-2}\pm2.61\times10^{-3}$
		41.10	$7.28\times10^{-3}\pm1.49\times10^{-3}$	30.96	$7.59\times10^{-4}\pm5.36\times10^{-4}$	19.04	$7.97\times10^{-3}\pm2.13\times10^{-3}$
		41.70	$6.07\times10^{-3}\pm1.36\times10^{-3}$	31.44	$1.52\times10^{-3}\pm7.59\times10^{-4}$	19.36	$6.26\times10^{-3}\pm1.89\times10^{-3}$
		42.30	$4.55\times10^{-3}\pm1.18\times10^{-3}$	31.92	$3.79\times10^{-4}\pm3.79\times10^{-4}$	19.68	$1.71\times10^{-3}\pm9.85\times10^{-4}$
		42.90	$2.73\times10^{-3}\pm9.10\times10^{-4}$	32.40	$7.59\times10^{-4}\pm5.36\times10^{-4}$	20.00	$2.28\times10^{-3}\pm1.14\times10^{-3}$
		43.50	$9.10\times10^{-4}\pm5.26\times10^{-4}$	32.88	$3.79\times10^{-4}\pm3.79\times10^{-4}$	20.32	$5.69\times10^{-4}\pm5.69\times10^{-4}$
		44.10	$6.07\times10^{-4}\pm4.29\times10^{-4}$			20.64	$2.28\times10^{-3}\pm1.14\times10^{-3}$
						20.96	$1.14\times10^{-3}\pm8.05\times10^{-4}$
						21.28	$5.69\times10^{-4}\pm5.69\times10^{-4}$

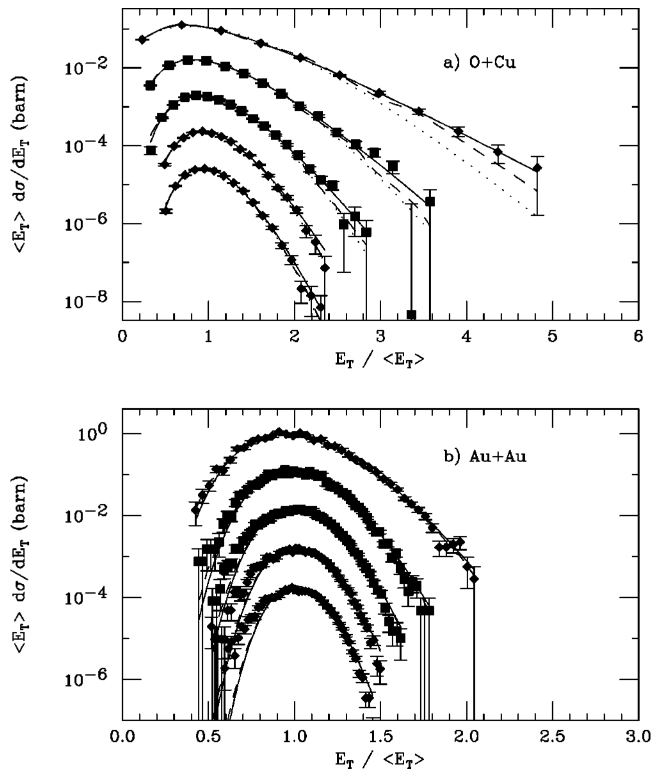

FIG. 7. (a) E_T distributions measured in [16]O+Cu central collisions at 14.6A GeV/c; (b) E_T distributions measured in Au+Au central collisions at 11.6A GeV/c. Measurements are shown for five $\delta\eta$ intervals, 0.17,0.378, . . . ,1.30, scaled by $\langle E_T \rangle$ on the interval. The scale in $\langle E_T \rangle$ $d\sigma/dE_T$ corresponds to the uppermost plot, $\delta\eta$=0.17. Succesive distributions have been normalized by factors of 10^{-1}–10^{-4} for clarity of presentation. The curves correspond to fits which are discussed in the text.

$\delta\eta$, w_n is the relative probability for n projectile participants in the $B+A$ reaction and $P_n(E_T)$ is the calculated E_T distribution on the $\delta\eta$ interval for n independently interacting projectile nucleons. If $f_1(E_T)$ is the measured E_T spectrum in the $\delta\eta$ interval for one projectile nucleon, in this case the

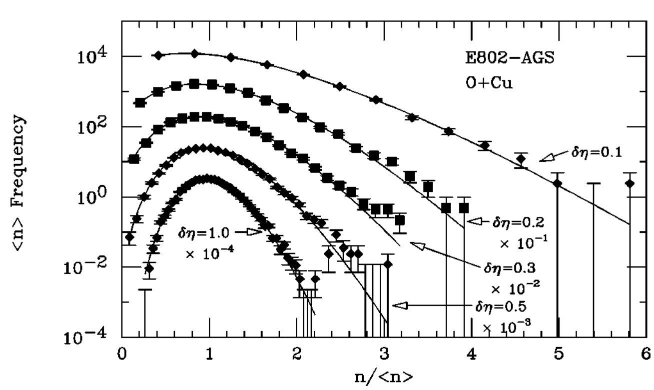

FIG. 8. Multiplicity distributions from Ref. [49] measured in [16]O+Cu central collisions at 14.6A GeV/c for five $\delta\eta$ intervals (indicated) around midrapidity, scaled by the $\langle n \rangle$ on the interval. Each successive distribution has been normalized downwards by the factor indicated for clarity of presentation. The curves correspond to NBD fits as discussed in the text.

TABLE X. Parameters from Gamma distribution fits to O+Cu and Au+Au central collision data. Errors quoted are statistical only.

		Gamma fit parameters		
		O+Cu (ZCAL)		
$\delta\eta$	σ (b)	$\langle E_T \rangle$ (GeV)	p	b (GeV^{-1})
1.30	0.160±0.001	4.45±0.08	15.7±0.2	3.53±0.04
0.966	0.159±0.001	3.43±0.07	12.4±0.2	3.62±0.04
0.624	0.158±0.001	2.28±0.04	8.7±0.1	3.82±0.05
0.378	0.157±0.001	1.38±0.02	5.6±0.1	4.04±0.05
		Au+Au (ZCAL)		
1.30	0.541±0.009	41.8±1.0	79.4±1.3	1.90±0.03
0.966	0.552±0.009	32.5±0.7	63.7±1.0	1.96±0.03
0.624	0.567±0.009	21.9±0.5	49.7±0.8	2.27±0.03
0.378	0.553±0.009	13.5±0.3	35.7±0.6	2.64±0.04

p+Au spectrum, and p_0 is the probability for a p+Au collision to produce no signal in the $\delta\eta$ interval, then $P_n(E_T)$ (including the p_0 effect) is

$$P_n(E_T)=\sum_{i=0}^{n}\frac{n!}{(n-i)!\ i!}p_0^{n-i}(1-p_0)^i f_i(E_T), \qquad (15)$$

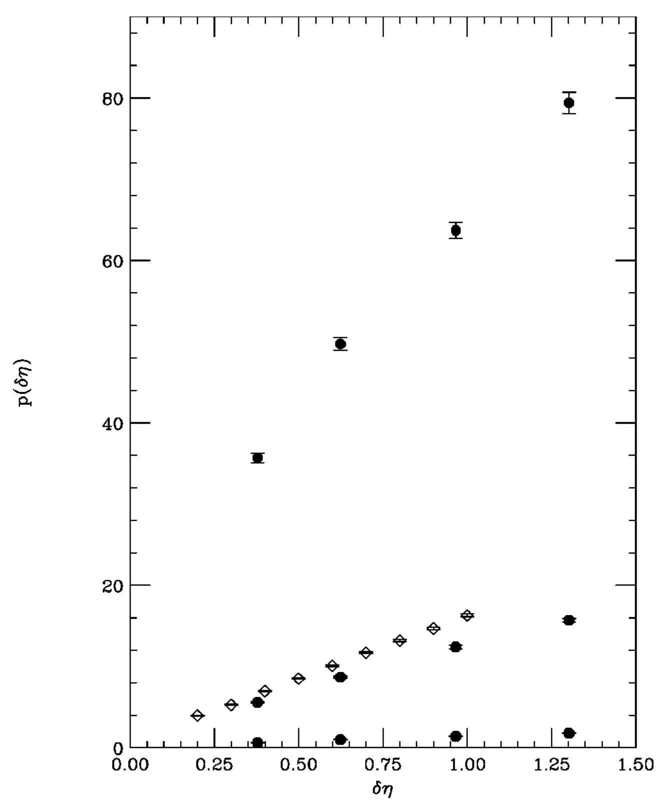

FIG. 9. Gamma distribution fit parameters $p(\delta\eta)$ as a function of $\delta\eta$ for E_T distributions (filled circles) from central collisions of Au+Au at 11.6A GeV/c, central collisions of O+Cu at 14.6A GeV/c , and from p+Au collisions 14.6 GeV/c. The open diamonds are $p(\delta\eta)$ from Gamma distribution fits [49] to O+Cu central multiplicity distributions at 14.6A GeV/c.

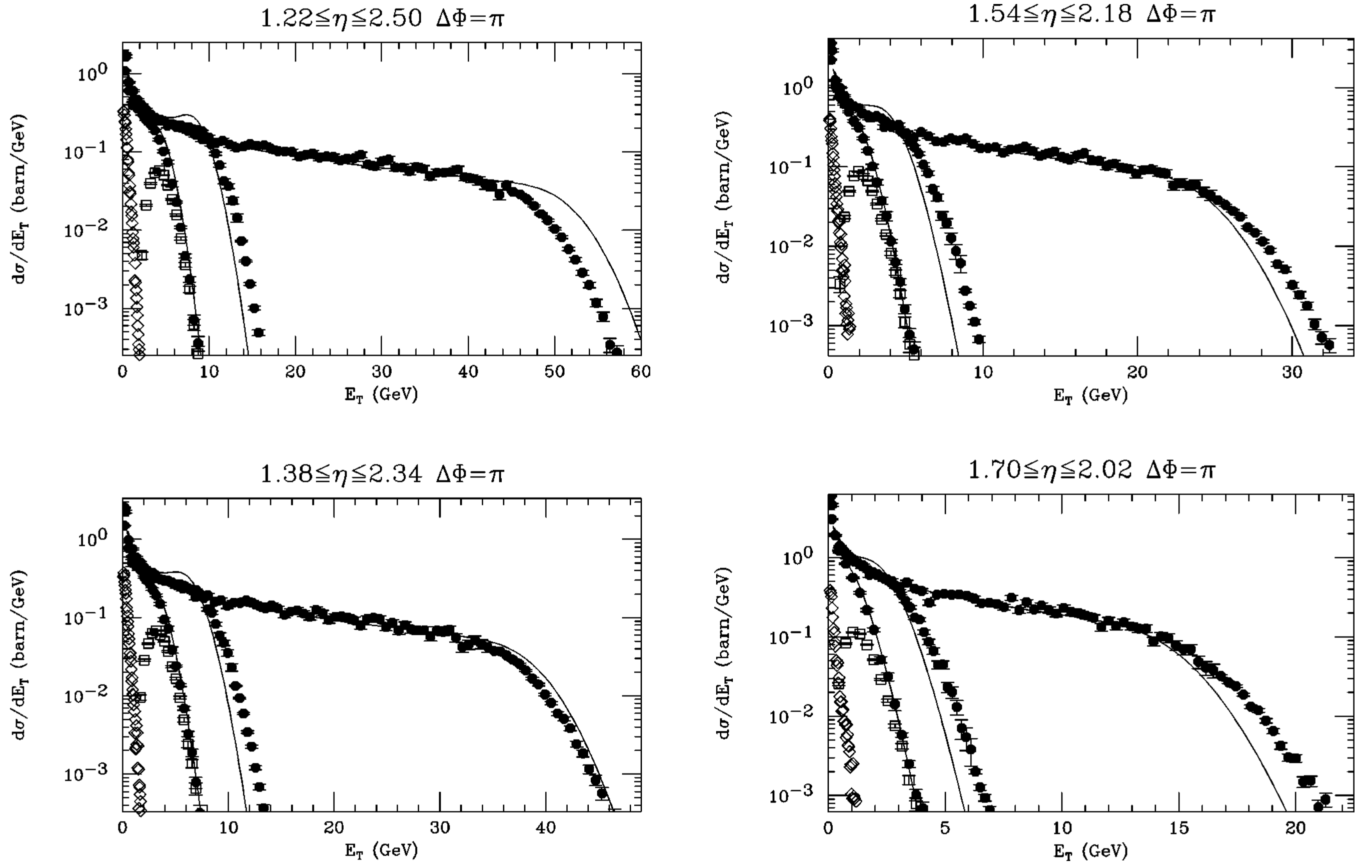

FIG. 10. E_T ($\Delta\phi=\pi$) distributions from Fig. 6 for the four $\delta\eta$ intervals indicated for (open diamonds) $p+$Au ($\times$0.10), and (filled points) for the reactions (in order of increasing maximum E_T) O+Cu, Si+Au, at 14.6A GeV/c and Au+Au at 11.6A GeV/c. The open squares on the O+Cu distribution represent the centrally triggered O+Cu (ZCAL) data. The WPNM calculations for O+Cu, Si+Au, and Au+Au are shown as solid lines. To correct for the difference in incident energies, the WPNM calculation for Au+Au has been scaled down in E_T by a factor of 1.155 [15] to correspond to the lower beam energy.

where $f_0(E_T)\equiv\delta(E_T)$ (the Dirac delta function) and $f_i(E_T)$ is the ith convolution of $f_1(E_T)$. Since the $p+$Au data in each $\delta\eta$ interval are nicely fit by Gamma distributions, the convolution is analytical [45]. Reversing the indices in Eqs. (14) and (15) gives a form that is less physically transparent, but considerably easier to compute

$$\left(\frac{d\sigma}{dE_T}\right)_{\rm WPNM}=\sigma\sum_{i=1}^{B} w_i'(p_0)\, f_i(E_T), \qquad (16)$$

where

$$w_i'(p_0)=(1-p_0)^i\sum_{n=i}^{B}\frac{n!}{(n-i)!\,i!}\,p_0^{n-i}\,w_n. \qquad (17)$$

As smaller and smaller $\delta\eta$ intervals are used for the E_T spectra, the probability p_0 for a $p+$Au reaction to produce zero signal on the interval becomes larger and larger. This effect is easily measured from the ratio of the detected cross section on the $\delta\eta$ interval for $p+$Au (Table IV) to the total inelastic $p+$Au cross section of 1662 mb from the nuclear geometry calculation [14,64], and must be taken into account when performing the WPNM. The values of p_0 are 0.08, 0.16, 0.23, 0.23 for the $\delta\eta$ intervals of Fig. 5, with statistical plus systematic error of $\pm$0.02 to $\pm$0.03. The results of the WPNM calculations for the data of Fig. 6 are shown in Fig. 10, with details of the calculation for O+Cu shown in Fig. 11. Clearly, the wounded projectile nucleon model continues to work well to relate the measured $p+$Au, O+Cu, Si+Au and Au+Au[5] E_T distributions, even for $\delta\eta$ intervals as small as 0.32 around midrapidity. This shows that midrapidity E_T distributions, even in relatively small apertures, provide excellent characterization of the nuclear geometry of $B+A$ collisions. As noted in Ref. [15], it is perhaps surprising that the WPNM, which treats the projectile and target asymmetrically, seems to work well even for the symmetric Au+Au system.

B. A simple exercise

Recently, electromagnetic E_T measurements in limited solid angles ($\delta\eta\sim1$) have been accepted as a characterization of the nuclear geometry of RHI collisions to such an extent

[5]The calculation for Au+Au is scaled down in E_T by a factor of 1.155 [15] to correspond to the lower beam energy.

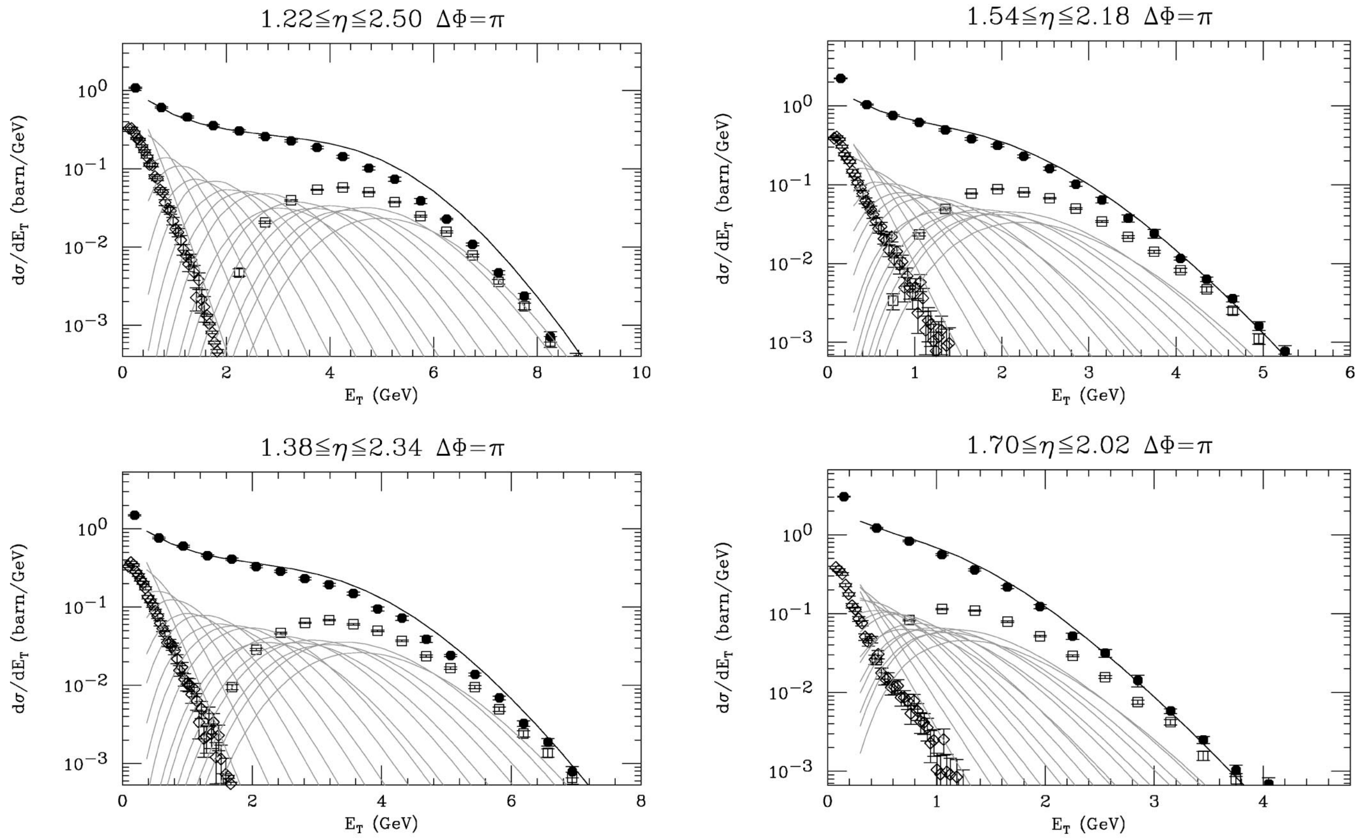

FIG. 11. WPNM calculations (lines) for the four $\delta\eta$ intervals indicated for the O+Cu E_T distributions (filled circles) from Fig. 10. The p+Au E_T distributions (open diamonds), which are the basis of the calculation in each $\delta\eta$ interval are also shown (normalized by a factor of 0.10 for presentation purposes). The centrally triggered O+Cu (ZCAL) distributions are shown as open squares. The individual components $w_n P_n(E_T)$ for $n=1,2,\ldots,16$ wounded projectile nucleons [Eq. (14)] are shown as lighter lines. Note that the present value for $p_0=0.083$ on the $1.22\leqslant\eta\leqslant2.50$ interval is different from the value $p_0=0.10$ used [14] in Fig. 2.

that the measured E_T tends to be treated as if it represented a microscopic quantity such as impact parameter or path-length in the nuclear medium to a high precision [22]. In the context of the WPNM calculation for the present data, it is straightforward to calculate from Eq. (14) the distribution, $P(m)|_{E_T}$, of the number of wounded projectile nucleons, m, for a fixed value of E_T

$$P(m)|_{E_T}=\frac{w_m\, P_m(E_T)}{\sum_{n=1}^{B} w_n\, P_n(E_T)}. \tag{18}$$

This is shown in Fig. 12 for the intervals $\delta\eta=1.30$ and $\delta\eta=0.624$ for five values of E_T ($\Delta\phi=\pi$) that correspond roughly to the upper 31 percentile, 7 percentile, 4 percentile, 2 percentile and 1/2 percentile of the Au+Au E_T distribution on the interval. For a fixed E_T (measured with $\leqslant1\%$ resolution), the number of projectile participants, N_{pp}, varies by 7–9 % (rms) (depending on the $\delta\eta$) around the mean, $\langle N_{pp}\rangle$, at the upper percentiles where *centrality* is normally defined, increasing to a variation of 10–15 % (rms) about the mean at the lower centrality values (~50 projectile participants), with continued proportionality $\sigma/\mu\propto1/\sqrt{\mu}$ at still lower values.[6] This is consistent with previous estimates [22,65]. It stands to reason that changes of any microscopic physical quantity as a function of measured E_T are unlikely to be sharper than the variation in the number of projectile participants at the same E_T value. Then, of course, E_T resolution different from the $\leqslant1\%$ of the present measurement would further affect the sharpness.

V. E_T DISTRIBUTIONS WITH APERTURE CORRECTED SCALE

One problem with the limited aperture EM calorimeter E_T distributions in comparison to 4π hadron calorimeters is the difficulty in relating the end points of the E_T spectra to the total available energy for the reaction. However, when the energy scale for each aperture is normalized by the measured

[6]For the $\delta\eta=0.624$ interval, the rms variation in the number of WPNM around the mean is given by the simple relation [65] $\sigma/\mu=1/\sqrt{\mu}$; but this relationship depends on the interval $\delta\eta$: for the smaller interval $\sigma/\mu>1/\sqrt{\mu}$ and for the larger intervals $\sigma/\mu<1/\sqrt{\mu}$.

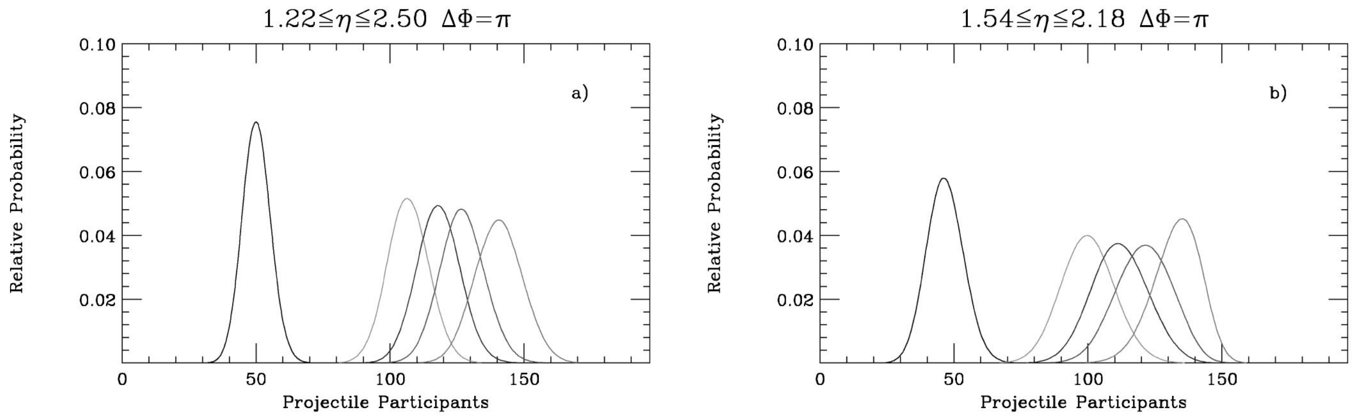

FIG. 12. Calculated distribution in projectile participants for a fixed value of E_T ($\Delta\phi=\pi$) in Au+Au collisions at 11.6A GeV/c for two $\delta\eta$ intervals: (a) $1.22\leqslant\delta\eta\leqslant2.50$, (b) $1.54\leqslant\delta\eta\leqslant2.18$. Calculations are for five values of E_T which correspond approximately to the upper 31 percentile, 7 percentile, 4 percentile, 2 percentile, 1/2 percentile of the distributions.

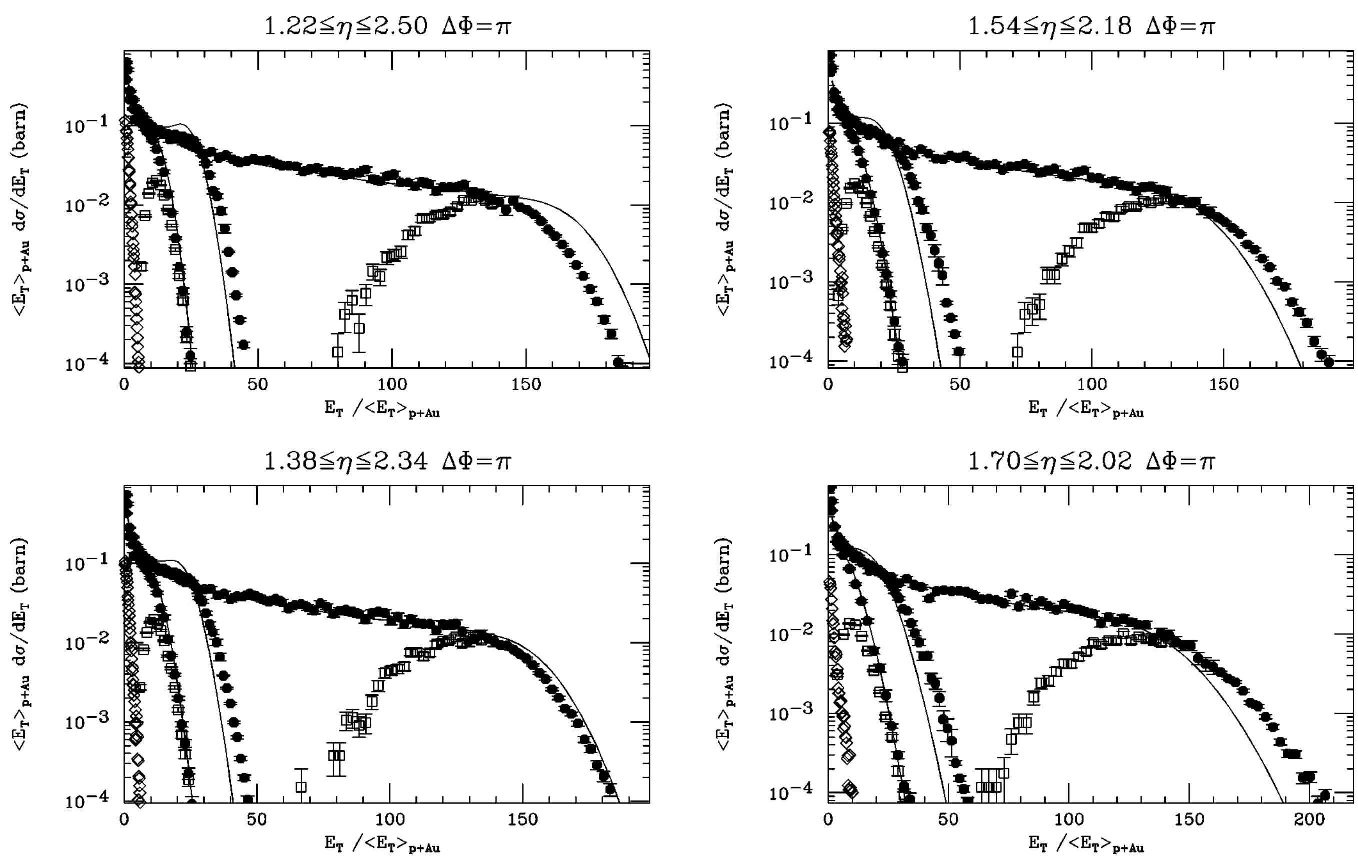

FIG. 13. E_T ($\Delta\phi=\pi$) distributions for the four $\delta\eta$ intervals indicated for (open diamonds) p+Au ($\times0.10$) and (filled points) for the reactions (in order of increasing maximum E_T) O+Cu, Si+Au at 14.6A GeV/c; Au+Au, corrected to 14.6A GeV/c. For each interval, the E_T scale is normalized by the measured $\langle E_T(\delta\eta)\rangle_{p+\mathrm{Au}}$ on the interval. The open squares on the O+Cu and Au+Au distributions represent the centrally triggered O+Cu (ZCAL) and Au+Au (ZCAL) data. The Au+Au measurements have been scaled up in E_T by a factor of 1.155 to correspond to 14.6 A GeV/c beam momentum [15]. The solid lines are wounded projectile nucleon model calculations.

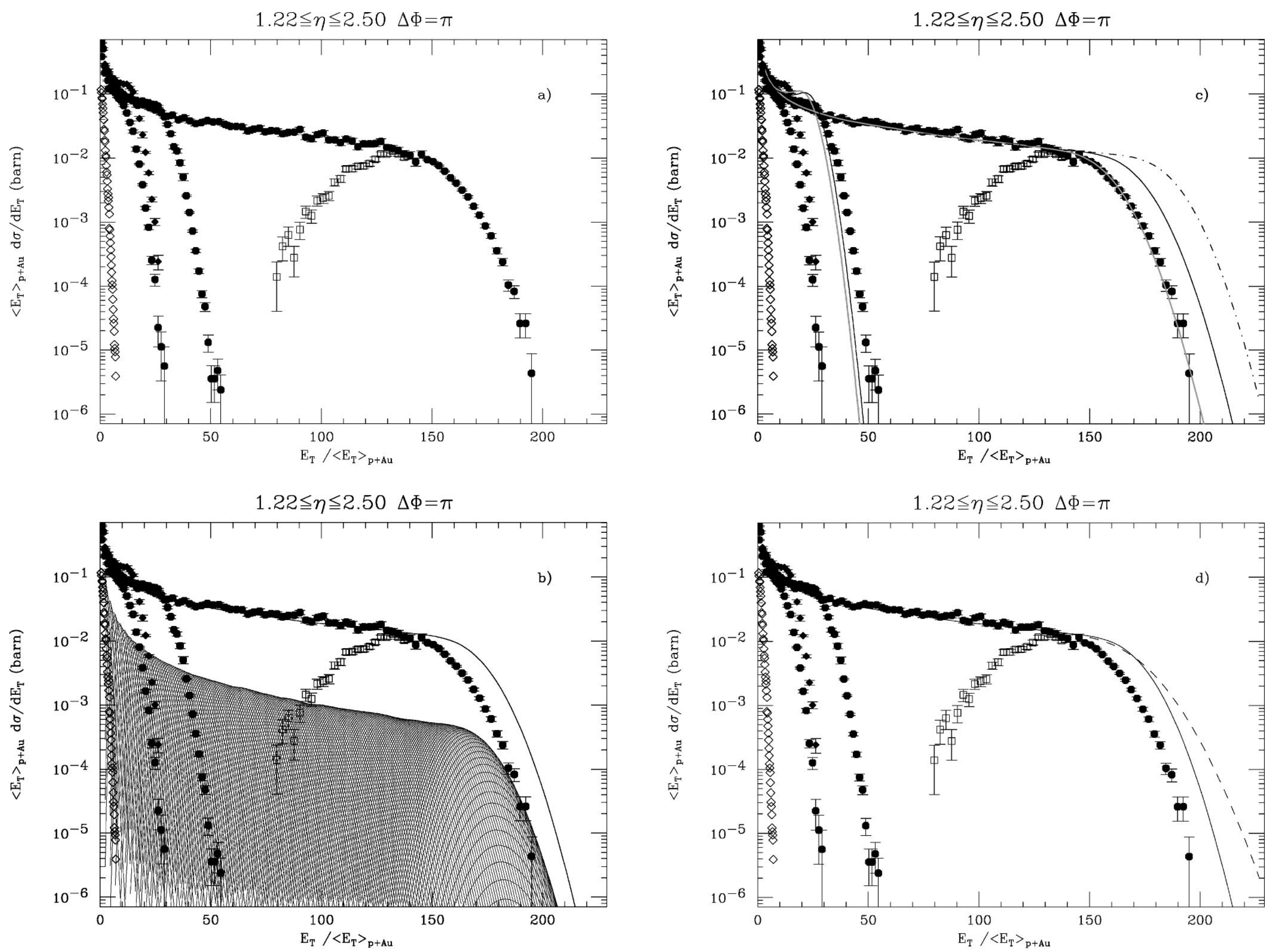

FIG. 14. (a) E_T ($\Delta\phi=\pi$,$1.22\leqslant\eta\leqslant2.50$) distributions (open diamonds) for $p+\mathrm{Au}$ ($\times0.10$) and (filled points) for the reactions (in order of increasing maximum E_T) O+Cu, O+Au, Si+Au at 14.6 A GeV/c; Au+Au corrected to 14.6A GeV/c as on Fig. 13. The open squares on the Au+Au distribution represent the centrally triggered Au+Au (ZCAL) data. The O+Au data [14] come from Fig. 2. (b) The same with standard WPNM calculation for Au+Au, with individual WPN components [Eq. (16)] shown. (c) Standard WPNM calculations (solid curves), $p_0=0.083$; WPNM calculation for Au+Au (dot-dash) with $p_0\rightarrow0$; WPNM calculations (lighter/dotted curves) with $p_0=0.156$. (d) WPNM calculation (dashes) with underlying $p+\mathrm{Au}$ $\Gamma(p,b)$ parameters changed keeping $\langle E_T\rangle_{p+\mathrm{Au}}$ fixed: $p\rightarrow p/2$, $b\rightarrow b/2$. Solid curve on all panels is the standard WPNM calculation.

$\langle E_T\rangle$ in the same aperture for $p+\mathrm{Au}$ collisions[7] (Table IV), the situation changes dramatically (see Fig. 13). Note that the Au+Au E_T distribution in Fig. 13 has been scaled up by a factor of 1.155 to correspond to 14.6A GeV/c beam momentum [15]. The dynamics of the reaction, in terms of projectile participants, can now be read directly from Fig. 13, e.g., the knees of the ^{16}O+Cu and ^{28}Si+Au E_T distributions for all $\delta\eta$ intervals occur at roughly 16 and 28 times the $\langle E_T\rangle_{p+\mathrm{Au}}$, corresponding to the A of the projectiles; but the knees of the Au+Au distributions are at roughly 150, clearly not $A_{\mathrm{Au}}=197$. The underlying dynamics and the difference in dynamics between the asymmetric ^{16}O+Cu, ^{28}Si+Au systems and the symmetric Au+Au system in all four $\delta\eta$ intervals is evident directly from Fig. 13, without recourse to a model.

VI. STUDIES OF THE UPPER EDGES FOR Au+Au

The details of the upper edge of the Au+Au distribution can be further understood in the context of the WPNM using the $\delta\eta$=1.30 interval for illustration (see Fig. 14). The position of and the steep fall-off above the upper *knee* of the Au+Au distribution is largely due to the steep fall-off of the contributions above 150 WPN, as shown in Fig. 14(b). This is both a nuclear geometry effect[8] and an acceptance effect in

[7]If multiple-collision effects were apparent in the $p+A$ data, as at CERN energies, then the measured $\langle E_T\rangle$ for p-p collisions (2 wounded nucleons) would be a better normalizing factor.

[8]The edges of heavy nuclei are dilute compared to the centers, so even zero-impact-parameter collisions for symmetric systems have, on the average, significant numbers of noninteracting nucleons at the periphery.

the limited aperture, i.e., $(1-p_0)^{197}$ tends to be considerably less than unity for most reasonable values of p_0, where p_0 is the measured probability for a WPN (a $p+\mathrm{Au}$ interaction) to produce zero signal on the $\delta\eta$ interval.

The sensitivity of the upper edge to p_0 can be studied by setting $p_0=0$ in the WPNM calculation [Fig. 14(c)]; and to the shape of the underlying $p+\mathrm{Au}$ E_T distribution by varying p and b, keeping $\langle E_T\rangle_{p+\mathrm{Au}}=p/b$ fixed [Fig. 14(d)]. The shape of upper edge is preserved as p_0 varies, but the position of the knee moves. For fixed $\langle E_T\rangle_{p+\mathrm{Au}}$, the upper edge flattens as b flattens (decreases), but the *knee* remains unchanged. Thus, the upper edges of Au+Au E_T distributions integrate over many WPN but retain their sensitivity to the underlying fundamental fluctuations on the interval as well as to the nuclear geometry.

Since the acceptance effect in the WPNM calculation has factors proportional to $(1-p_0)^{A_P}$, one could imagine that the slight discrepancies of the WPNM calculations compared to the ^{197}Au+Au measurements in Figs. 11 and 13 could be improved by varying p_0, without affecting the better agreement for the ^{16}O and ^{28}Si projectiles with smaller A_p. This is shown in Fig. 14(c) where p_0 is empirically varied to 0.156 from its measured value of 0.083 ± 0.011 (Table IV), $\pm\sim0.02$ systematic, which in fact does give curves (lighter/dotted curves) that pass through the Au+Au data. The change in p_0 of 7.3% is equivalent to an E_T scale change of roughly 8% for Au+Au, while making a smaller change ($\sim5\%$ in E_T) in the Si+Au and O+Cu (not shown) calculations.[9] Without arguing whether the WPNM describes the present data within the quoted errors on p_0 and the relative E_T scale ($\pm3\%$), it is clear that the WPNM provides in detail a reasonable description of the present data within $\pm5\%$ in E_T for all cases. Without recourse to a model, the plots in units of $E_T/\langle E_T\rangle_{p+\mathrm{Au}}$ lead to the same conclusion.

VII. A_P DEPENDENCE OF MIDRAPIDITY E_T DISTRIBUTIONS IN A_P+Au COLLISIONS AT 14.6A GeV/c

The projectile dependence of midrapidity E_T distributions as a function of the centrality—defined as a fixed upper percentile—was determined as a function of the interval $\delta\eta$ from the data of Fig. 13 for ^{16}O+Cu, ^{16}O+Au, ^{28}Si+Au, and ^{197}Au+Au, where the Au+Au data have been scaled up [15] by a factor of 1.155 in E_T to correspond to 14.6A GeV/c beam momentum and the O+Au distributions were extrapolated from O+Cu using the WPNM. Centralities of 7 percentile, 4 percentile, 2 percentile, 1 percentile, 0.5 percentile were examined (see Table XI). The convenience of normalizing the E_T scales in each interval, $\delta\eta$, by $\langle E_T(\delta\eta)\rangle_{p+\mathrm{Au}}$ is apparent since the percentiles are given in the physically meaningful units of ''number of average $p+\mathrm{Au}$ collisions,'' equivalent to average number of projectile participants, $\langle N_{pp}\rangle$. The effect of the variation in shape of the upper edges of the E_T distributions on the percentiles of the distributions is small for the ranges of $\delta\eta$ and percentiles studied. The 4 percentile results shown in Fig. 15(a) are typical. A given percentile centrality on the $\delta\eta=0.378$ and $\delta\eta=1.30$ intervals tends to correspond to a slightly ($\leqslant5\%$) larger number of equivalent projectile participants than on the 0.966 and 0.624 intervals for all three projectiles. This small-observed variation is actually significantly less than would be expected if the data were perfectly described by the WPNM and calls attention to the systematic variation of the WPNM with respect to the data evident in Fig. 13—in the largest $\delta\eta$ bin, the upper edge of the WPNM curve is $\sim8\%$ higher in E_T than the measurements and moves systematically lower with respect to the measurements as $\delta\eta$ is reduced, becoming $\sim7\%$ lower in E_T than the measurements for the smallest $\delta\eta$. In other words, if the WPNM were strictly correct as a function of $\delta\eta$, the measured percentiles in units of ''number of average $p+\mathrm{Au}$ collisions'' in each $\delta\eta$ interval would be equal to the true average number of projectile participants $\langle N_{pp}\rangle$ times $1-p_0$, a roughly 18% monotonic variation, rather than the $\leqslant5\%$ variation observed.[10]

TABLE XI. Upper percentiles of E_T distributions at 14.6A GeV/c as a function of the interval $\delta\eta$ in units of $\langle E_T(\delta\eta)\rangle_{p+\mathrm{Au}}$ on the interval.

$\delta\eta$	7 percentile	4 percentile	2 percentile	1 percentile	0.5 percentile
	Au+Au corrected to 14.6A GeV/c				
1.30	122.76	135.30	147.27	155.02	161.38
0.966	118.12	131.25	143.05	151.20	157.66
0.624	116.15	129.16	141.88	151.14	158.71
0.378	119.18	133.07	146.85	157.82	167.43
	Si+Au				
1.30	27.05	29.52	32.07	34.45	36.26
0.966	26.01	28.67	31.36	33.85	35.84
0.624	25.79	28.83	31.88	34.67	37.36
0.378	26.55	30.17	34.20	37.90	41.26
	O+Cu				
1.30	12.58	14.16	15.69	17.17	18.39
0.966	12.20	13.78	15.49	17.03	18.46
0.624	11.88	13.65	15.74	17.61	19.29
0.378	12.52	14.79	17.14	19.66	22.10
	O+Au WPNM calculation				
1.30	16.06	17.34	18.73	19.89	21.08
0.966	15.28	16.68	18.18	19.55	20.80
0.624	14.77	16.40	18.12	19.75	21.27
0.378	15.88	17.73	20.08	22.27	24.45

[9] To the extent that the E_T spectrum is dominated by the nuclear geometry rather than the shape (p,b) of the underlying $p+\mathrm{Au}$ E_T distribution, i.e., for E_T values up to the *knee* of the distribution, the effect of p_0 as a change in the E_T scale by a factor of $1-p_0$ can be understood from Eq. (15). The average value of E_T for n collisions with $p_0\neq0$, $\langle E_T(p_0)\rangle_n$, is equal to the true average E_T for n collisions, $\langle E_T\rangle_n$, times $(1-p_0)/(1-p_0^n)$ which equals $1-p_0$ for large n.

[10] Since the WPNM calculation happens to describe the Au+Au data best in the $\delta\eta=0.966$ interval, correcting the measured percentiles for Au+Au in Table XI by $1-p_0$ gives values for this interval that are closest to the true percentiles of the WPNM in units of $\langle N_{pp}\rangle$.

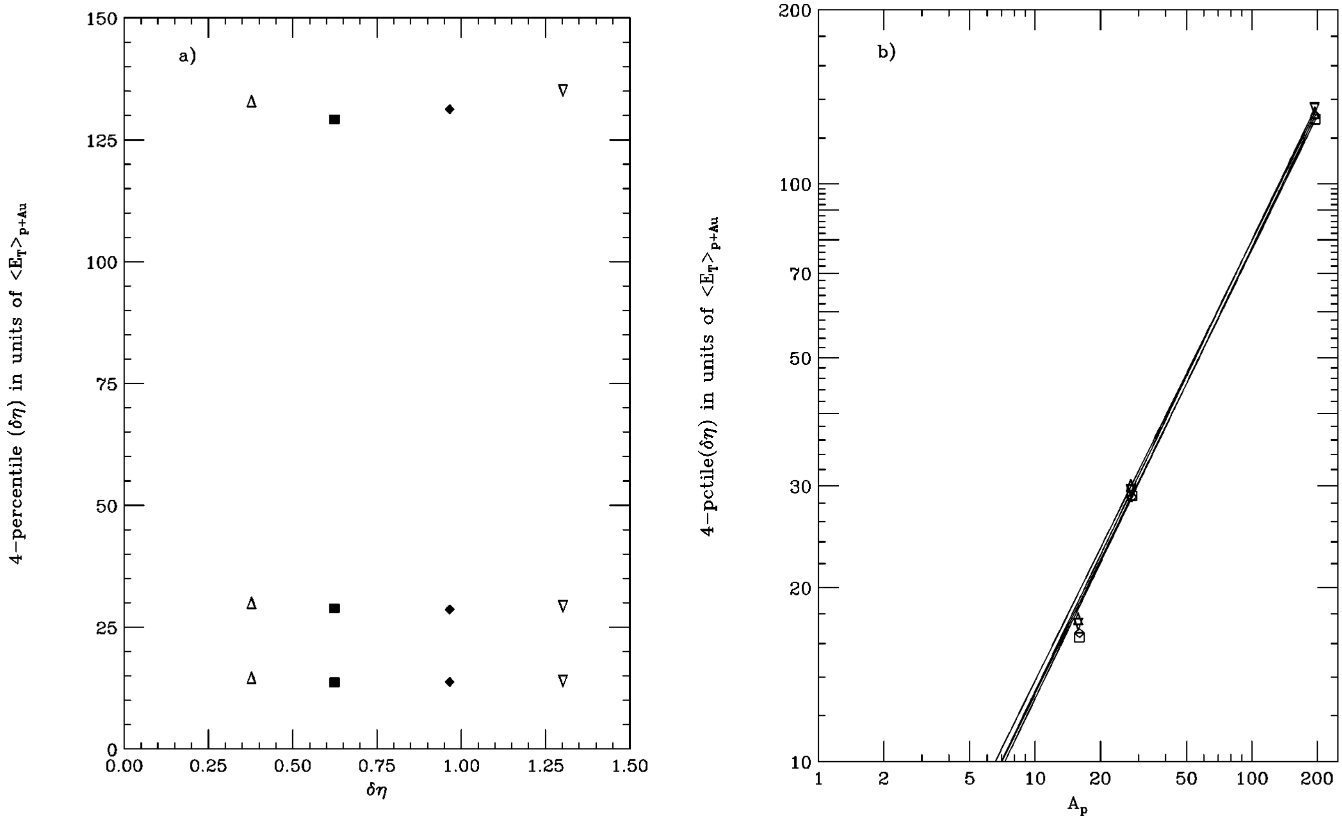

FIG. 15. (a) 4 percentile of E_T distributions as a function $\delta\eta$, measured in units of $\langle E_T(\delta\eta)\rangle_{p+\mathrm{Au}}$, for Au+Au (corrected to 14.6*A* GeV/*c*) and Si+Au, O+Cu at 14.6*A* GeV/*c*. (b) Projectile (A_p)-dependence in an Au target of the 4 percentile of E_T distributions for the four $\delta\eta$ bins, measured in units of $\langle E_T(\delta\eta)\rangle_{p+\mathrm{Au}}$. Lines are fits to $A_p^{\alpha_p}$ from Si+Au to Au+Au (corrected to 14.6*A* GeV/*c*). The points for $A_p=16$ are extrapolated from O+Cu to O+Au using the WPNM.

The projectile A_p dependence at fixed percentile centrality [see Fig. 15(b]) cannot be represented as a simple power law, $A_p^{\alpha_p}$, from O+Au, Si+Au to Au+Au. However, the A_p dependence is nearly A_p^1, from O+Au to Si+Au ($\alpha_p=0.94-1.00$ depending on percentile and $\delta\eta$), changing to $\alpha_p=0.73$–0.78 from Si+Au to Au+Au depending on percentile and $\delta\eta$. The relatively small systematic variation of α_p over the ranges of percentile and $\delta\eta$ studied shows that centrality definition by a fixed upper percentile of midrapidity E_T distributions is surprisingly robust. There are previous measurements of the target dependence [66,14] of E_T production at AGS energies; but previous measurements of the projectile dependence [31] were for symmetric systems and given relative to the *isotropic fireball model* [38], making comparisons difficult.

VIII. SUMMARY AND CONCLUSIONS

Systematic measurements of E_T distributions of produced particles for $p+$Be, $p+$Au, O+Cu, Si+Au, and Au+Au collisions at 11.6–14.6 *A* GeV/*c* incident momentum in a half-azimuth ($\Delta\phi=\pi$) electromagnetic calorimeter as a function of the pseudorapidity interval $\delta\eta$ from 0.2 to 1.3 around midrapidity are presented. The shapes of the E_T distributions vary with the $\delta\eta$ interval, like multiplicity, with larger fluctuations (flatter upper tails) for smaller intervals. This variation has little effect on the projectile A_p dependence measured at a constant centrality defined as a fixed upper percentile of the E_T distributions for the typical values, 7 percentile, 4 percentile, 2 percentile, 1 percentile, 0.5 percentile, which were investigated.

The nuclear geometry characterization of the midrapidity E_T distributions remains valid for all $\delta\eta$ intervals studied as demonstrated by the success of the wounded projectile nucleon model in relating the spectra for O+Cu, Si+Au, and Au+Au to the $p+$Au E_T spectrum measured in the same $\delta\eta$ interval. The success in reproducing the shapes of the upper tails of the E_T distributions in Au+Au collisions, where the number of participants is so large that combinatoric acceptance effects play an important role, further illustrates the sensitivity of the method to the underlying dynamics as well as to the nuclear geometry.

An effective way of demonstrating the systematics of the projectile dependence without recourse to a model is to plot the the $E_T(\delta\eta)$ distribution in each $\delta\eta$ interval in units of the measured $\langle E_T(\delta\eta)\rangle_{p+\mathrm{Au}}$ in the same $\delta\eta$ interval for $p+$Au collisions. These plots, in the physically meaningful units of ''number of average $p+$Au collisions,'' are nearly universal as a function of $\delta\eta$, confirming that the reaction dynamics for E_T production at midrapidity at AGS energies is governed by the number of projectile participants.

A particularly striking result comes from $p+A$ collisions, where a large change in shape with $\delta\eta$ is observed for both the $p+$Be and $p+$Au E_T distributions; yet in each $\delta\eta$ interval the $p+$ Be and $p+$Au distributions remain identical in shape to each other, dramatically illustrating the absence of multiple-collision effects at AGS energies at midrapidity over a wide range of pseudorapidity intervals, from $\delta\eta=0.3$ to $\delta\eta=1.3$. This demonstrates that the large projectile stopping at AGS energies, originally inferred from early measurements of midrapidity E_T distributions [11,12], and subsequently confirmed by direct measurements of the nucleon-rapidity distributions [28–30] is not an artifact of a particular $\delta\eta$ interval.

Attempts to understand in detail the differences in fluctuations about the mean for E_T and multiplicity distributions [49] in O+Cu central collisions, where the centrality definition is very clean (<1 projectile spectator), were inconclusive, leaving unresolved the issue of whether multiplicity or energy emission is primary.

It seems clear that midrapidity is indeed a reasonable place for robust event characterization and studies of reaction dynamics in relativistic heavy ion collisions using E_T distributions in limited apertures. Independent of any model, results can be expressed in the physically meaningful units of average number of *p-p* or $p+A$ collisions by using measurements of these reactions in the same apertures, which serve as *in situ* calibration of the detector, and which works remarkably well at AGS energies.

[1] J. D. Bjorken, Phys. Rev. D **8**, 4098 (1973).

[2] W. Ochs and L. Stodolsky, Phys. Lett. **69B**, 225 (1977).

[3] P. V. Landshoff and J. C. Polkinghorne, Phys. Rev. D **18**, 3344 (1978).

[4] R. L. Cool *et al.*, CCR Collaboration, in *Proceedings of the XVI International Conference on High Energy Physics*, Chicago-Batavia, 1972, edited by J. D. Jackson and A. Roberts (NAL, Batavia, 1973), Vol. 3, p. 317. See also B. Alper *et al.*, Phys. Lett. **44B**, 521 (1973); M. Banner *et al.*, *ibid.* **44B**, 537 (1973); F. W. Büsser *et al.*, *ibid.* **46B**, 471 (1973).

[5] C. DeMarzo *et al.*, Phys. Lett. **112B**, 173 (1982); see also K. Pretzl, *et al.*, in *Proceedings of XX International Conference on High Energy Physics, Madison, 1980*, edited by L. Durand and L. G. Pondrom (AIP, New York, 1981), pp. 92–97.

[6] E.g., see G. Giacomelli and M. Jacob, Phys. Rep. **55**, 1 (1979); P. Capiluppi *et al.*, Nucl. Phys. **B79**, 189 (1974); **B70**, 1 (1974).

[7] E.g., see M. J. Tannenbaum, Int. J. Mod. Phys. A **4**, 3377 (1989).

[8] J. D. Bjorken, Phys. Rev. D **27**, 140 (1983).

[9] G. Sterman and S. Weinberg, Phys. Rev. Lett. **39**, 1436 (1977).

[10] M. Plümer and R. M. Weiner, Phys. Rev. D **37**, 3136 (1988); S. Raha, *et al.*, in *Correlations and Multiparticle Production, Marburg, 1990*, Proceedings of the International Workshop, edited by M. Plümer, S. Raha, and R. M. Weiner (World Scientific, Singapore, 1991), pp. 283–289.

[11] T. Abbott *et al.*, E802 Collaboration, Phys. Lett. B **197**, 285 (1987).

[12] T. Abbott *et al.*, E802 Collaboration, Z. Phys. C **38**, 35 (1988).

[13] T. Abbott *et al.*, E802 Collaboration, Phys. Rev. C **44**, 1611 (1991).

[14] T. Abbott *et al.*, E802 Collaboration, Phys. Rev. C **45**, 2933 (1992).

[15] L. Ahle *et al.*, E802 Collaboration, Phys. Lett. B **332**, 258 (1994).

[16] J. Barrette *et al.*, E814/E877 Collaboration, Phys. Rev. Lett. **70**, 2996 (1993); **64**, 1219 (1990); P. Braun-Munzinger *et al.*, Z. Phys. C **38**, 45 (1988); M. Rosati *et al.*, Nucl. Phys. **A566**, 597c (1994).

[17] T. Åkesson *et al.*, Helios Collaboration, Z. Phys. C **58**, 239 (1993); Nucl. Phys. **B353**, 1 (1991); Z. Phys. C **38**, 383 (1988); **38**, 397 (1988); Phys. Lett. B **214**, 295 (1988).

[18] R. Albrecht *et al.*, WA80 Collaboration, Phys. Lett. B **199**, 297 (1987); Phys. Rev. C **44**, 2736 (1991); Z. Phys. C **55**, 539 (1992).

[19] S. P. Sorensen *et al.*, WA80 Collaboration, Z. Phys. C **38**, 3 (1988).

[20] A. Bamberger *et al.*, NA35 Collaboration, Phys. Lett. B **184**, 271 (1987); W. Heck *et al.*, Z. Phys. C **38**, 19 (1988); T. Alber *et al.*, NA49 Collaboration, Phys. Rev. Lett. **75**, 3814 (1995).

[21] J. Bächler *et al.*, NA35 Collaboration, Z. Phys. C **52**, 239 (1991).

[22] M. C. Abreu *et al.*, NA50 Collaboration, Phys. Lett. B **450**, 456 (1999).

[23] H. R. Schmidt and J. Schukraft, J. Phys. G **19**, 1705 (1993).

[24] T. Peitzmann and M. Aggarwal *et al.*, WA98 Collaboration, Nucl. Phys. **A610**, 200c (1996).

[25] J. E. Elias *et al.*, Phys. Rev. D **22**, 13 (1980); C. Halliwell *et al.*, Phys. Rev. Lett. **39**, 1499 (1977); W. Busza *et al.*, *ibid.* **34**, 836 (1975).

[26] A. Białas, A. Błeszynski, and W. Czyż, Nucl. Phys. **B111**, 461 (1976).

[27] A. J. Baltz, Phys. Rev. C **43**, 1420 (1991).

[28] Y. Akiba *et al.*, E802 Collaboration, Nucl. Phys. **A610**, 139c (1996); H. Hamagaki *et al.*, *ibid.* **A566**, 27c (1994); M. Gonin *et al.*, *ibid.* **A566**, 601c (1994).

[29] T. Abbott *et al.*, E802 Collaboration, Phys. Rev. C **50**, 1024 (1994).

[30] L. Ahle *et al.*, E802 Collaboration, Phys. Rev. C **57**, R466 (1998).

[31] J. Barrette *et al.*, E814/E877 Collaboration, Phys. Rev. Lett. **70**, 2996 (1993); thanks to Professors J. Stachel and T. Hemmick for permission to show these measurements.

[32] G. Arnison *et al.*, UA1 Collaboration, Phys. Lett. **122B**, 103 (1983); M. Banner *et al.*, UA2 Collaboration, *ibid.* **122B**, 476 (1983).

[33] Also see W. J. Willis, in *ISABELLE Physics Prospects*, edited by R. B. Palmer (Brookhaven National Laboratory, Upton, NY, 1972), pp. 207–234.

[34] C. De Marzo *et al.*, Phys. Rev. D **29**, 2476 (1984); **26**, 1019 (1982).

[35] Y. Akiba, Ph.D. thesis, Department of Physics, University of Tokyo, Report No. INS-IM6, 1989.
[36] J. Ftáčnik *et al.*, Phys. Lett. B **188**, 279 (1987).
[37] J. Stachel, Nucl. Phys. **A527**, 167c (1991).
[38] J. Stachel and G. R. Young, Annu. Rev. Nucl. Part. Sci. **42**, 537 (1992).
[39] G. D. Westfall *et al.*, Phys. Rev. Lett. **37**, 1202 (1976).
[40] S. Das Gupta and A. Z. Mekjian, Phys. Rep. **72**, 131 (1981).
[41] S. Nagamiya, J. Randrup, and T. J. M. Symons, Annu. Rev. Nucl. Part. Sci. **34**, 155 (1984).
[42] P. M. Fishbane and J. S. Trefil, Phys. Rev. D **3**, 238 (1971); **9**, 168 (1974); Phys. Lett. **51B**, 139 (1974); A. Dar and J. Vary, Phys. Rev. D **6**, 2412 (1972); A. S. Goldhaber, *ibid.* **7**, 765 (1973); K. Gottfried, Phys. Rev. Lett. **32**, 957 (1974); see also A. Białas and W. Czyż, Phys. Lett. **51B**, 179 (1974); B. Andersson and I. Otterlund, Nucl. Phys. **B88**, 349 (1975).
[43] T. Abbott *et al.*, E802 Collaboration, Phys. Rev. D **45**, 3906 (1992).
[44] T. Abbott *et al.*, E802 Collaboration, Nucl. Instrum. Methods Phys. Res. A **290**, 41 (1990).
[45] A full discussion on the Gamma distribution is given in Sec. III A.
[46] T. Abbott *et al.*, E802 Collaboration, Phys. Rev. Lett. **66**, 1567 (1991).
[47] See also I. Chemakin *et al.*, BNL-E910 Collaboration, nucl-ex/9902009.
[48] L. Ahle *et al.*, E802 Collaboration, Phys. Rev. C **59**, 2173 (1999).
[49] T. Abbott *et al.*, E802 Collaboration, Phys. Rev. C **52**, 2663 (1995).
[50] G. J. Alner *et al.*, UA5 Collaboration, Phys. Lett. **160B**, 193 (1985); **160B**, 199 (1985); **167B**, 476 (1986).
[51] M. J. Tannenbaum *et al.*, BCMOR Collaboration, in *Proceedings of Quark Matter 1984*, edited by K. Kajantie (Springer, Berlin, 1985), pp. 174–186.
[52] B. Callen *et al.*, AFS Collaboration, *Proceedings of Quark Matter 1984* (Ref. [51]), pp. 133–142.
[53] A. L. S. Angelis *et al.*, BCMOR Collaboration, Phys. Lett. **168B**, 158 (1986); **141B**, 140 (1984).
[54] T. Åkesson *et al.*, Phys. Lett. B **231**, 359 (1989).
[55] E.g., see A. Bialas and R. Peschanski, Phys. Lett. B **207**, 59 (1988).
[56] G. N. Fowler and R. M. Weiner, Phys. Lett. **70B**, 201 (1977); Phys. Rev. D **17**, 3118 (1978).
[57] A. Giovannini and L. Van Hove, Z. Phys. C **30**, 391 (1986).
[58] E.g., see citations in Ref. [49].
[59] H. Bøggild *et al.*, AFS Collaboration, Report No. CERN-EP-82/104.
[60] T. Åkesson and H-U Bengtsson, Phys. Lett. **120B**, 233 (1983).
[61] H. Gordon *et al.*, AFS Collaboration, Phys. Rev. D **28**, 2736 (1983).
[62] T. Åkesson *et al.*, AFS Collaboration, Phys. Lett. **119B**, 464 (1982).
[63] H. Brody, S. Frankel, W. Frati, and I. Otterlund, Phys. Rev. D **28**, 2334 (1983).
[64] The value of 1662 mb is very close to the extrapolated value of 1675 $\pm$ 30 mb for the total inelastic $p+$Au cross section at 20 GeV/c from the measurements of S. P. Denisov *et al.*, Nucl. Phys. **B61**, 62 (1973).
[65] D. Kharzeev, C. Lourenço, M. Nardi, and H. Satz, Z. Phys. C **74**, 307 (1997).
[66] Also see J. Stachel, Nucl. Phys. **A525**, 23c (1991) for target (A_t) dependences for O and Si/S projectiles.